Performance Analysis of Power Control and Cell Association in Heterogeneous Cellular Networks

by

Prasanna Herath Mudiyanselage

A thesis submitted in partial fulfillment of the requirements for the degree of

Doctor of Philosophy
in
Communications

Department of Electrical and Computer Engineering
University of Alberta

Abstract

The research investigation focuses on modeling and mitigation of interference in Heterogeneous networks (HetNets). Stochastic geometry-based analytical tools are used to develop tractable mathematical models. The idea is to abstract the spatial distribution of nodes and users by points of suitable point processes. Developed mathematical models are used to identify the effects of various parameters and network configurations on the performance of cellular networks. In particular, the aims of this research project are to: (i) develop analytical tools to comprehensively capture practical conditions of HetNets, including the spatial distribution of nodes and different environmental conditions (fading, shadowing, and path loss); (ii) develop new power control schemes for HetNet uplink transmission; (iii) develop simple cell association policies for HetNets; and (iv) investigate the impact of practical limitations in cell association policies on the performance of HetNets. Overall, the research findings will pave the way to the design of new energy-efficient and spectrally-efficient high-throughput cellular systems.

~

Preface

This thesis is an original work conducted by Prasanna Herath Mudiyanselage.

Chapter 3 of this thesis has been published as P. Herath, C. Tellambura, and W. A. Krzymień, "Coverage probability analysis of three uplink power control schemes: Stochastic geometry approach," *EURASIP Journal on Wireless Communications and Networking*, vol. 141, pp. 1-14, June 2018. A part of the contribution of this chapter has been also published as P. Herath, C. Tellambura, and W. A. Krzymień, "Stochastic geometry modeling of cellular uplink power control under composite Rayleigh-lognormal fading," in *Proc. IEEE 82nd Vehicular Technology Conference*, September 2015.

Chapter 4 of this thesis has been published as P. Herath, W. A. Krzymień, and C. Tellambura, "Coverage and rate analysis for limited information cell association in stochastic-layout cellular networks," *IEEE Trans. Veh. Technol.*, vol. 65, no. 9, pp. 6962-6971, September 2016. A part of the contribution has also been published as P. Herath, W. A. Krzymień, and C. Tellambura, "A novel base stations - mobile stations association policy for cellular networks," in *Proc. 80th IEEE Vehicular Technology Conference*, September 2014.

~

Dedicated to my beloved parents, wife, and daughter...

Acknowledgements

First of all, I express my sincere gratitude and respect to my supervisors, Prof. Chintha Tellambura and Prof. Witold A. Krzymień. They indeed gave me total freedom to define and conduct my research, while providing encouragement, guidance, and invaluable expertise throughout my Ph.D. program. It was my great pleasure to work and collaborate with them, and their open approach towards research and professionalism have immensely facilitated my work. I extend my sincere gratitude to the Ph.D. supervisory committee member Prof. Yindi Jing for evaluating my thesis and providing constructive feedback and comments. I would also like to convey my special thanks to Prof. Hong-Chuan Yang from University of Victoria and Prof. Hai Jiang for their valuable feedback during my final Ph.D. defense. I am thankful to Prof. Scott Dick for chairing my final Ph.D. defense.

I also wish to thank the Natural Sciences and Engineering Research Council of Canada (NSERC), and TRTech, Edmonton, for the financial support I received in the form of a NSERC Industrial Postgraduate Scholarship, and the Government of Alberta for financial support received through a Queen Elizabeth II Graduate Scholarship. Furthermore, I am grateful to the faculty and the administrative staff of the Department of Electrical and Computer Engineering for their support and for creating an environment conducive to research excellence.

My most heartfelt gratitude goes to my beloved parents, my three brothers, and my loving wife for their immeasurable support and encouragement throughout my graduate studies. I would also like to thank my former and current labmates, including Gayan, Saman, Damith, Sachitha, Shashindra, Shuangshuang, Vesh, Yamuna, Yun, Bitan, Khagendra, Mahmoud, Wu, and Chao for the useful discussions we had and enjoyable times we spent together. Moreover, the rich and diverse learning environment of my research lab provided me a golden opportunity to gain invaluable experience.

~

Table of Contents

List of Tables

List of Figures

List of Symbols

Elementary & Special Functions

Notation	Definition
$\exp(\cdot)$	Exponential function
$\log(\cdot)$	natural logarithm
$\log_2(\cdot)$	logarithm to base 2
$\Gamma(z)$	gamma function [5, Eqn. (8.310.1)]
$\gamma(\alpha, z)$	lower incomplete gamma function [5, Eqn. (8.350.1)]
$\Gamma(\alpha, z)$	upper incomplete gamma function [5, Eqn. (8.350.2)]
${}_2F_1(\cdot, \cdot; \cdot, \cdot)$	Gauss Hypergeometric function [5, Eqn. (9.14.1)]

Probability & Statistics

Let X and A be a random variable and an arbitrary event, respectively.

Notation	Definition
$\mathcal{E}_X\{\cdot\}$	expected value with respect to X; $\mathcal{E}\{\cdot\}$, if X is implied
$f_X(\cdot)$	probability density function (PDF) of X
$F_X(\cdot)$	cumulative distribution function (CDF) of X
$\bar{F}_X(\cdot)$	complimentary cumulative distribution function (CCDF) of X
$\mathcal{L}_X(\cdot)$	Laplace transform of the PDF of X
$\mathrm{var}_X(\cdot)$	variance of X; $\mathrm{var}(\cdot)$, if X is implied.
$\Pr(A)$	probability of A
$X \sim \mathcal{CN}(\mu, \sigma^2)$	X is complex normal distributed with mean μ and variance σ^2
$X \sim \exp(\mu)$	X is exponentially distributed with mean μ
$X \sim \mathrm{lognormal}(\mu, \sigma)$	random variable X is a lognormal random variable with mean μ, and $\mathrm{var}(X) = \sigma^2$

Miscellaneous

Notation	Definition
$\mathbb{N}$	Natural numbers (including 0)
$\mathbb{R}^d$	Real coordinate space of d dimensions
$\|\|a\|\|$	Euclidean norm of $\mathbf{a}$
$\|\|x - y\|\|$	Euclidean distance between point x and y
$\|z\|$	absolute value of a complex number z

$\lvert \cdot \rvert$	Lebesgue measure of relevant dimension of the argument
$Re\ z$	real component of complex number z
$Im\ z$	imaginary component of complex number z
$k!$	factorial of k [6, Eqn. (6.1.5)]
$\binom{n}{k}$	binomial coefficient n choose k [6, Sec. 3.1]
$\mathbf{1}(x)$	Indicator function; $\mathbf{1}(x) = 1$, if x holds, else 0
$b(x, R)$	ball centered at point x and have radius R

List of Abbreviations

Abbreviation	Definition
2G	second generation cellular networks
3G	third generation cellular networks
3GPP	3rd generation partnership project
4G	fourth generation cellular networks
5G	fifth generation cellular networks
AP	access point
AWGN	additive white Gaussian noise
BPP	binomial point process
BS	base station
CAGR	compound annual growth rate
CCDF	complimentary cumulative distribution function
CCI	co-channel interference
CDF	cumulative distribution function
CSG	closed subscriber group
D2D	device-to-device
DFT-S-OFDMA	discrete Fourier transform-spread OFDMA
DS-CDMA	direct sequence code division multiple access
DSL	digital subscriber line
eMBB	enhanced mobile broadband
Gbps	gigabits per second
HetNet	Heterogeneous network
i.i.d.	independent and identically distributed
ICI	inter-cell interference
IMT-A	International Mobile Telecommunications-Advanced
kbps	kilobits per second

Abbreviation	**Definition**
LAA	license assisted access
LoS	line-of-sight
LTE	Long Term Evolution
LTE-A	Long Term Evolution-Advanced
LTE-A	Long Term Evolution-Advanced
M2M	machine to machine
Mbps	megabits per second
MGF	moment generating function
MIMO	multiple-input multiple-output
mMTC	massive machine-type communication
MRC	maximal ratio combining
MS	mobile station
NLoS	non-line-of-sight
NR	new radio
NSA 5G	non-standalone 5G
OFDM	orthogonal frequency division multiplexing
OFDMA	orthogonal frequency division multiple access
PCP	Poisson cluster process
PDF	probability density function
PGFL	probability generating functional
PHP	Poisson hole process
PLI	path loss inversion
PLSI	path loss and shadowing inversion
PPP	Poisson point process
RF	radio frequency
RRH	remote radio head
RSSI	received signal strength indicator
RV	random variable
SA 5G	standalone 5G
SINR	signal-to-interference-plus-noise ratio
SIR	signal-to-interference ratio
SNR	signal-to-noise ratio
TPC	transmit power control
UR-LLC	ultra-reliable, low-latency communication
XOR	(bitwise) exclusive OR (operation)

Chapter 1

Introduction

From being an expensive technology enjoyed by a select few three decades ago, mobile communications have become everyday commodity accessible to all today. During this period, the world has witnessed the evolution of four generations of cellular mobile communication systems. Each generation has revolutionized the way people live their day-to-day lives.

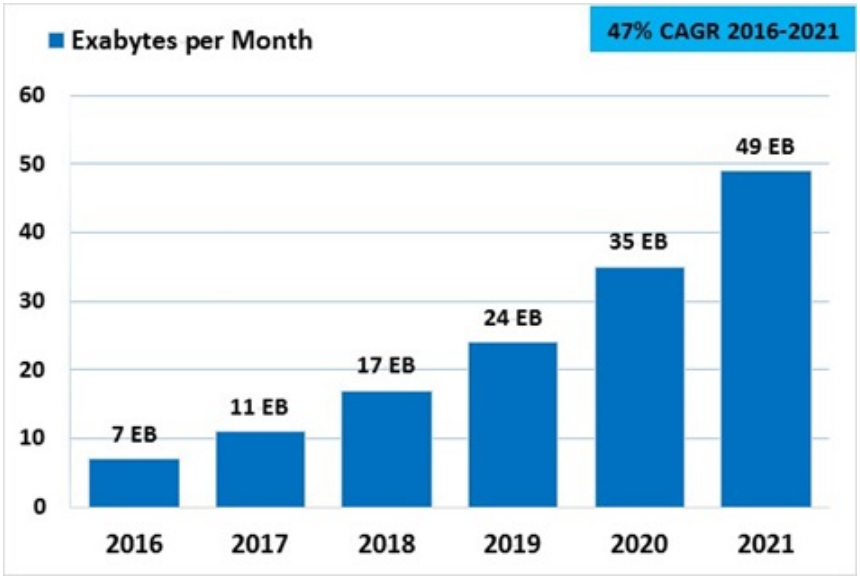

Figure 1.1: Cisco mobile traffic forecast 2016-2021 [1]

Today's mobile communication networks have to cater a diverse set of services with a range of performance requirements. This includes meeting the high data rates of capacity-hungry services (video and audio streaming, online gaming, social networking, cloud computing [7, 8], augmented/virtual reality [9]), providing low latency and ultra-reliable communications for critical services (autonomous driving,

drones), and providing network connectivity in user-dense areas (offices, stadiums, urban centers). Meeting all of these service requirements has put the networks and system designers under tremendous pressure. Addition of a multitude of new connections and services has increased the severity of the problem. For example, in 2016 alone, almost half a billion (429 million) mobile devices and connections were added to wireless systems, increasing the number of the global mobile connections and devices to approximately 8 billion [1]. As a result, global mobile data traffic grew by 63% in 2016 and reached 7.2 exabytes (7.2×10^{18} bytes) per month, compared to 4.4 exabytes per month in 2015, see Figure 1.1 [1]. This trend is expected to continue at compound annual growth rate (CAGR) of 47% from 2016 to 2021, reaching 49 exabytes per month by 2021. During this period the number of mobile-connected devices, including machine to machine (M2M) modules is expected to reach 11.6 billion, which is 1.5 mobile devices per capita [1].

To cope with increasing demand, mobile networks have constantly evolved by adding new technologies and features (enhanced multiple-input multiple-output (MIMO) technologies [10–13] , carrier aggregation [14,15], dual connectivity, device-to-device (D2D) communications [16–18], license assisted access (LAA) [19–21]), introducing new types of base stations (BSs) (pico BSs, femto access points (APs), enabling service off-loading to wireless LANs (WiFi) [22]), and adding more frequency bands (millimeter waves [23, 24]). A new generation of cellular mobile communications standards has been introduced approximately every decade. Each new generation has brought major changes to mobile communication systems. In between two generations system designers and standardizing bodies constantly add new technical solutions to meet increasing demand. In keeping with this trend, currently the fifth generation cellular networks (5G) systems are in the development stage. These communication systems are expected to be commercially deployed by 2020 [25, 26].

1.1 5G New Radio: The Air Interface for Next Generation of Mobile Communications

5G networks are expected to result in dramatic improvements in the capabilities of the current International Mobile Telecommunications-Advanced (IMT-A) networks (Figure 1.2) [2]. These include providing peak data rates of 20 Gbps, user experienced data rates of 100 Mbps, area traffic capacity of 10 Mb/s/m^2, connec-

tion density of 1 million devices/km^2, user mobility of 500 km/h, and end-to-end network latency of 1 ms. Further, 5G networks are expected to result in a 3-fold increase in spectral efficiency and a 100-fold increase in energy efficiency compared to current IMT-A networks. To meet these demands the new air interface of 5G, commonly known as 5G new radio (NR), is currently being developed [27].

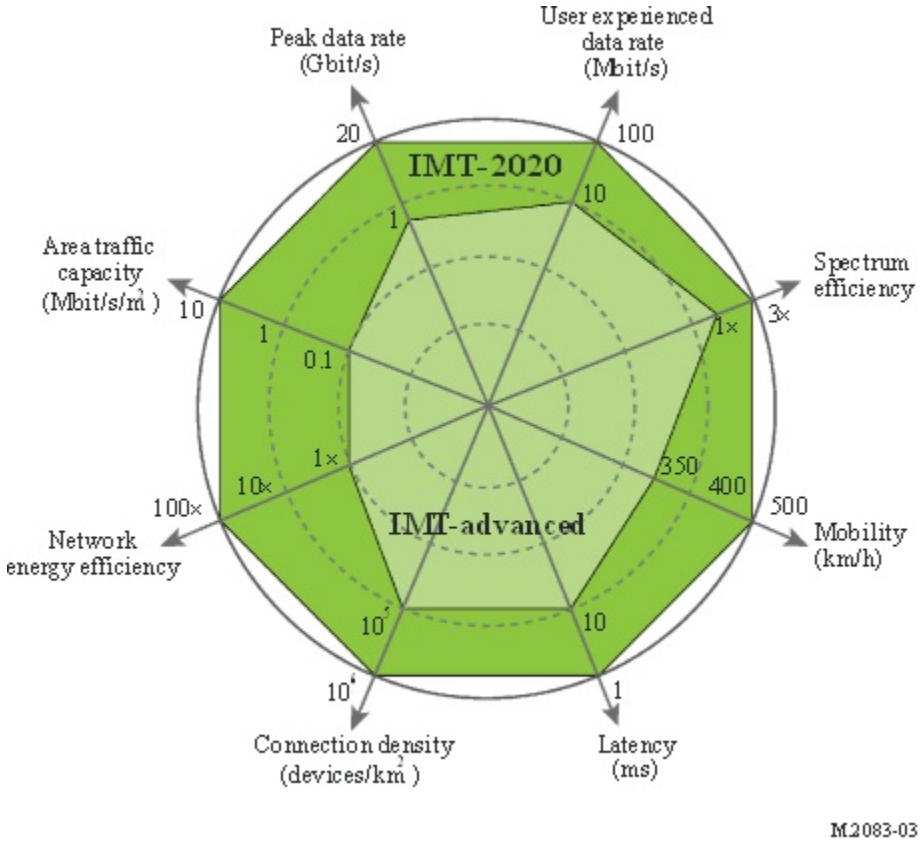

Figure 1.2: ITU recommendation ITU-R M.2083-0 [2]

The challenging (and also conflicting) IMT-2020 performance requirements will be met by three implementation varieties of 5G cellular networks, known as usage scenarios [2] (see Figure 1.3), as follows:

1. Enhanced mobile broadband (eMBB): This usage case aims to serve users that demand very high data rates [2, 28]. These include high-speed access in user-dense areas (offices, stadiums, urban centers), broadband connectivity everywhere (suburban, rural, and road networks), and high-speed mobility (trains, planes, etc.) to meet the people's demand for an increasingly digital lifestyle [28, 29].

2. Massive machine-type communication (mMTC): The aim of the mMTC is to meet demands of a developed digital society including high deployment density scenarios such as smart cities and smart agriculture [28]. These scenarios are typically characterized by a very large number of connected devices transmitting relatively low volumes of non-delay-sensitive data [2]. mMTC devices need to be low cost and have very long battery life [2].

3. Ultra-reliable, low-latency communication (UR-LLC): Meeting the industrial and health-care expectations by focusing on latency-sensitive services, such as automated driving, remote management, wireless control of manufacturing or production processes, remote medical surgery, and distribution automation in a smart grid, are among the aims or UR-LLC [2,28]. This usage case has strict requirements for throughput, latency, and connectivity [2].

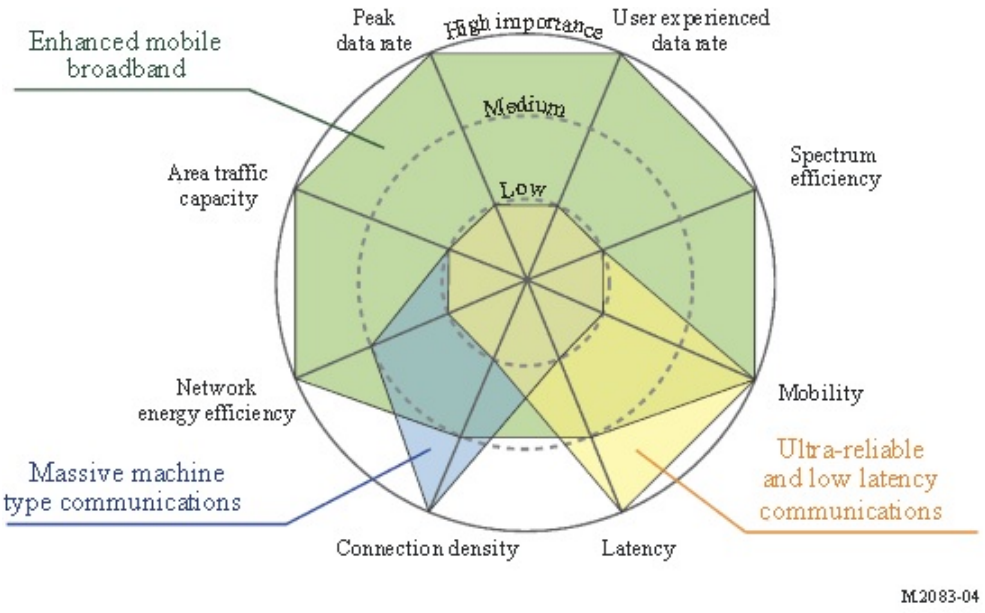

Figure 1.3: 5G usage scenarios and their target capabilities [2]

Phased Deployment of 5G NR

To enable early launch of 5G services and to make the development process manageable, there is an industry-wide plan to introduce 5G networks in two phases, non-standalone 5G (NSA 5G) and standalone 5G (SA 5G). NSA 5G specifications

are expected be finalized in mid-2018, as part of 3rd generation partnership project (3GPP) Release 15 (see Figure 1.4) and commercially deployed by early 2019 [3]. These networks will utilize the existing Long Term Evolution (LTE) radio and core network as an anchor for mobility management and coverage, while adding new 5G carriers. The main focus is on enabling eMBB services, while some of the features of mMTC and UR-LLC are also expected to be realized in NSA 5G [29]. In parallel to the development of NSA 5G, 3GPP and its organizational partners are currently working towards the larger vision of 5G NR; SA 5G NR, supporting all three usage cases eMBB, mMTC, and UR-LLC. These networks are expected to be commercially deployed in 2020. Similar to three previous generations of cellular mobile communication systems, second generation cellular networks (2G), third generation cellular networks (3G), and fourth generation cellular networks (4G) [30], the first release and commercial deployment will be just the starting point. Eventually more features will be added to 5G systems to meet the future demands [29].

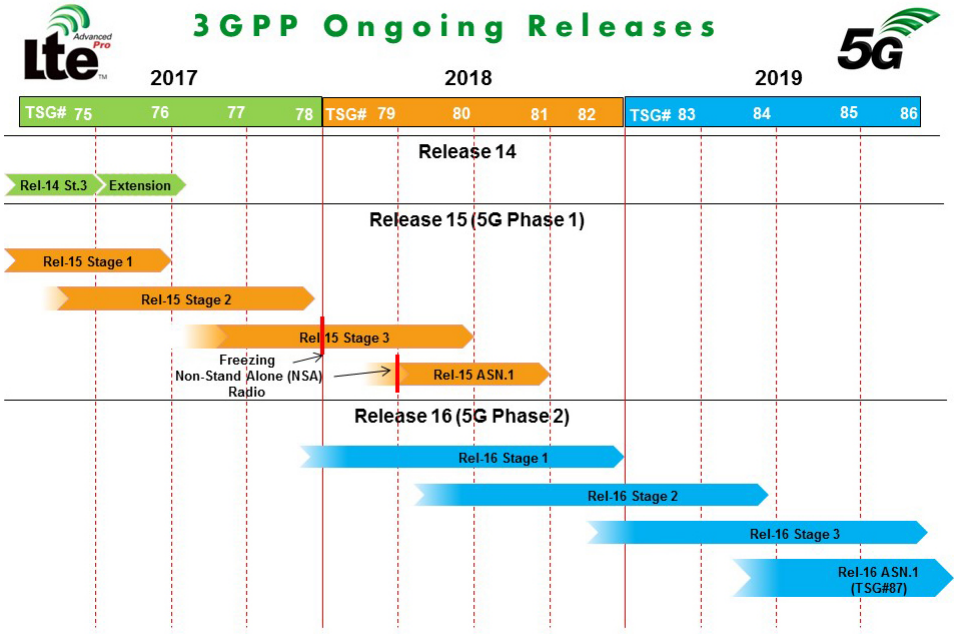

Figure 1.4: 3GPP ongoing releases and the development of 5G NR [3]

1.2 Heterogeneous Cellular Networks

The Heterogeneous network (HetNet) concept involves overlaying low-cost low-power nodes, for example, pico BSs, femto APs, relay stations, remote radio heads

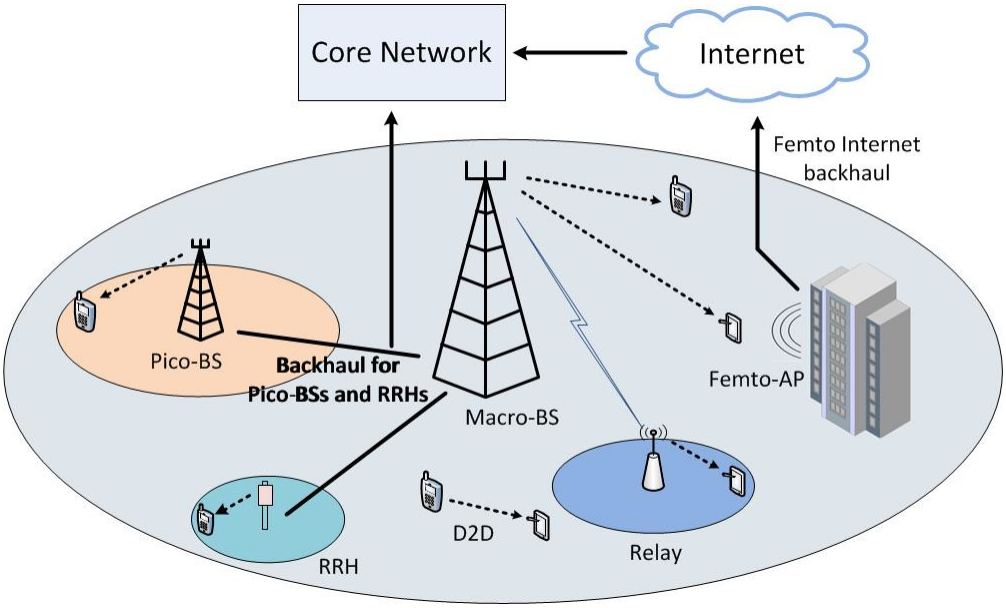

Figure 1.5: Heterogeneous cellular network architecture

(RRHs), on coverage holes or capacity-demanding hotspots within a conventional macro-cellular network [31–35]. Deploying such small nodes aims at off-loading the macrocells, boosting the local capacity, extending the indoor coverage, and improving the cell-edge user performance. Further, these nodes can be deployed with relatively low network overhead, and potentially reduce network power consumption. HetNets architecture is expected to play a key role in the next generation cellular standards such as 5G NR and beyond. With network densification destined to cope with ever increasing demand, future networks will be more heterogeneous and will be more densely deployed than today's networks.

A typical HetNet is shown in Figure 1.5. Macro BSs which are typically deployed by the operator in a planned layout provide the umbrella coverage. They transmit at high power level compared to other types of nodes (typically between 20 W to 40 W). Dedicated optical fiber connections are used to backhaul macro BSs traffic. Pico BSs are also deployed by the operators. However, they are deployed on coverage holes or capacity demanding hotspots, and thus follow a relatively random placement. While their backhaul implementation is similar to that of macro BSs, they transmit at lower power levels, in the order of 250 mW to 2 W. Femto AP or home BSs are typically deployed by users and are intended to boost indoor coverage. While the transmit power is less than 100 mW, they are connected to the core network via users' Internet connections, such as digital subscriber line (DSL) or TV cable

modem. Access to a femto AP can be either restricted to users within a closed subscriber group (CSG), unrestricted making service available to all devices coming within its coverage or a combination of both, giving priority to CSG. These access schemes are called open, closed and hybrid access, respectively [36]. A relay extends the coverage of a BS by forwarding signals it receives wirelessly from the BS to the users, and vice versa [37]. They are classified as in-band and out-of-band depending on the type of backhaul connection. An in-band relay uses the same frequency band as the access link for its backhaul, while an out-of-band relay uses a different set of frequencies [38]. A RRH, also known as a fiber repeater, is connected to a BS by an optical fiber and repeats signals it receives from the BS. It is an attractive solution to provide wireless connectivity to users in dense urban areas [39]. A summary of different types of nodes in HetNets is given in the Table 1.1.

Table 1.1: Different nodes in heterogeneous cellular networks

Node type	Transmit power	Features
Macro	5 W - 40 W	Operator deployed, open access, dedicated backhaul (often by optical fiber), provides umbrella coverage
Pico	250 mW - 2 W	Features are similar to those of macro BSs
Femto	$\leq$ 100 mW	User deployed, can be closed access open access or hybrid type, backhaul is enabled by user's digital subscriber line or TV cable modem
Relay	250 mW - 2 W	Operator deployed, RF wireless backhaul (usually in-band)

1.2.1 Spatial Modeling of Nodes and Users

A major change in the HetNet setup compared to traditional single-tier cellular networks is the placement of BSs and their coverage or association regions [34]. Considering the fact that macro BSs are approximately evenly spaced, usually they have been modeled as lying on a hexagonal grid. The association regions are then simply the corresponding hexagons. However, smaller base stations, are not regularly spaced nor their association regions homogeneous. These nodes are generally scattered or clustered within the existing macrocell network due to the demand based deployment, and form their own embedded smaller association regions. Con-

sequently, the traditional hexagonal grid-based model is not suitable for modeling the spatial distribution of nodes and users in a HetNet. One other major drawback of grid-based model is its mathematical intractability. Therefore, researchers have to rely on complex system level simulations to evaluate the performance of various configurations. However, as networks become more complex with the addition of irregularly deployed low-power nodes (pico BSs, femto APs etc.), simulations become even more complex and time consuming. Thus, stochastic geometry characterization of the spatial distribution of nodes and users has been developed [35, 40–43]. Stochastic geometry models permit deriving conclusions about entire classes of cellular networks, instead of restricting to just one specific configuration of the network [42, 43]. In these models, the nodes and users are abstracted by a suitable point process, the Poisson point process (PPP) for example. Stochastic geometry modeling of wireless networks is reviewed in Section 2.2.

1.2.2 Cell Association

In a traditional single-tier cellular network, cell association is based on the downlink signal strength, which provides the best signal-to-interference-plus-noise ratio (SINR). When all cells are fully loaded, i.e., transmitting and receiving signals in all their time-frequency resource blocks at all times, such a strategy maximizes total throughput [34]. However, this strategy is not appropriate for HetNets. This is mainly because, in a HetNet setup which consists of multiple classes of BSs with different transmit powers, antenna gains and heights, and receiver capabilities, downlink signal strength based cell association will result in lightly loaded small BSs and congested macro BSs. Therefore, even when the strongest signal is received from a macro BS, which is already heavily loaded, a user can achieve a better data rate by connecting to a nearby small BS (off-loading) and utilizing more radio resources. Such user off-loading helps to reduce the load on macro BSs, thus the remaining macro users can enjoy better data rates. The process of off-loading users to small BSs can be achieved by adding carefully determined extra values (bias values) to the received signal strengths from small BSs and employing the conventional maximum signal strength association by using the modified signal strengths from different BSs.

1.3 Uplink Transmit Power Control in Cellular Networks

Uplink transmit power control (TPC) plays a major role in modern cellular networks, and is employed to maintain the strength of received signals from mobile stations (MSs) at appropriate levels to successfully demodulate signals. Another key aspect of power control is to minimize the interference to other transmissions in the same or adjacent cells. Uplink TPC also helps to prolong the battery life of small hand held devices.

In LTE and Long Term Evolution-Advanced (LTE-A), uplink TPC is usually a combination of two mechanisms, open-loop and closed-loop power control [44]. In open-loop power control, the transmit power of an MS depends on the downlink path loss and shadow fading estimates, maximum transmit power level and the target received power. In the closed-loop power control mechanism, the network adjusts the device transmit power by means of power-control commands transmitted on the downlink, accounting for various link level and network level parameters.

1.4 Motivation and Objectives

HetNet has shown tremendous potential in meeting traffic demand, massive numbers of connections, and high power and area spectral efficiencies envisioned in future generation cellular networks. However, the demand based deployment of much of the small, low power nodes in the existing macro-cellular infrastructure results in an extremely complicated muti-tier cellular network. This makes mathematical modeling, system level analysis and design of HetNets very challenging. To make this problem tractable, stochastic geometry and especially the point process theory can be used. Some of the commonly used stochastic geometry models are briefly discussed in 2.2. Although, initial results have shown stochastic geometry modeling as a very effective tool, existing models have many limitations in capturing practical network configurations and conditions. Further, since HetNet is a very complicated network architecture, it naturally involves a vast number of possible network configurations. Only a handful of these configurations have been investigated, leaving many gaps in the literature. This thesis identifies such limitations in the analytical tools and develops a comprehensive framework for modeling and analysis of HetNet. Further, potential network configurations which have not been investigated in the

current literature are identified and investigated in detail. The main objectives of this research are listed below.

1. Develop analytical tools to comprehensively capture practical conditions of HetNets, including the spatial distribution of nodes and different environmental conditions (path loss, shadowing due to large objects, multipath fading, etc.).

2. Develop new uplink TPC schemes for HetNet and investigate their performance using stochastic geometry based analytical tools.

3. Investigate the effect of different TPC parameters and network densification on the performance of power control schemes.

4. Develop new simple cell association policies and investigate their performance. Investigate the impact of various network configurations and practical limitations on overall network performance.

5. Investigate the impact of limited candidate size for cell association on the gains of user off-loading.

1.5 Significance of the Thesis

Future generation wireless communication systems, for example 5G cellular networks, are expected to be very energy efficient compared to the existing 4G cellular networks [2]. In particular two out of three usage cases of 5G networks, i.e., eMBB and mMTC, are expect to be very energy efficient [2]. As the energy efficiency of a network can be improved by reducing radio frequency (RF) transmit power [2], the developed power control schemes will help to achieve efficiencies envisioned in future generation cellular networks. Further, the investigation of the impact of various network parameters will help provide useful guidelines for the selection of power control parameters. Also the developed uplink TPC schemes will help prolong the battery life of small hand-held mobile devices. As smart cell association is a key aspect for harnessing the benefits of HetNet, the developed simple cell association policies will help to provide the best user-perceived data rates with limited network overhead. The study of the size of the search domain for candidate BS to serve a given MS will provide useful guidelines on complexity and performance trade-offs of

cell association policies. Moreover, the developed stochastic geometry based mathematical tools will help to speed up the candidate technology selection process for 5G and beyond cellular networks by reducing the time and resources required to perform complex system-level simulations.

1.6 Thesis Outline and Contributions

This thesis focuses on modeling and analyzing HetNet, investigating new TPC schemes and simple cell association policies. The thesis outline is as follows. The theoretical background on wireless channels, different stochastic geometry models used to model wireless networks, and other related topics are covered in Chapter 2. The main contributions of this research are presented in Chapter 3 and 4. Chapter 5 highlights the the conclusions derived from this research study and gives future research directions.

1.6.1 Novel Contributions of the Thesis

The major contributions of this thesis are as follows:

- Chapter 3 introduces three TPC schemes for cellular uplink. They include partial compensation of: (1) path loss only; (2) the aggregate effect of path loss and shadowing; and (3) path loss and complete inversion of shadowing. An analytical framework for the coverage probability evaluation considering path loss, shadowing due to large objects and multipath fading is developed. This analytical framework considers orthogonal channel assignment to match the network configurations of modern cellular networks, such as LTE and 5G NR, which are based on orthogonal frequency division multiple access (OFDMA) or discrete Fourier transform-spread OFDMA (DFT-S-OFDMA). Using the developed framework, several observations are made on the suitable TPC strategies and parameters under various networks conditions. First, at low SINRs, i.e. for cell-edge users or users experiencing severe shadowing, compensating for the aggregate effects of path loss and shadowing (Scheme 2) provides better coverage compared to the other two schemes. However, at high SINRs, i.e., for cell-center users, inverting only path loss (Scheme 1) provides the best coverage. Second, we show that the network densification (adding more BSs) has little effect on the coverage under power control scheme

1 and 3 at all shadowing levels, and for Scheme 2 a similar trend holds under light shadowing conditions. Third, we observe that the level to which path loss and shadowing should be compensated for in a network, depends on the operating SINR of the network. Analytical expressions are also derived for the probability density function (PDF) and cumulative distribution function (CDF) of the transmit power under three TPC schemes. These results help to understand battery power utilization by each scheme.

- Chapter 4 proposes and investigates simple cell association schemes for single-tier and two-tier networks. In particular, for a single-tier network a given user is proposed to be associated with the highest instantaneous SINR BS from among BSs, providing average received power above a predetermined threshold value. Two methods are given to determine the threshold received power. This approach is extended to a two-tier HetNet, assuming two different conditions for the availability of SINR information. We show that the proposed policy enables flexible user off-loading in two-tier networks. A stochastic geometry-based mathematical framework is developed to investigate the coverage probability and achievable data rates by an MS in coverage. Using the developed analytical framework and extensive simulation results, several observations are made. First, it is observed that monitoring the received signal strength indicator (RSSI) from few candidate BSs is sufficient for cellular networks. The candidate BSs can be selected based on the average RSSI from BSs that provide meaningful signal quality. Second, user off-loading to small cells through association bias will result in lower average data rates for small cell users due to their lower SINR. Hence, the average user data rate in a two-tier HetNet will also be reduced. However, the network capacity will increase, since many more users will be served by small cells in addition to those already served by macrocells at higher average data rates per user.

$\sim$

Chapter 2

Background

Analysis of modern cellular communication systems requires proper modeling of mobile radio channel impediments, the spatial distribution of mobile stations (MSs) and the various types of nodes (base stations (BSs), access points (APs), relays). This chapter reviews these key wireless communications concepts that are employed in this thesis. In particular, various channel impediments and their mathematical modeling are discussed in Section 2.1. Various stochastic geometry models and the special properties of the Poisson point process (PPP) are discussed in Section 2.2 and Section 2.3.

2.1 Mobile Radio Channel

The mobile radio channel poses severe challenges for reliable high-speed communication. It is susceptible to co-channel interference (CCI), noise and channel impediments. Three mechanisms contribute to the channel impediments: reflection, diffraction and scattering. As a result, the received signal strength exhibits random changes over time. In the analysis of radio wave propagation, these impediments are characterized by three nearly independent phenomena: path loss with distance, shadowing and multipath fading. Figure 2.1 shows the channel power gain in dB versus log-distance for these three phenomena. This section briefly discusses co-channel interference and the three channel impediments.

Co-channel Interference

Cellular systems rely heavily upon frequency reuse, where geographically separated cells simultaneously use the same carrier frequencies and/or time slots (time-frequency resource blocks). Due to frequency reuse, communication between a BS

and an MS in one cell is interfered with by one or many BS-MS pairs belonging to adjacent cells. This is referred to as CCI, and is the primary factor that limits capacity of modern cellular systems [30].

Multipath Fading

In cellular communication systems, MSs and small BSs (pico-BSs or femto-APs, for example) are typically surrounded by local scatterers due to their low-elevation antennas. Except in rural or open environments where line-of-sight (LoS) conditions exist, a non-line-of-sight (NLoS) condition typically exists between the BSs and MSs. Consequently, radio waves must propagate between the BSs and MSs via reflections, diffraction and scattering. This generates multiple replicas of the transmitted signal that arrive at the MS (or BS) receiver antenna(s) from different directions, with each having a distinct polarization, amplitude, phase and delay. In wireless communications, this phenomenon is referred to as multipath propagation. These multiple plane waves combine vectorially at each MS (or BS) and produce a composite received signal resulting in rapid fluctuations in the received signal amplitude and phase, commonly referred to as multipath fading. If all the frequency components in the received signal experience the same time-variant amplitude gains, the fading is known as frequency flat; otherwise the fading is called frequency selective. For communication system designers, frequency selective fading poses numerous challenges, while frequency flat fading is easier to deal with. Wideband communication systems such as Long Term Evolution (LTE) use orthogonal frequency division multiplexing (OFDM) to obtain multiple frequency flat subchannels (sub-carriers). 5G new radio (NR) is also expected to use OFDM [27, 45]. In frequency flat fading, channel gain due to multipath fading can be represented by a single complex coefficient $b = |b|e^{j\phi}$, where |b| is the amplitude (envelope) gain, and ϕ is the phase shift. In NLoS fading, ϕ is usually uniformly distributed in $\{0, 2\pi\}$. Various distributions are used to model the amplitude gains based on the wireless communications environment. In this thesis we consider the Rayleigh distribution given by [30]

$$f_{|b|}(t) = \frac{2t}{\mu}\exp\left(\frac{-t^2}{\mu}\right),\ t \geq 0, \tag{2.1}$$

where the average fading envelope power $\mathcal{E}[|b|^2] = \mu$. The corresponding squared envelope $g = |b|^2$ is exponentially distributed and its probability density function

(PDF) is given by [30]

$$f_g(t) = \frac{1}{\mu}\exp\left(\frac{-t}{\mu}\right),\ t \geq 0. \tag{2.2}$$

A more general model is Nakagami$-m$ fading, in which the PDF of the channel amplitude is given by

$$f_{|b|}(t) = 2\left(\frac{m}{\mu}\right)^m \frac{t^{2m-1}}{\Gamma(m)}\exp\left(-\frac{mt^2}{\mu}\right),\ t \geq 0,\ m \geq \frac{1}{2}, \tag{2.3}$$

where $\Gamma(m)$ is the gamma function. With Nakagami-m fading, the squared envelope has the Gamma distribution given by

$$f_g(t) = \left(\frac{m}{\mu}\right)^m \frac{t^{m-1}}{\Gamma(m)}\exp\left(-\frac{mt}{\mu}\right),\ t \geq 0,\ m \geq \frac{1}{2}. \tag{2.4}$$

Shadowing

Signals transmitted over a wireless channel also experience random variations due to blockage from large objects in their paths, such as buildings and trees. Shadowing is also caused by changes in the reflecting surfaces and scattering objects. Since the spatial distribution, size and dielectric properties of the blocking objects causing these random blockages are generally unknown, statistical models are used to characterize their attenuation [4, 30]. The most common model is log-normal shadowing [4,30]. Empirical results have confirmed that the lognormal distribution is an accurate model, which captures the signal strength variations in both outdoor and indoor environments. The lognormal distribution of shadow (large-scale) fading of the local mean received envelope power is given by [30]

$$f_\mu(t) = \frac{1}{t\sigma_{\text{dB}}\delta\sqrt{2\pi}}\exp\left(-\frac{\left(10\log_{10}(t) - \varsigma_{(\text{dBm})}\right)^2}{2\sigma_{\text{dB}}^2}\right), \tag{2.5}$$

where σ_{dB} is the shadowing standard deviation in decibel units, and $\delta = \ln(10)/10$. $\varsigma_{(\text{dBm})} = 10\ \mathcal{E}\left[\log_{10}(\mu)\right]$ is the mean value (the area mean determined by the path loss). For macro cellular networks σ_{dB} is typically in the range of 5 dB to 12 dB, with 8 dB being a commonly used value [4,30]. Further, studies has shown that σ_{dB} is nearly independent of transmitter to receiver distance [30].

Composite Shadowing-Fading Distributions

When both shadowing and multipath fading affect a communication system, it is desirable to obtain the composite distribution of the envelope of the complex channel

gain due to these two fading mechanisms. To this end, two different approaches have been proposed in the literature.

1. Express the probability density function of the squared envelope of the channel gain as conditional, conditioned on the channel envelope power due to shadowing, μ, and then integrate over the PDF of μ to obtain the distribution of the composite fading. When the envelope of the channel gain due to small-scale fading is modeled by Rayleigh distribution, i.e., (2.2) and envelope power due to shadowing (large-scale fading) by (2.5), the composite shadow and multipath fading distribution is given by [30]

$$f_h(t) = \int_0^\infty \frac{1}{\mu} \exp\left(-\frac{t}{\mu}\right) \frac{1}{\mu \sigma_{\text{dB}} \delta \sqrt{2\pi}} \exp\left(-\frac{\left(10\log_{10}(\mu) - \varsigma_{(\text{dBm})}\right)^2}{2\sigma_{\text{dB}}^2}\right) d\mu, \; t \geq 0. \tag{2.6}$$

   Similarly, when the envelope of the channel gain due to fading is modeled by Nakagami-m distribution, i.e., (2.4), and envelope power due to shadowing by (2.5), the composite shadowing-fading distribution is given by [30]

$$f_h(t) = \int_0^\infty \left(\frac{m}{\mu}\right)^m \frac{t^{m-1}}{\Gamma(m)} \exp\left(-\frac{mt}{\mu}\right) \times \frac{1}{\sqrt{2\pi}\delta\sigma_{\text{dB}}\mu} \exp\left(-\frac{\left(10\log_{10}(\mu) - \varsigma_{(\text{dBm})}\right)^2}{2\sigma_{\text{dB}}^2}\right) d\mu, \; t \geq 0, m \geq \frac{1}{2}. \tag{2.7}$$

   Unfortunately, both distributions (2.6) and (2.7) cannot be expressed in closed form, but can be efficiently evaluated using Gauss-Hermite quadrature integrations [30, 46].

2. The second approach expresses composite squared envelope of the channel gain due to shadowing and multipath fading as the product of the squared envelope due to multipath fading and shadow fading, g and μ, i.e., $h = g \times \mu$ [30, 47], and assume that g and μ are statistically independent.

In Chapter 3, (2.6) is used to characterize the effect of composite shadowing-fading on cellular uplink tansmissions.

Path Loss

Path loss reduces the received average power of a radio wave as it propagates through space. In addition to the distance between the transmitter and receiver, it also

depends on frequency, antenna heights and topography [4, 30]. Path loss is the largest and most variable quantity in a communication link budget [30]. A variety of theoretical and empirical path loss models exist in the literature. In this thesis, a power-law path loss model is used. In this model, signal power attenuates at the rate of $||x - y||^{-\alpha}$, where x and y are the location of the transmitter and receiver respectively. Parameter alpha is the path loss exponent. The value of α can be empirically evaluated, and is typically in the range of 1.6 to 6.5 [4].

Composite Effect of Path Loss, Shadowing, and Multipath Fading

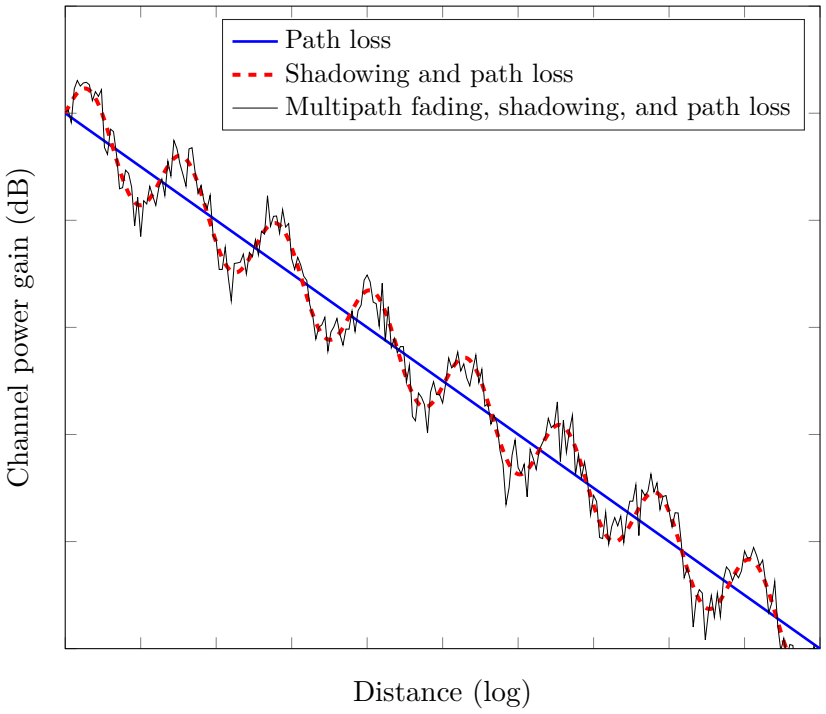

Figure 2.1: Path loss, shadowing and multipath versus distance [4]

Figure 2.1 shows the variation of channel power gain (and hence the received signal power) in dB versus log-distance due to the aggregate effect of path loss, shadowing and multipath fading [4]. In a radio channel, received signal strength variations due to path loss occur over large distances, so that variations due to shadow fading are averaged out [30]. Random shadowing occurs over distances proportional to the lengths of the obstructing objects, and are obtained by averaging out variations due to multipath fading over distances of about 20 wavelengths [30]. Since both variations due to path loss and shadowing take place over relatively

larger distances, they are commonly referred to as large scale propagation effects [4]. Variations due to multipath fading occur over distances on the order of signal wavelength [4]. Therefore, these variations are commonly referred to as small-scale propagation effects.

2.2 Stochastic Geometry for Analysis and Design of Cellular Networks

The demand-based deployment of many low-cost low-power BSs, for example, pico BSs and femto APs, makes a network arrangement more irregular than that of the traditional homogeneous cellular networks [48]. Furthermore, certain types of cells, e.g. femtocells, may be deployed by their users, thus falling under the random deployment category. All of these deployments result in a complex multi-tier network, in which each tier represents a different kind of BSs (macro and pico BSs, femto AP, etc.). It has been shown that the spatial distribution of BSs of such an irregular and random network can be adequately modeled by points of stochastic random processes [33,34,40,41,49,50]. The random spatial modeling of the locations of BSs is surprisingly tractable analytically and captures some of the main Heterogeneous network (HetNet) performance trends [33]. Some of the most commonly-used point processes to model locations of nodes and MSs are discussed below.

1. **Poisson point process (PPP)**: PPP with intensity measure $\lambda(x)$, is a point process $\Phi = \{x_1, x_2, ...\} \in \mathbb{R}^d$ such that [42,51,52]

   - The number of points in any compact set A denoted by $\Phi(A)$ is Poisson-distributed with mean $\mu(A) = \mathcal{E}[\Phi(A)] = \int_A \lambda(x)dx$, i.e.,

   $$\Pr\left(\Phi(A) = k\right) = \frac{\mu(A)^k}{k!} e^{-\mu(A)},\ k = 0, 1, 2, 3, ... \text{ and,} \tag{2.8}$$

   - If $A_1, A_2, ..., A_m$ are disjoint bounded sets, then $\Phi(A_1), \Phi(A_2), ..., \Phi(A_m)$ are independent random variables.

   When $\lambda(x) = \lambda$, a constant, the resultant point process is a homogeneous PPP. Figure 2.2 shows a cellular network consisting of a single class of BSs, macro BS for example, and MSs characterized by two independent homogeneous PPPs. Homogeneous PPP has been extensively used in the cellular network research to characterize the spatial distribution of nodes and MSs [40, 41, 53].

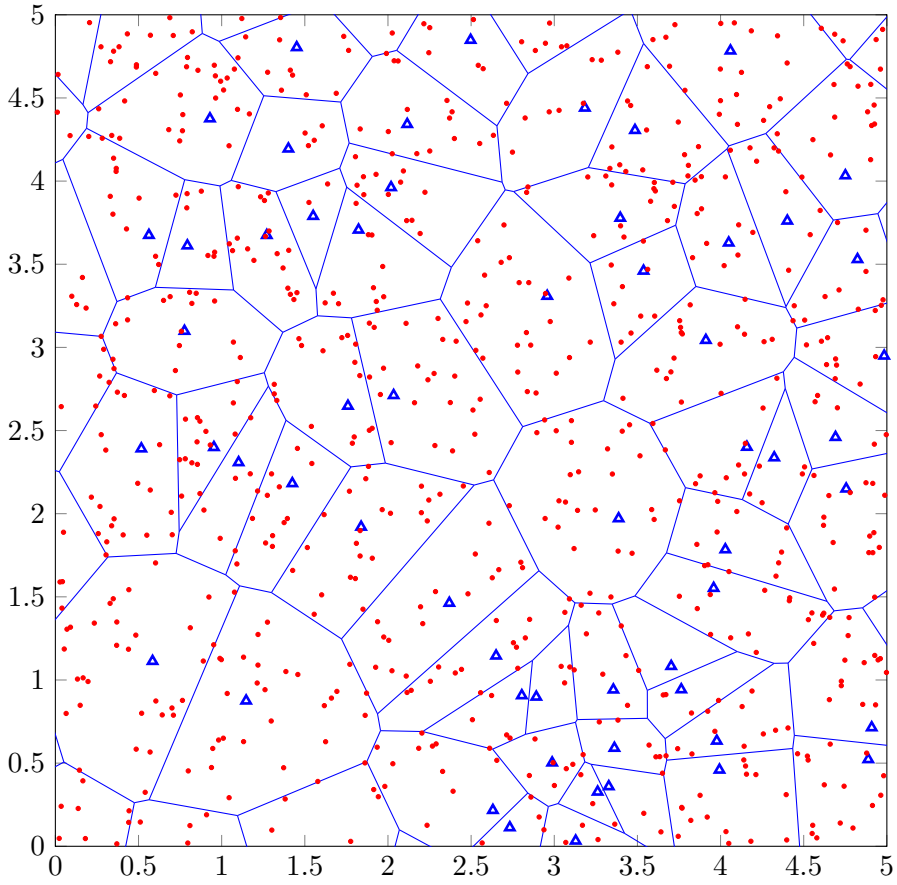

Figure 2.2: Poisson distributed BSs and MSs in a 5 km $\times$ 5 km cellular network, with each mobile associated with the nearest BS. The cell boundaries are shown and form a Voronoi tessellation. Legend: blue triangles - BSs, red squares - MSs. Poisson-Voronoi cell boundaries are denoted by blue lines.

In [40] the downlink coverage probability and data rate of a cellular network consisting of a single class of BSs are investigated. Homogeneous PPP is used to characterize the spatial distribution of BSs and MSs. In [41] independent PPPs with different intensities are used to characterize the spatial distribution of various types of BSs in a multi-tier network, and to investigate the downlink coverage probability and achievable data rates. In [53] the spatial distribution of MS is characterized by a homogeneous PPP, and uplink coverage probability and the mean data rate of a single-tier cellular network are investigated. The PPP model has been shown to provide pessimistic bounds on the performance metrics (e.g., the coverage probability and the mean rate) that are as tight as the optimistic bounds provided by the conventional grid-based model for actual cellular networks [40, 41]. Non-homogeneous PPP has also been used

to model cellular networks in several studies [54, 55]. Circularly symmetric power-law, polynomial and Gaussian intensity functions have been considered in most studies. PPP can be used to model communication networks, in which both the number of devices (BSs, MSs) and their locations are random, but the densities are known.

2. **Binomial point process (BPP):** A point process over $W \in \mathbb{R}^d$ is a binomial point process $\Phi_W^n = \{x_1, x_2, ..., x_n\}$, if the number of points in any set $A \subset W$ is a binomial random variable (RV) with parameters n and $p = |A|/|W|$, i.e.,

$$\Pr\left(\Phi_W^n(A) = k\right) = \binom{n}{k} p^k (1-p)^{n-k}, k = 0, 1, 2, ..., n, \tag{2.9}$$

where $|\cdot|$ is the Lebesgue measure in d-dimensional Euclidean space.

When the total number of nodes is known and they are independently and uniformly distributed in a finite area (volume in $\mathbb{R}^2$ and distance in $\mathbb{R}^1$), their spatial distribution can be modeled by a BPP [56,57]. In [57], the BPP is used to characterize the spatial distribution of nodes in an ad-hoc network.

3. **Cluster process:** A cluster process is generated by using a parent point process and daughter point processes, one per parent, and translating each daughter process to the position of their parent [42]. The union of all the points of the daughter processes represents the cluster process. Consider a parent point process denoted by $\Phi_p = \{x_1, x_2, ...x_n\}$ and number of parent points by $n \in \mathbb{N} \cup \{\infty\}$. Also let $\Phi_i,\ i \in \mathbb{N}$, be the untranslated daughter process of x_i. The cluster process is the union of the translated daughter processes, i.e.,

$$\Phi = \bigcup_{i \in [n]} \Phi_i + x_i. \tag{2.10}$$

When both parent process and the daughter processes are PPPs, the resulting cluster process is a Poisson cluster process (PCP). In practical cellular networks, operators deploy more BSs in highly populated areas, while few in sparsely populated suburban or rural areas. PCP is useful for modeling these networks. In [58] and [59], cluster processes are used to model interferer distributions in large cellular networks and ad-hoc networks, respectively.

4. **Hard-core process:** Hard-core processes are point processes with a given minimum distance between two points [42]. A hard core process can be gen-

erated by first generating a point process that has no restriction on the minimum distance and then deleting all the points that violate this condition. There are two commonly used hard-core processes, Matérn hard-core process of type I and II [42]. A Matérn hard-core process of type I can be generated by starting with a homogeneous PPP of intensity λ_b, and then identifying all points that have a neighbor within minimum distance r_{m} and deleting all identified points. The intensity of the resultant type I process is given by $\lambda = \lambda_b \exp\left(-\lambda_b c_d r_m^d\right)$, where $c_d = \pi^{d/2}/\Gamma(d/2+1)$ [42] and $\Gamma(\cdot)$ is the gamma function. A Matérn hard-core type II process can be generated as follows. Start by generating a PPP of intensity λ_b. Add a mark $m(x)$, an independent and uniformly-distributed random variable on $[0,1]$ to each point x. Flag all points that have a neighbour within distance r_m that has a smaller mark. Then remove all flagged points. The resultant intensity is given by $\lambda = \left(1-\exp(-\lambda_b c_d r_m^d)\right)/c_d r_m^d$ [42].

5. **Poisson hole process (PHP)**: PHP is generated by carving out holes in a PPP. Let Φ_1 and Φ_2 be two PPPs with intensities λ_1 and λ_2 ($\lambda_2 > \lambda_1$) respectively. For each $x \in \Phi_1$, remove all the points in $\Phi_2 \cap b(x,R)$, where $b(x,R)$ is a ball centered at point x with readius R. The remaining points of Φ_2 form a PHP with intensity $\lambda = \lambda_2 \exp\left(-\pi\lambda_1 R^2\right)$ [42,60]. PHP is a very suitable point process to model the placement of small cells around macro cell edges [61], device-to-device (D2D) communication systems where cell edge users are allowed to directly communicate with each other without going through the cellular system or with its limited involvement [62], and cognitive radio networks where underutilized licensed sprectrum is opportunistically accessed by unlicensed users [63].

2.3 Selected Properties of the Poisson Point Process

PPP has number of special properties, which often make the calculation of associated probabilities mathematically tractable. Some of these properties used in this thesis are described below. Further details on these properties of PPP and additional useful properties can be found in [42, 51, 52, 64].

1. Superposition Property

   Let $\Phi_1, \Phi_2, ...$ be a countable collection of independent PPPs on space S and

let the mean measure of Φ_i is given by μ_i, $\forall i$. Then the superposition of PPPs,

$$\Phi = \bigcup_{i=1}^{\infty} \Phi_i, \tag{2.11}$$

is a PPP with mean measure [52] $\mu = \sum_{i=1}^{\infty} \mu_i$. Consequently, when $\Phi_1, \Phi_2, ...$ are homogeneous PPPs with intensities $\lambda_1, \lambda_2, ...$, $\Phi = \bigcup_{i=1}^{\infty} \Phi_i$ is a homogeneous PPP with intensity $\lambda = \sum_{i=1}^{\infty} \lambda_i$.

2. Restriction Theorem

   Let Φ be a PPP with mean measure μ on space S, and let S_1 be a measurable subset of S. The random countable set $\Phi_1 = \Phi \cap S_1$ is a PPP on S with mean measure $\mu_1(A) = \mu(A \cap S_1)$ or a PPP on S_1 whose mean measure is the restriction of μ to S_1.

3. Colouring Theorem and Independent Thinning

   Let Φ be a PPP on space S with mean measure μ. Let the points of Φ are coloured randomly with k colours such that the probability that a point receives the ith colour is P_i and the colours of different points are independent of one another and of the position of the point. The set of points that receive ith colour, Φ_i forms an independent PPP with mean measure $\mu_i = p_i\mu$.

   Independent thinning a PPP can be considered as a special case of $k = 2$. One colour represents not deleted and the other represents points deleted in the thinning process. Points are deleted with probability $1 - p$, where $0 \leq p \leq 1$, from a PPP of intensity λ. Points remaining and deleted in the thinning process form two independent PPPs, with intensities $p\lambda$ and $(1-p)\lambda$, respectively. Superposition of these two point processes yields the original point process.

4. The Probability Generating Functional and Campbell's Theorem

   The probability generating functional (PGFL) of a point process Φ on $\mathbb{R}^d$ is defined as

$$G(\nu) = \mathcal{E}\left[\prod_{x \in \Phi} \nu(x)\right], \tag{2.12}$$

   for all non-negative functions $v : \mathbb{R}^d \to [0, 1]$. PGFL of PPP is given by the Campbell's theorem. The moment-generating function (or the Laplace transform) of sums over PPP can be obtained using the Campbell's theorem or the PGFL of PPP. The theorem is formally stated below [42, 52].

Campbell's Theorem: Let Φ be a PPP on space S with mean measure μ and $f : S \to \mathbb{R}$ a measurable function. Then the sum over Φ

$$\Sigma = \sum_{x \in \Phi} f(x), \tag{2.13}$$

is absolutely convergent if and only if

$$\int_S \min\left(|f(x)|, 1\right) \mu(dx) < \infty. \tag{2.14}$$

If (2.14) holds, then for any complex θ

$$\mathcal{E}\left[e^{-\theta\Sigma}\right] = \exp\left(-\int_S \left(1 - e^{-\theta f(x)}\right) \mu(dx)\right). \tag{2.15}$$

Further, the sum of f over Φ is given by

$$\mathcal{E}\left(\sum_{x \in \Phi} f(x)\right) = \int_S f(x)\mu(dx), \tag{2.16}$$

in the sense that expectation exists if and only if the integral (2.16) converges. If (2.16) converges, then

$$\text{var}\left(\sum_{x \in \Phi} f(x)\right) = \int_S f(x)^2 \mu(dx). \tag{2.17}$$

Note that replacing $\theta f(x)$ in (2.15) by $-\log\left(\nu(x)\right)$, we can obtain PGFL of PPP.

5. Slivnyak's Theorem

   Before presenting Slivnyak's theorem, we will first introduce the Palm distribution and the reduced Palm distribution. The Palm distribution, denoted by P^x is the conditional point process distribution given that a point exists at a specific location x. In the reduced Palm distribution, denoted by $\mathrm{P}^{x!}$, the point at x on which we condition is not included in the distribution. These two concepts play a very important role when wireless networks are modeled using Point processes. For example, assuming all transmitting nodes form a point process, one may want to consider one of them as the desired transmitter, while the others are interferers. Then the desired transmitter should not be included in the set of interferers.

   The independence property of the PPP states that the number of points in a ball centered at point x with radius ϵ denoted by $b(x, \epsilon)$ is independent of the

number of points in any region outside this ball, for an arbitrarily-small ϵ. This suggests that conditioning on a point at x does not change the distribution of the rest of the point process. This is formally stated in the Slivnyak's theorem.

Slivnyak's theorem: For a PPP the reduced Palm distribution equals to its (original) distribution P of PPP, i.e.,

$$\mathrm{P}^{x!} = \mathrm{P}. \tag{2.18}$$

Using the Slivnyak's theorem and (2.8) with $k = 0$, for a PPP with intesity measure $\lambda(x)$ the PDF of the nearest neighbour distance r_0 can be obtained as follow.

$$\begin{aligned} F_{r_o}(r) &= \Pr\left(\Phi(b(x,r)) = 0\right), \\ &= \exp\left(-\int_{b(x,r)} \lambda(x)dx\right). \end{aligned} \tag{2.19}$$

For a homogeneous PPP in $\mathbb{R}^2$ with intensity λ, (2.19) simplifies to

$$F_{r_o}(r) = \exp\left(-\pi\lambda r^2\right),\ 0 \leq r \leq \infty. \tag{2.20}$$

Differentiating (2.20) with respective to r_0, we can obtain the PDF or r_0 given by

$$f_{r_o}(r) = 2\pi\lambda r\, \exp\left(-\pi\lambda r^2\right),\ 0 \leq r \leq \infty. \tag{2.21}$$

2.4 Aggregate Interference and Signal-to-Interference-Plus-Noise Ratio Analysis in Poisson Wireless Networks

Many performance metrics used in wireless network analysis are directly or indirectly related to signal-to-interference-plus-noise ratio (SINR). Therefore, characterizing the aggregate interference and the resultant SINR is very important. However, in many situations, these parameters cannot be directly computed. Alternatively, the moment generating function (MGF) or equivalently the Laplace transform of the PDF of aggregate interference and SINR can be computed, and use for the performance analysis. This approach has been used in many studies related to various types of wireless networks including HetNet [41,50,65,66], D2D communications [62,67], cognitive radio networks [68–70], and point-to-point communications with and without diversity reception [71–74]. In the following we briefly discuss how

the properties of PPP can be used to compute the MGF or the Laplace transform of the aggregate interference in a Poisson wireless network.

Let us consider a network with nodes distributed according to a homogeneous PPP Φ in $\mathbb{R}^2$ with density λ. Also assume that one of the node $x \in \Phi$ is the receiver and all the other nodes $z \in \Phi \backslash x$ generate interference to x. Following the Slivnyak's theorem and using the stationary property of homogeneous PPP in $\mathbb{R}^2$ [51], the aggregate interference at x does not depend on the location of the receiver or whether the point x belongs to Φ. The aggregate interference is then given by

$$I = \sum_{z \in \Phi} Pl(x, z) h_{xz}, \tag{2.22}$$

where P is the transmit power by each node (a constant). $l(x, z)$ represents the channel power gain due to path loss. h_{xz} is the channel envelope power gain due to shadowing (large-scale fading) and small-scale fading. The Laplace transform of the PDF of I can be obtained as

$$\begin{aligned} \mathcal{L}_I(s) &= \mathcal{E}\left[e^{-sI}\right], \\ &= \mathcal{E}\left[e^{-s\sum_{z\in\Phi} Pl(x,z)h_{xz}}\right], \\ &= \mathcal{E}_{\Phi, h_{xz}}\left[\prod_{z\in\Phi} e^{-sPl(x,z)h_{xz}}\right]. \end{aligned} \tag{2.23}$$

Assuming PPP Φ and shadowing-fading process are statistically independent (2.23) can be written as

$$\mathcal{L}_I(s) = \mathcal{E}_{\Phi}\left[\prod_{z\in\Phi} \mathcal{E}_{h_{xz}}\left[e^{-sPl(x,z)h_{xz}}\right]\right]. \tag{2.24}$$

Using the definition of PGFL of PPP $\mathcal{L}_I(s)$ can be written as

$$\mathcal{L}_I(s) = \exp\left(-\int_{\mathbb{R}^2}\left(1 - \mathcal{E}_{h_{xz}}\left[e^{-sPl(x,z)h_{xz}}\right]\right)\mu(dz)\right). \tag{2.25}$$

$\sim$

Chapter 3

Uplink Power Control in Cellular Networks under Composite Rayleigh-lognormal Fading Channels

In cellular networks each mobile station (MS) adjusts its power level under control of its base station (BS), i.e., through uplink transmit power control (TPC), which is essential to reach signal-to-interference-plus-noise ratio (SINR) at the BS and to limit inter-cell interference (ICI). The optimal transmit power of an MS depends on channel impediments; path loss, shadowing and multipath fading, as well as the network configuration. However, since path loss is distance dependent and the cell association distances are correlated due to the cell association policies, the performance analysis of the uplink TPC is very complicated. Consequently, the impact of a specific power control algorithm on network performance is hard to quantify. In this Chapter [1], using tools from stochastic geometry, we analyze uplink TPC schemes. Three schemes are considered which either completely or partially invert the effect of path loss and/or shadowing. We assume the standard power-law path loss and composite Rayleigh-lognormal fading. The cumulative distribution function (CDF), the probability density function (PDF) of uplink transmit power and the resulting network coverage probability are derived and validated via computer simulations. With the aid of the mathematical expressions derived, the impact of various networks and TPC parameters on the network performance are investigated

[1] A version of this chapter has been published in EURASIP Journal on Wireless Communications and Networking [75]. A part of the contribution of this chapter has been also published in 2015 IEEE 82nd Vehicular Technology Conference, Boston, MA, USA [76].

and several observations are made. The study shows that the coverage is highly dependent on the severity of shadowing, the power control scheme and its parameters, but invariant of the density of deployment of BSs when the shadowing is mild and power control is partial. Study also shows that when the operating SINR is low, which is the typical scenario for cell edge users, compensating both path loss and shadowing by power control improves the coverage. However, when the operating SINR is high (for cell center users) compensating for path loss only improves coverage. It was also observed that increase in the severity of shadowing significantly reduces the coverage.

3.1 Introduction

Both uplink and downlink TPC is an integral part of modern cellular system standards (e.g., Long Term Evolution (LTE) and Long Term Evolution-Advanced (LTE-A) to control the transmit power of MSs and BSs, respectively, in order to mitigate inter-cell and intra-cell interference, while achieving energy savings, improving connectivity and maintaining a required signal-to-interference-plus-noise ratio (SINR) [44]. Uplink TPC is essential to the operation of CDMA cellular systems (e.g. the 3G cellular systems). Without the uplink TPC these systems would simply not work, due to the near-far effect on their uplink [30]. The simplest uplink TPC is to ensure that all user transmissions reach the same SINR at the base station (BS), which however requires that those encountering high path loss to transmit with much higher power. In contrast, partial power control, standardized by 3rd generation partnership project (3GPP) for LTE [44], LTE-A [44], and non-standalone 5G (NSA 5G) new radio (NR) [77], compensates for the path loss and possibly shadowing between the MS and its serving BS, and higher path loss users (e.g., cell-edge users) are allowed to operate at a lower SINR, thus reducing ICI. TPC (both downlink and uplink) is especially important for dense Heterogeneous networks (HetNets), the layouts of which may be very irregular. In HetNets, uplink interference from a neighbouring cell can be very strong [66], and battery-powered MS handsets need to save energy. All these reasons have motivated the development of various uplink TPC schemes to improve the total network throughput, cell-edge user performance, and energy efficiency [48, 53, 66, 76, 78–87].

Therefore, it is critically important to understand and quantify the performance of both uplink and downlink TPC schemes. Fortunately, the downlink has

been widely modeled and optimized using stochastic geometry [40–42, 50, 53, 66, 88]. Stochastic geometry facilitates tractable analysis of HetNets, where the locations of the BSs, access points (APs), and MSs are distributed according to mathematically tractable point processes [34, 41, 42]. For example, the homogeneous Poisson point process (PPP) has been widely used to study HetNets [34, 41, 42]. However, the uplink studies have been relatively limited, but have become necessary due to, for example, applications such as cloud processing and storage [89].

Location dependent power control and orthogonal multiple access make mathematical modeling cellular uplink more challenging. To elaborate, there is only one randomly located MS per cell per resource block due to the use of orthogonal frequency division multiple access (OFDMA) (see Figure 3.1). Thus cell association policy couples the locations of MSs. Consequently, even when all MS in the network form a PPP, the set of active MSs in a given resource block does not form a PPP. Moreover, the transmit powers of MSs, which typically depend on the MS-BS distances and random channel gains due to shadowing and multipath fading, are highly variable and correlated. This is because, although MS-BS distances of different cells are identically distributed, they are not statistically independent. All these conditions pose fundamental challenges for the analysis of uplink TPC performance.

In previous research, the aforementioned challenges have been overcome in two ways. First, one neglects or only partially captures the dependency among locations of interfering MSs and simply assumes them to form a homogeneous/inhomogeneous PPP. Therefore, we call this the *PPP approximated MSs model*. The correlation between the tagged MS (MS under investigation) and the interfering MS is captured by considering an appropriate interference protection region around the serving BS considering the cell association policy adapted. For example, with closest-BS association policy, no other co-channel MS can be closer to the serving BS than the tagged MS. In that model, the MS transmit powers are also assumed to be independent and identically distributed (i.i.d.). The exact distribution depends on the power control scheme and the cell association policy adapted. Second, one considers a fully loaded network, i.e., each cell has an active uplink transmission scheduled per time-frequency resource block. The spatial dependency between co-channel MSs is neglected and assumed to form a homogeneous PPP [90]. This makes the density of MSs per resource block equal to the density of BSs in the network. Each MS is assumed to be associated with the BS that provides the highest area averaged

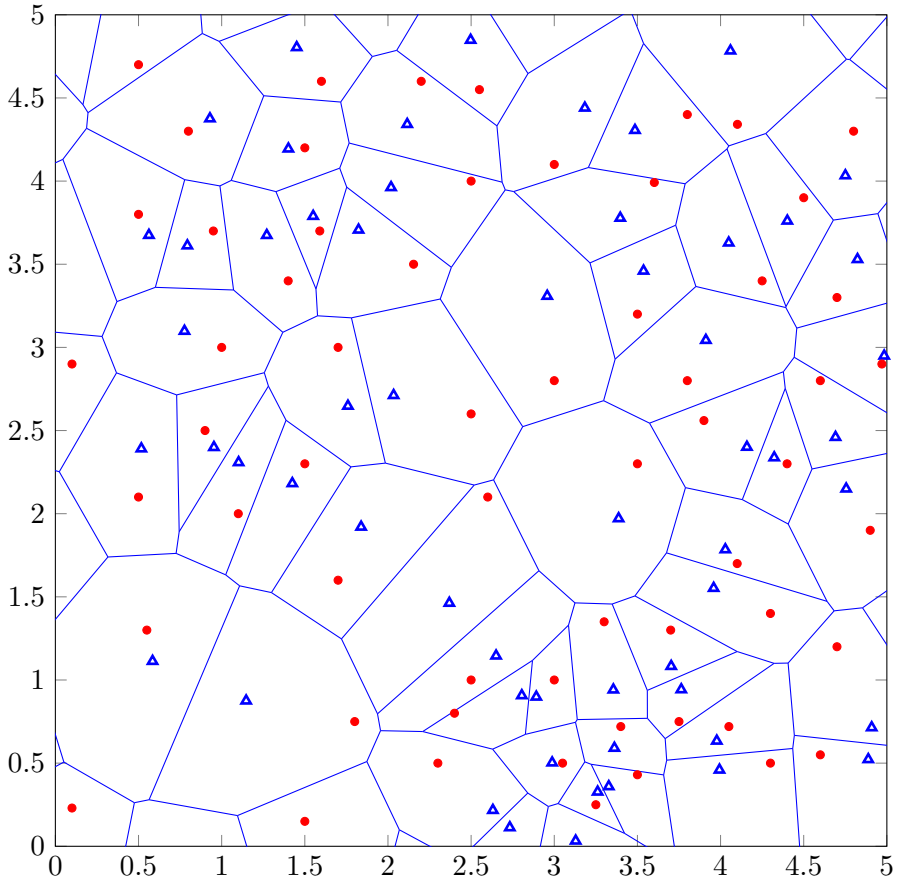

Figure 3.1: Poisson distributed BSs and MSs in a cellular network with orthogonal multiple access. MSs associated with the nearest BS. The cell boundaries are shown and form a Voronoi tessellation. Legend: blue triangles - BSs, red circles - active MSs per resource block. Poisson-Voronoi cell boundaries are denoted by blue lines.

received signal power. To capture the correlations among MS-BS distances, the associated BS of each MS is assumed to be uniformly distributed in the Voronoi cell of the MS. We refer to this approach as the *downlink equivalent model* [53].

3.1.1 Prior Related Research

For modern OFDMA-based or similar cellular networks, TPC attempts full/partial compensation of path loss and/or shadowing [53, 91]. Common schemes are path loss inversion (PLI) and path loss and shadowing inversion (PLSI). In the following, we summarize recent uplink TPC studies and highlight their contributions.

PLI, which compensates for path loss only, is considered in [53, 66, 78–81, 85–87, 90, 92]. The *downlink equivalent model* is used by [53, 90], while the *PPP approximated MSs model* is adopted by [66, 78–81, 85–87, 92]. Reference [53] has introduced

the *downlink equivalent model* and has derived the coverage and average rate of uplink partial PLI power control in a single-tier network. ICI mitigation through uplink partial frequency reuse [93, 94] and partial PLI power control is investigated in [90]. For a multi-tier HetNet, [80] proposes a tractable and general model to characterize the uplink signal-to-interference ratio (SIR) and rate distribution. First uplink analysis with multiple antenna BSs is presented in [81] considering a generalized version of partial PLI power control. The coverage probability and achievable data rate are derived for maximal ratio combining (MRC) and optimum combining at the BS. All works thus far consider partial PLI. In contrast, full PLI, which maintains a constant area mean (after averaging over variations due to shadowing and multipath fading [30]) received power at BSs, is considered in [66, 79, 92]. The outage probability and spectral efficiency of both single-tier and multi-tier cellular networks are investigated in [66]. Symbol error rate analysis of multi-tier HetNets is presented in [79]. A two-tier HetNet consisting of femtocells and macrocells is considered in [92]; upper and lower bounds for the outage probability of femtocell and macro users are derived there. SIR distribution in a two-tier HetNet is investigated in [78], where the MS transmit power is selected out of a finite set of discrete values to maintain the area mean received power above or equal to a predefined target value. Reference [85] investigates uplink outage probability in a multi-channel environment and captures the load variation on BSs. Uplink SINR and rate distribution in a massive multiple input multiple output (MIMO) network are investigated in [87].

In all previously mentioned references, uplink performance is investigated by averaging over the respective underlying point processes considered for the spatial distribution of users and BSs. Recently, [95,96] have investigated the uplink coverage probability of arbitrary, but fixed, realization (meta distribution of SIR) of Poisson cellular networks. Both these references consider partial PLI power control.

References [48, 76, 82, 83, 86] consider PLSI power control (i.e., compensation of both path loss and shadowing). The *downlink equivalent model* is adopted by [76], but *PPP approximated MSs model* is used by [48,82,83,86]. Reference [82] considers an interference aware PLSI scheme, where interference from each MS to the most interfered BS is kept under a predefined value. Reference [83] evaluates the uplink interference in a two-tier HetNet considering multi-type users and BSs. Uplink capacity in a two-tier direct sequence code division multiple access (DS-CDMA) HetNet consisting of macro BSs and femto APs is considered in [48]. Reference

[76] investigates coverage probability of a single-tier cellular network in composite Rayleigh-lognormal fading channels considering partial inversion of path loss and complete compensation of shadowing. Uplink SINR and rate distribution in a multi-tier cellular network are investigated in [86]. Joint uplink and downlink rate coverage (joint probability of uplink and downlink data rate/SINR exceeding their respective thresholds) is also investigated there.

3.1.2 Motivation and Our Contribution

The main goal of this study is the investigate and characterize the impact of TPC and shadowing on the uplink performance. The effectiveness of shadowing compensation by power control is also in the focus. Shadowing may degrade the performance of modern HetNets that include both macro and low-power, small form-factor small cells, which have low antennas. In such environments, a significant impact of shadowing is to be expected. Shadowing specifically refers to variations in the signal strength over distances proportional to the length of an obstructing object (10-100 meters) in outdoor environments and less in indoor environments [4]. Experiments have confirmed that typical shadowing effects can be modeled as log-normal [4, 30], and that distribution has thus been widely used to study the effects of shadowing [4, 30, 97, 98]. Overall, power control schemes that alleviate shadowing in addition to path loss (i.e., PLSI) will undoubtedly have a beneficial effect on the uplink coverage, data rates, and power efficiency.

Although uplink PLSI studies exist in the literature [48, 82, 83], their system models appears to be not flexible enough to investigate the effect of uplink TPC in modern cellular networks. For example, [82, 83] consider shadowing as a random displacement on the MS point process. This prevents the consideration of different shadowing levels for different radio channels, desired and interfering channels for example. Reference [48] investigates the cellular uplink with PLSI power control. However, it investigates a two-tier DS-CDMA cellular network. Therefore, the results of this research are not fully applicable for modern orthogonal frequency division multiplexing (OFDM) or discrete Fourier transform-spread OFDMA (DFT-S-OFDMA) based cellular uplink such as LTE or fifth generation cellular networks (5G) NR.

All above mentioned reasons and gaps in the literature motivate the investigation of TPC schemes which compensates for path loss and shadowing. Thus we consider

three TPC schemes which provide full and/or partial compensation for

1. Path loss only,
2. The aggregate effect of path loss and shadowing,
3. partial compensation of path loss and complete inversion of shadowing.

With these, the transmit power of an MS becomes a random variable, whose statistics depend on the MS−BS distance, shadowing, and power control parameters. The MS battery power utilization has a direct relationship with these statistics. Thus we derive the CDF and the PDF of the transmit power under each scheme. Further, these TPC can have a significant impact on the uplink signal quality (signal-to-noise ratio (SNR)). Therefore, a refined mathematical framework is also developed to investigate the coverage probability under each TPC scheme. The developed framework help us to quantify the impact of power control, shadowing, and other network parameters on the coverage probability. Specifically, the main contributions of this study can be summarized as follows:

- We provide analytical expressions for PDF, CDF and the mean transmit power, and coverage probability for the three power control schemes considering composite Rayleigh-lognormal fading and path loss. To evaluate the complicated integrals, we use the Gauss-Hermite and Gauss-Laguerre quadratures to express them as weighted sums of function evaluations. This provides a powerful, flexible platform to evaluate the effects of different shadowing levels. Computing the Gauss quadrature nodes and weights is very simple with Golub-Welsch algorithm [99], which utilizes the eigenvalues and eigenvectors of the symmetric tridiagonal matrix formed by the recurrence relations to compute the nodes and weights.
- We investigate in detail the effects of shadowing, power control factor, and BSs' density on the coverage probability using analysis and simulations. We show that under all three power control schemes, density of BSs has no significant effect on the coverage.
- Comparing the performance of three power control schemes, we show that at low SINRs (cell edge users or users subject to severe shadowing), compensating for both path loss and shadowing improves the coverage probability. However,

at high SINRs (users closer to their serving BSs) compensating for path loss only is more effective.

3.2 System Model, Power Control and Assumptions

This section presents the network setup, three power control schemes considered, and key assumptions needed for tractable mathematical analysis.

3.3 System Model

This research considers uplink transmission in a cellular network with the following network configurations and assumptions. We use the downlink equivalent model proposed in [53], which is described by the following 6 points.

1. Network consists of a single class of BSs with density $\lambda > 0$. Similarly to [53,66] we consider minimum path loss based association policy. Therefore, each MS is associated with the BS providing the highest area mean received power [30]. This is equivalent to connecting to the closest BS. Considering minimum path loss association is motivated by two reasons. First, investigating the effectiveness of compensating for shadowing as a part of power control is one of the aims of this study. Therefore, we refrain from considering shadowing and fast fading for the cell association. Second, this association policy is simple and also avoids frequent handoffs [100]. An orthogonal multiple access technique is used, for example OFDMA or DFT-S-OFDMA.

2. Universal frequency reuse [30], which allows every cell in the network to reuse the same set of carrier frequencies. The network is fully loaded, i.e., each BS has an active uplink transmission scheduled for each time-frequency resource block.

3. The locations of MSs operating in a particular time-frequency channel form a homogeneous PPP Φ. Due to orthogonal channel assignment and the assumption of a fully loaded network, $\Phi = \{x_1, x_2, \ldots\}$, where $x_k \in \mathbb{R}^2$ has the intensity λ.

4. With this network setup, each BS is uniformly distributed in the Voronoi cell of its corresponding MS [53,90]. This is referred to as the downlink equivalent model for uplink communication.

5. All the radio channels are subject to power-law path loss and composite Rayleigh-lognormal fading. Although the severity of shadowing depends on the density and locations of shadowing objects, considering different shadowing levels for each cell is mathematically intractable. Therefore, we consider only two values for the standard deviation of the shadowing process: σ for the local environment (locality of the BS serving MS z_0), and ξ for interfering cells. Channel power gains due to small-scale fading and shadowing are assumed to be independently distributed across all MS-BS pairs.

6. We investigate the coverage probability of a randomly chosen MS $z_0 \in \Phi$. Since a homogeneous PPP in $\mathbb{R}^2$ is translation and rotation invariant, without loss of generality the BS associated with z_0 is assumed to be located at the center of the network.

Reference [53] has investigated the accuracy of this model and has shown that it accurately models the uplink transmissions in a cellular network.

3.3.1 Power Control Schemes

We consider three partial power control schemes, which compensate for path loss and shadowing. For a selected power control scheme, we assume all the MSs use the same set of power control parameters.

Scheme 1: Partial/Full Path Loss Compensation

This scheme aims to compensate for the effect of path loss on the received signal power. Therefore, the transmit power P_z of MS $z \in \Phi$ associated with the BS y [2] is given by

$$P_z = \rho \left(l(z, y) \right)^{-\eta}, \tag{3.1}$$

where ρ is a constant and $l(z, y)$ is the channel power gain due to path loss. For power-law path loss model, $l(z, y) = ||z - y||^{-\alpha}$, where $\alpha > 2$ is the path loss exponent. The power control factor is denoted by $\eta \in [0, 1]$. η can be interpreted as a fairness parameter, where higher value helps the cell edge users meet their SINR target but at the cost of increasing the interference level in the network [86]. This can reduce the SINR experienced by cell center users. $\eta = 1$ represents complete

[2] with a slight abuse of notation we will use z to denote both the location of MS and MS itself. Similarly for BS y.

elimination of path loss while $\eta = 0$ represents no power control. For a given network ρ is a constant; value is the same for all the MSs.

Scheme 2: Partial/Full Compensation for both Path Loss and Shadowing

With this power control, the transmit power of MS $z \in \Phi$ is given by

$$P_z = \rho \left(l(z, y) h_{zy} \right)^{-\eta}, \tag{3.2}$$

where h_{zy} is the shadowing power gain. Therefore, $\eta = 1$ ($\eta = 0$) represents complete compensation for path loss and shadowing (no power control).

Scheme 3: Partial Compensation for Path Loss and Complete Inversion of Shadowing

This scheme completely eliminates the shadowing effect, but only partially inverts path loss. Therefore, the transmit power of MS $z \in \Phi$ is given by

$$P_z = \rho \left(l(z, y) \right)^{-\eta} h_{zy}^{-1}. \tag{3.3}$$

In (3.3), power control factor $\eta \in [0, 1]$ determines the degree of path loss compensation. That is, $\eta = 1$ ($\eta = 0$) gives a complete inversion of path loss (path loss is not compensated for and only shadowing is inverted).

3.3.2 Downlink Equivalent Model

As mentioned before, correlations among transmit powers and the locations complicate the analysis. To overcome this, we will use the downlink equivalent model [53] and make two additional assumptions to obtain the PDF of the transmit power for each TPC scheme.

Assumption 1

According to the system model described earlier, the BS is uniformly distributed in the Voronoi cell of the MS being served. We approximate this choice by selecting the closest BS from a networks with BSs forming a PPP with intensity λ. This assumption is also made in [53], and it is shown that the loss of accuracy due to it is minimal. This assumption will play a key role in the derivations of the PDFs of the MS transmit powers.

With Assumption 1, the distance between an MS and its associated BS follows the Rayleigh PDF given by

$$f_r(t) = 2\pi\lambda t \exp\left(-\pi\lambda t^2\right),\ 0 < t < \infty. \tag{3.4}$$

Proof: Since each MS associates with the closest BS, the CDF of the the distance r between any MS located at point $x \in \Phi$ to its associated BS can be written as

$$F_r(t) = \Pr\left[\Phi(b(x,t)) = 0\right]. \tag{3.5}$$

$\Pr\left[\Phi(b(x,t)) = 0\right]$ can be obtained by assigning $k = 0$ in (2.8). Therefore,

$$F_r(t) = \exp\left(-\lambda\pi t^2\right). \tag{3.6}$$

PDF (3.4) can be obtained by differentiating (3.6) with respect to variable t.

Assumption 2

All MS-BS distances are i.i.d. with PDF (3.4).

In all three power control schemes, transmit power of an MS depends on path loss, power control parameter η and ρ. As path loss is a function of MS-BS distance and path loss exponent, with Assumption 2, transmit power from different MSs become i.i.d..

References [53, 66] showed that the dependencies between MS-BS distances and transmit powers are in fact weak, and above assumptions yield accurate results. In Section 3.6, we also test the validity of these assumptions by comparing numerical and simulation results and show that the loss of accuracy due to these assumptions is negligible.

3.4 Transmit Power Analysis

Here we derive the transmit power PDFs and CDFs.

3.4.1 Scheme 1: Partial Compensation for Path Loss

In this scheme, each MS adjusts its transmit power according to (3.1). Using Assumptions 1, 2, and (3.4), approximate expressions for the CDF and PDF of the transmit power at MSs $z \in \Phi$, P_z, can be derived as given in the following lemma.

Lemma 1

In a single-tier Poisson cellular network with closest BS cell association and partial path loss inversion power control, the CDF and the PDF of the transmit power P_z are given by

$$F_{P_z}(t) = 1 - \exp\left(-\pi\lambda\rho^{-\frac{2}{\alpha\eta}}t^{\frac{2}{\alpha\eta}}\right), \quad 0 < t < \infty \text{ and} \tag{3.7}$$

$$f_{P_z}(t) = \frac{2\pi\lambda}{\alpha\eta\rho^{\frac{2}{\alpha\eta}}} \exp\left(-\pi\lambda\rho^{-\frac{2}{\alpha\eta}}t^{\frac{2}{\alpha\eta}}\right) t^{\frac{2}{\alpha\eta}-1} \quad , 0 < t < \infty. \tag{3.8}$$

Proof: Using (3.1), the CDF of P_z can be written as

$$\begin{aligned} F_{P_z}(t) &= \Pr\left[\rho r^{\alpha\eta} < t\right], \\ &= \Pr\left[r < \left(\frac{t}{\rho}\right)^{\frac{1}{\alpha\eta}}\right]. \end{aligned} \tag{3.9}$$

Substituting the PDF of r given by (3.4) in (3.9) we obtain the CDF of P_z given in (3.7). By differentiating (3.7) we obtain the PDF of P_z given in (3.8).

3.4.2 Scheme 2: Partial Compensation for the Aggregate Effect of Path Loss and Shadowing

For partial inversion of the path loss and shadowing, the transmit power at the MS $z \in \Phi$, P_z, is given by (3.2). The CDF and PDF of the transmit power are given below.

Lemma 2

In a single-tier Poisson cellular network with closest BS cell association and partial path loss and shadow inversion power control, the CDF of P_z is given by

$$F_{P_z}(t) = 1 - \sum_{k=1}^{N} \frac{w_k}{\sqrt{\pi}} \exp\Big(- \pi\lambda \left(\frac{t}{\rho}\right)^{\frac{2}{\alpha\eta}} \exp\Big(\frac{2\sqrt{2}\xi u_k}{\alpha}\Big)\Big) + O_N, 0 < t < \infty. \tag{3.10}$$

The PDF of the transmit power is given by

$$f_{P_z}(t) = \frac{2\sqrt{\pi}\lambda}{\alpha\eta\rho^{\frac{2}{\alpha\eta}}} \sum_{k=1}^{N} w_k t^{\frac{2}{\alpha\eta}-1} \exp\Big(\frac{2\sqrt{2}\xi u_k}{\alpha} - \pi\lambda \left(\frac{t}{\rho}\right)^{\frac{2}{\alpha\eta}} \exp\Big(\frac{2\sqrt{2}\xi u_k}{\alpha}\Big)\Big) + \epsilon_N \quad , \ 0 < t < \infty. \tag{3.11}$$

Here $N > 1$ is an integer which determines the accuracy of the approximation. O_N, and ϵ_N represent the error terms that decrease to zero as N increases to infinity.

w_k and u_k are weights and abscissas for Gauss-Hermite quadrature of order N. For different values of N, w_k and u_k are available in [6, Table (25.10)] or can be calculated by a simple MATLAB® program.

Proof: See Section A.1.

3.4.3 Scheme 3: Partial Compensation for Path Loss and Complete Inversion of Shadowing

The transmit power of each MS $z \in \Phi$, P_z, is given by (3.3). The CDF and PDF are given by the following lemma.

Lemma 3

In a single-tier Poisson cellular network with closest BS cell association, partial path loss compensation and complete shadow inversion power control, the CDF is given by

$$F_{P_z(t)} = 1 - \sum_{k=1}^{N} \frac{w_k}{\sqrt{\pi}} \exp\Big(- \pi\lambda \left(\frac{t}{\rho}\right)^{\frac{2}{\alpha\eta}} \exp\left(\frac{2\sqrt{2}\xi u_k}{\alpha\eta}\right)\Big) + O_N,\ 0 < t < \infty. \quad (3.12)$$

The PDF of the transmit power P_z is given by

$$f_{P_z}(t) = \frac{2\sqrt{\pi}\lambda}{\alpha\eta\rho^{2/\alpha\eta}} \sum_{k=1}^{N} w_k t^{\frac{2}{\alpha\eta}-1} \exp\Big(\frac{2\sqrt{2}\xi u_k}{\alpha\eta} - \pi\lambda \left(\frac{t}{\rho}\right)^{\frac{2}{\alpha\eta}} \exp\Big(\frac{2\sqrt{2}\xi u_k}{\alpha\eta}\Big)\Big) + \epsilon_N , \quad 0 < t < \infty. \quad (3.13)$$

Similarly to in Lemma 1, w_k and u_k are the weights and abscissas for Gauss-Hermite quadrature of order N. O_N and ϵ_N are the error terms.

Proof: See Section A.2.

3.5 Coverage Probability Analysis

Next we derive the coverage probability of the network for the three power control schemes (Section 3.3). Similarly to [40], the coverage probability is defined as the probability that a randomly chosen MS $z_0 \in \Phi$ achieves the uplink SINR target of T.

3.5.1 Scheme 1: Partial Compensation for Path Loss

Under this power control scheme, the SINR at the BS serving MS $z_0 \in \Phi$ can be written as

$$\text{SINR} = \frac{\rho r_{z_0}^{\alpha(\eta-1)} h_{z_0}}{\sum_{z\in\Phi\setminus z_0} P_z r_z^{-\alpha} h_z + N_0}, \tag{3.14}$$

where r_{z_0} is the distance between MS z_0 and its associated BS at the origin. Variance of the additive white Gaussian noise (AWGN) is given by N_0. The channel power gain due to composite shadowing-fading modeled by Rayleigh-lognormal distribution is given by h_{z_0}. The set $\Phi\setminus z_0$ represents all the active co-channel interfering MSs (all MSs of Φ except z_0). For MS $z \in \Phi$, where $z \neq z_0$, $r_z = ||z||$ and h_z are the Euclidean distance from the BS at the origin and channel power gain (modeled by Rayleigh-lognormal distribution) to the BS. The coverage probability is given by the following theorem.

Theorem 1

The uplink coverage probability of an MS in a single-tier cellular network under partial path loss inversion power control is

$$\begin{aligned} P_c(T) =& 2\sqrt{\pi}\lambda \sum_{i=1}^{L} \zeta_i \int_0^\infty r_{z_0} \exp\left(-\pi\lambda r_{z_0}^2 - \frac{N_0 T \exp\left(-\sqrt{2}\sigma v_i\right)}{\rho r_{z_0}^{\alpha(\eta-1)}}\right) \\ & \times \mathcal{L}_{I_{\Phi\setminus z_0}}\left(s = \frac{T\,\exp\left(-\sqrt{2}\sigma v_i\right)}{\rho r_{z_0}^{\alpha(\eta-1)}}\right) dr_{z_0} + \epsilon_L, \end{aligned} \tag{3.15}$$

where

$$\begin{aligned} \mathcal{L}_{I_{\Phi\setminus z_0}}(s) = \exp\Bigg(& \frac{-2\pi^{\frac{1-\alpha\eta}{2}} \lambda^{\frac{2-\alpha\eta}{2}} s\rho\; r_{z_0}^{2-\alpha}}{\alpha-2} \sum_{j=1}^{M} \kappa_j \exp(\sqrt{2}\sigma x_j) \sum_{q=1}^{Q} \beta_q \\ & \times\; {}_2F_1\left(1, \frac{\alpha-2}{\alpha}, 2-\frac{2}{\alpha}, \frac{-s\rho\,\exp\left(\sqrt{2}\sigma x_j\right)\delta_q^{\frac{\alpha\eta}{2}}}{r_{z_o}^{\alpha}\,(\pi\lambda)^{\frac{\alpha\eta}{2}}}\right)\Bigg) + R_{MQ}. \end{aligned} \tag{3.16}$$

Here, ζ_i and v_i are the weights and nodes for the Gauss-Hermite quadrature of order L. Similarly, κ_j and x_j are the weights and nodes for Gauss-Hermite quadrature of order M. Finally, β_q and δ_q are the weight and nodes for the Gauss-Laguerre quadrature of order Q. Weights and nodes for Gauss-Laguerre quadrature of different orders are available in [6, Table (25.9)] or can be calculated by a low-complexity MATLAB program [99]. Terms ϵ_L and R_{MQ} are the errors of the approximations.
Proof: See Section A.3.

3.5.2 Scheme 2: Partial Compensation for the Aggregate Effect of Path Loss and Shadowing

When Scheme 2 is employed, SINR at the BS serving MS $z_0 \in \Phi$ can be written as

$$\text{SINR} = \frac{\rho r_{z_0}^{\alpha(\eta-1)} \hat{h}_{z_0}}{\sum_{z \in \Phi \setminus z_0} P_z r_z^{-\alpha} h_z + N_0}. \tag{3.17}$$

Since power control partially inverts the effect of shadowing, $\hat{h}_{z_0} \sim \exp(\mu)$, where $\mu \sim \text{lognormal}(0, (1-\eta)\sigma)$. The coverage probability for this power control is given by the following theorem.

Theorem 2

In a single-tier Poisson cellular network with closest BS cell association, partial path loss and shadow inversion power control, the coverage probability can be given by

$$P_c(T) = 2\sqrt{\pi}\lambda \sum_{i=1}^{L} \zeta_i \int_0^{\infty} r_{z_0} \exp\left(-\pi\lambda r_{z_0}^2 - \frac{N_0 T \exp\left(-\sqrt{2}\sigma(1-\eta)v_i\right)}{\rho r_{z_0}^{\alpha(\eta-1)}} \right) \times \mathcal{L}_{I_{\Phi \setminus z_0}}\left(s = \frac{T \exp\left(-\sqrt{2}(1-\eta)\sigma v_i\right)}{\rho r_{z_0}^{\alpha(\eta-1)}} \right) dr_{z_0} \epsilon_L, \tag{3.18}$$

where

$$\mathcal{L}_{I_{\Phi \setminus z_0}}(s) = \exp\Bigg(\frac{-2\lambda}{\alpha - 2} \sum_{k=1}^{N} w_k \sum_{j=1}^{M} \kappa_j \sum_{q=1}^{Q} \beta_q \frac{r_{z_0}^{2-\alpha} s\rho \exp\left(\sqrt{2}\sigma x_j\right) \delta_q^{\frac{\alpha\eta}{2}}}{(\pi\lambda)^{\frac{\alpha\eta}{2}} \exp\left(\sqrt{2}\xi u_k \eta\right)} \times {}_2F_1\left(1, \frac{\alpha-2}{\alpha}, 2 - \frac{2}{\alpha}, \frac{-s\rho \exp\left(\sqrt{2}\sigma x_j\right) \delta_q^{\frac{\alpha\eta}{2}}}{r_{z_0}^{\alpha} (\pi\lambda)^{\frac{\alpha\eta}{2}} \exp\left(\sqrt{2}\xi u_k \eta\right)}\right) \Bigg) + R_{NMQ}. \tag{3.19}$$

Here, ζ_i and v_i are the weights and abscissas for the Gauss-Hermite quadrature of order $L > 1$. Similarly, w_k and u_k are the weights and abscissas for the Gauss-Hermite quadrature of order $N > 1$. κ_j and x_j are the weights and abscissas for Gauss-Hermite quadrature of order $M > 1$. β_q and δ_q are the weight abscissas for the Gauss-Laguerre quadrature of order Q. Terms ϵ_L and R_{NMQ} are the errors of the approximations.

Proof: See Section A.4.

3.5.3 Scheme 3: Partial Compensation for Path Loss and Complete Inversion of Shadowing

In Scheme 3, path loss is partially compensated while the shadowing is completely inverted. Therefore, the SINR at BS serving MS $z_0 \in \Phi$ can be written as

$$\text{SINR} = \frac{\rho r_{z_0}^{\alpha(\eta-1)} g_{z_0}}{\sum_{z\in\Phi\setminus z_0} P_z r_z^{-\eta} h_z + N_0}, \tag{3.20}$$

where $g \sim \exp(1)$ is the power gain of the serving BS-MS channel due to Rayleigh multipath fading. The uplink coverage probability under this power control scheme is given by the following theorem.

Theorem 3

In a single-tier Poisson cellular network with closest BS cell association and partial path loss compensation and complete shadow inversion power control, the coverage probability is approximated by

$$P_c = 2\pi\lambda \int_0^\infty r_{z_0} \exp\left(-\pi\lambda r_{z_0}^2 - \frac{N_0 T}{\rho r_{z_0}^{\alpha(\eta-1)}}\right) \mathcal{L}_{I_{\Phi\setminus z_0}}\left(\frac{T r_{z_0}^{\alpha(1-\eta)}}{\rho}\right) dr_{z_0}, \tag{3.21}$$

where

$$\mathcal{L}_{I_{\Phi\setminus z_0}}(s) = \exp\Bigg(\frac{-2\lambda}{\alpha-2} \sum_{k=1}^{N} w_k \sum_{j=1}^{M} \kappa_j \sum_{q=1}^{Q} \beta_q \frac{r_{z_0}^{2-\alpha} s\rho \exp\left(\sqrt{2}\sigma x_j\right) \delta_q^{\frac{\alpha\eta}{2}}}{(\pi\lambda)^{\frac{\alpha\eta}{2}} \exp\left(\sqrt{2}\xi u_k\right)} \times {}_2F_1\left(1, \frac{\alpha-2}{\alpha}, 2-\frac{2}{\alpha}, \frac{-s\rho \exp\left(\sqrt{2}\sigma x_j\right) \delta_q^{\frac{\alpha\eta}{2}}}{r_{z_0}^{\alpha} (\pi\lambda)^{\frac{\alpha\eta}{2}} \exp\left(\sqrt{2}\xi u_k\right)}\right)\Bigg) + R_{NMQ}. \tag{3.22}$$

Here, w_k and u_k are the weights and abscissas for the Gauss-Hermite quadrature of order $N > 1$. κ_j and x_j are the weights and abscissas for the Gauss-Hermite quadrature of order $M > 1$. β_q and δ_q are the abscissas and weight factors for the Gauss-Laguerre quadrature of order $Q > 1$. Term R_{NMQ} is the errors of the approximation.

Proof: See Section A.5.

3.6 Numerical Results

This section presents numerical and simulation results, and investigates the effect of power control factor, standard deviations of shadowing, and intensity of BSs on

the uplink coverage probability. In the numerical derivations (Appendix A) natural logarithm is used instead of logarithm with base 10. Therefore, PDFs (A.3) and (A.9) are scaled versions of the actual PDFs [30]. Thus the standard deviations of shadowing in dB σ_{dB} and ξ_{dB} given in the following figures are $\sigma_{\text{dB}} = (10/\ln 10)\sigma$ dB and $\xi_{\text{dB}} = (10/\ln 10)\xi$ dB.

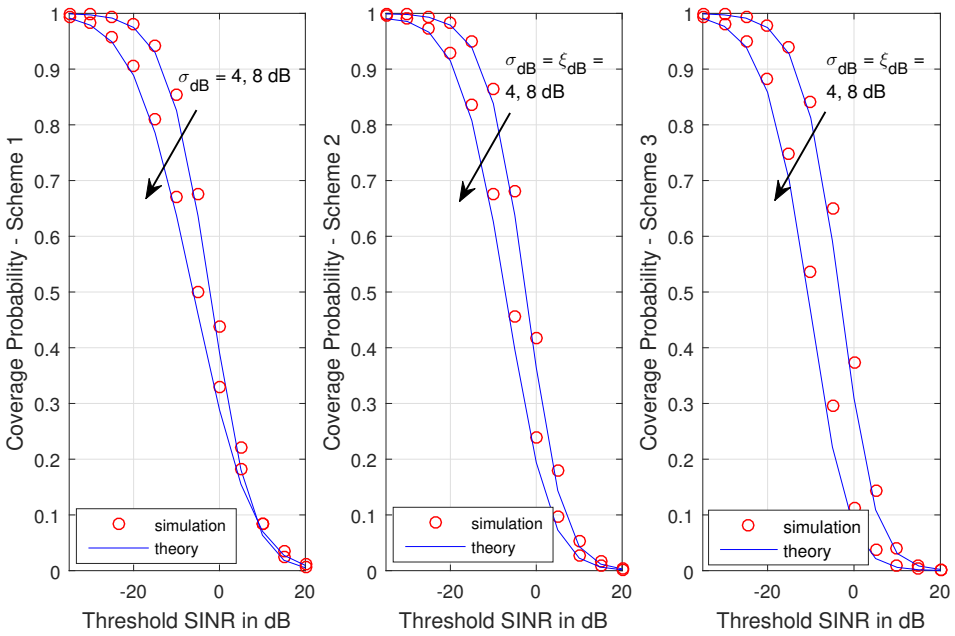

Figure 3.2: Coverage probability vs SINR threshold for three Schemes under different degrees of shadowing, $\eta = 0.5$, $\lambda = 0.5$ BS km^{-2}, $\alpha = 3.5$, $N_0 = 0$.

Fig. 3.2 we compare analytical coverage probability curves with the simulation results for three TPC schemes and different degrees of shadowing. We observe that our analytical expressions closely match the simulation results and accurately capture the performance trends. Further, lower σ_{dB} and ξ_{dB} (less severe shadowing) improve coverage. For analytical expressions, we use 30-points Hermite quadratures and 15-points Gauss-Laguerre quadratures.

Fig. 3.3 compares the coverage of the three TPC schemes under various degrees of shadowing. When shadowing is less severe, they achieve similar performance. For example, their coverage probabilities are more or less the same when $\sigma_{\text{dB}} = \xi_{\text{dB}} = 4$ dB. This suggests that, in an environment with less severe shadowing, path loss inversion using TPC is sufficient. Consequently, frequent channel state measurements such that they capture the variations due to shadowing are not

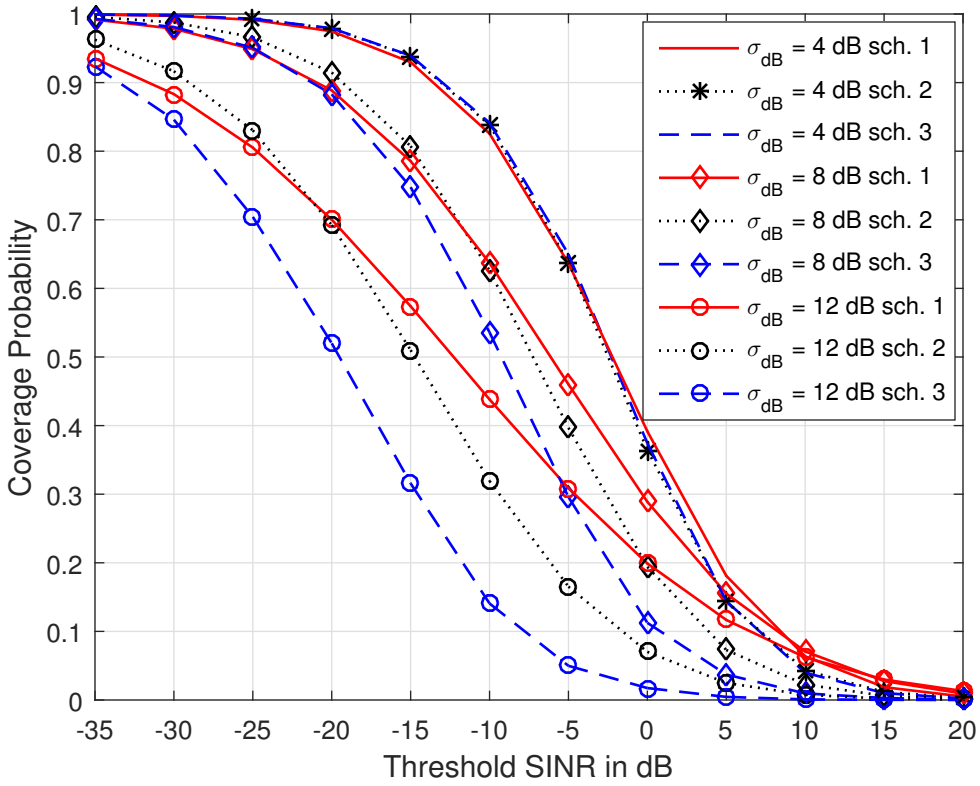

Figure 3.3: Comparison of coverage of three schemes for different degrees of shadowing. $\eta = 0.5$. $\lambda = 0.5$ BS km^{-2}, $\alpha = 3.5$, $\sigma_{\text{dB}} = \xi_{\text{dB}}$, $N_0 = 0$.

essential for proper power control. It is sufficient to capture channel state changes due to path loss. However, as the shadowing increases, the coverage probabilities differ significantly. Of these three, Schemes 3 results in the lowest coverage except when threshold SINR is very low (high coverage region). This is because, although complete inversion of shadowing (Scheme 3) improves the received signal strength of the desired signal, it also increases the transmit powers of interfering MSs, resulting in higher aggregate interference power.

Fig. 3.3 also shows that at low SINR thresholds, compensating for the aggregate effect of path loss and shadowing (Scheme 2) improves coverage, especially for higher degrees of shadowing. However, at high SINR thresholds, path loss inversion (Scheme 1) provides better coverage compared to other two TPC schemes. Reasons for these two trends can be explained as follows. Generally cell-edge users operate at low SINR due to high path loss and compensating for shadowing significantly improves their SINR. Cell-center users operates at high SINR as they experience

lower path loss. For these users, compensating for shadowing results in less significant SINR improvement, but negatively impacts cell-edge users and capacity of the network due to increased interference.

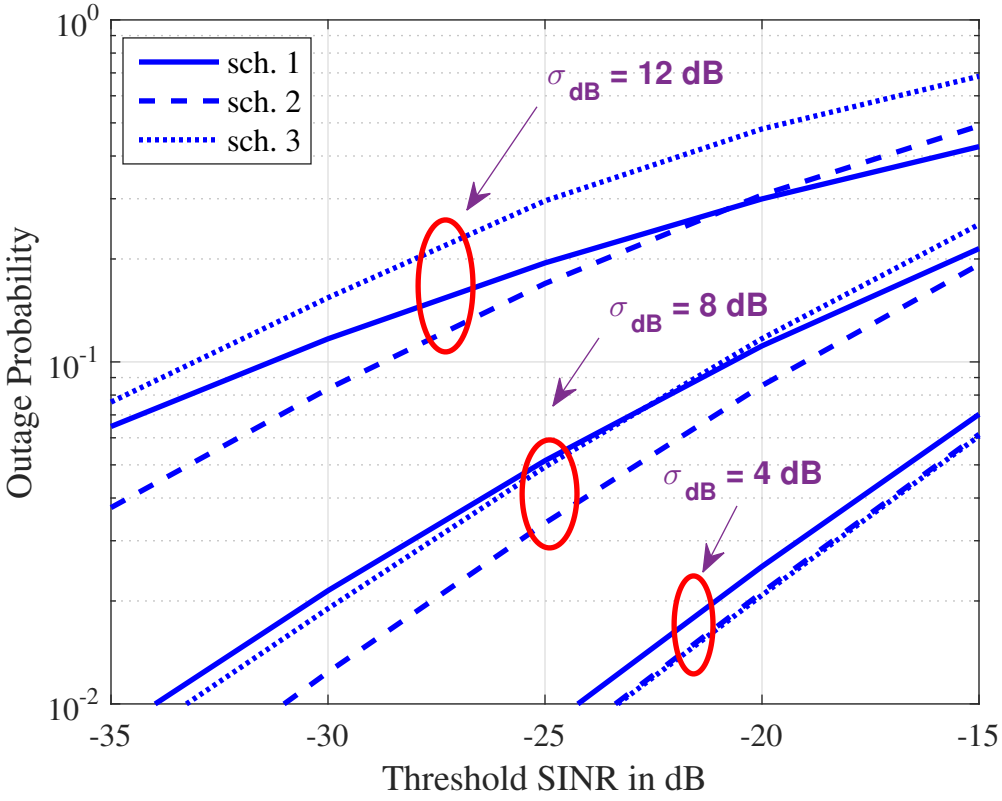

Figure 3.4: Comparison of outage probability of three schemes at lower threshold SINR. $\eta = 0.5$. $\lambda = 0.5$ BS km^{-2}, $\alpha = 3.5$, $\sigma_{\text{dB}} = \xi_{\text{dB}}$, $N_0 = 0$.

Fig. 3.4 highlights the outage probability (1-coverage probability) at low SINR threshold values, i.e., when coverage probability is high. The negative impact of higher shadowing standard deviation can be clearly identified. For example, to reach 10% outage probability, a network experiencing $\sigma_{\text{dB}} = 12$ dB needs more than 10 dB extra SINR compared to a network with $\sigma_{\text{dB}} = 8$ dB. Also results strongly indicate that partially compensating for both path loss and shadowing (Scheme 2) helps to lower the outage probability of the network in low SINR threshold region. For example, when $\sigma_{\text{dB}} = 8$ dB, to reach outage probability of 0.05% Scheme 3 gives a 2 dB advantage over other two Schemes.

Fig. 3.5 shows the coverage for different BS densities and shadowing levels. We see that the BS density has no impact on the coverage probabilities of Schemes

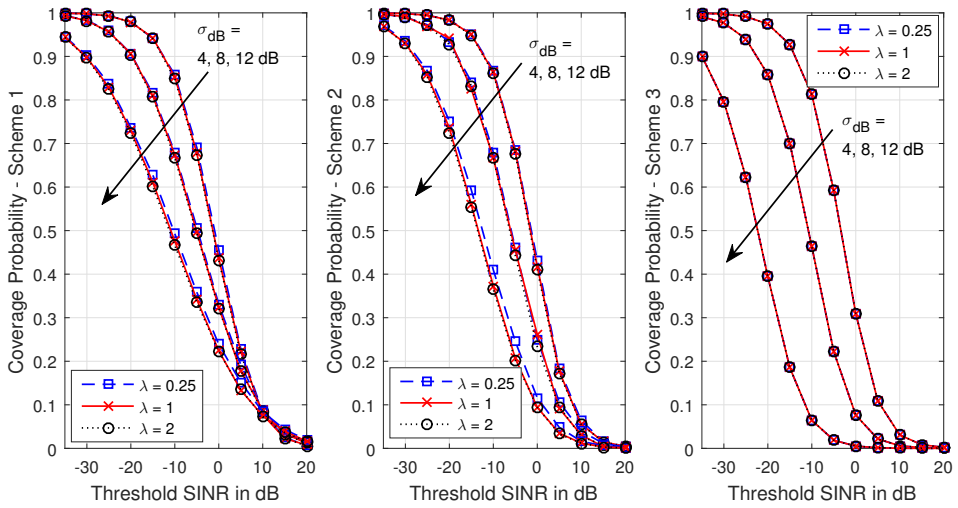

Figure 3.5: Coverage probability of three Schemes vs SINR threshold for different BS intensities and degrees of shadowing. $\eta = 0.5$. λ is in BSs/km^2, $\alpha = 3.5$, $\sigma_{\text{dB}} = \xi_{\text{dB}}$, $N_0 = 0$.

1 and 3, but severity of shadowing does. A similar observation can be made for Scheme 2, except for higher shadowing standard deviations values. For example, for $\sigma_{\text{dB}} = \xi_{\text{dB}} = 12$ dB, coverage slightly lowers as the BS intensity increases. This is because increasing the intensity of BSs not only increases the intensity of co-channel interfering users, but also increases the received signal power at the serving BSs by bringing in BSs closer to their users. Reference [80] has shown that with minimum path loss association and full PLI power control (Scheme 1 with $\eta = 1$), uplink coverage is invariant of the BS density. Fig. 3 corroborates this claim also for partial power control ($\eta < 1$) under Schemes 1 and 3 for all shadowing levels and for lower shadowing levels under Scheme 2.

Fig. 3.6 shows the coverage probability of Scheme 1 for different values of η and different degrees of shadowing. Clearly the coverage is smallest when the path loss is completely compensated. This is because higher value of η helps the cell edge users meet their SINR target, but at the cost of higher interference level in the network. This also reduces the SINR experienced by cell center users. Therefore, the spatially averaged coverage probability is reduced. Therefore, careful choice of TPC parameters is essential for proper designing of a cellular network. We also observe that at high threshold SINR ($T > 0$ dB), the $\eta = 0$ (no power control; each MS transmits with the same transmit power regardless of the path loss), results in better coverage. Further, the variation of coverage with η is similar for the two

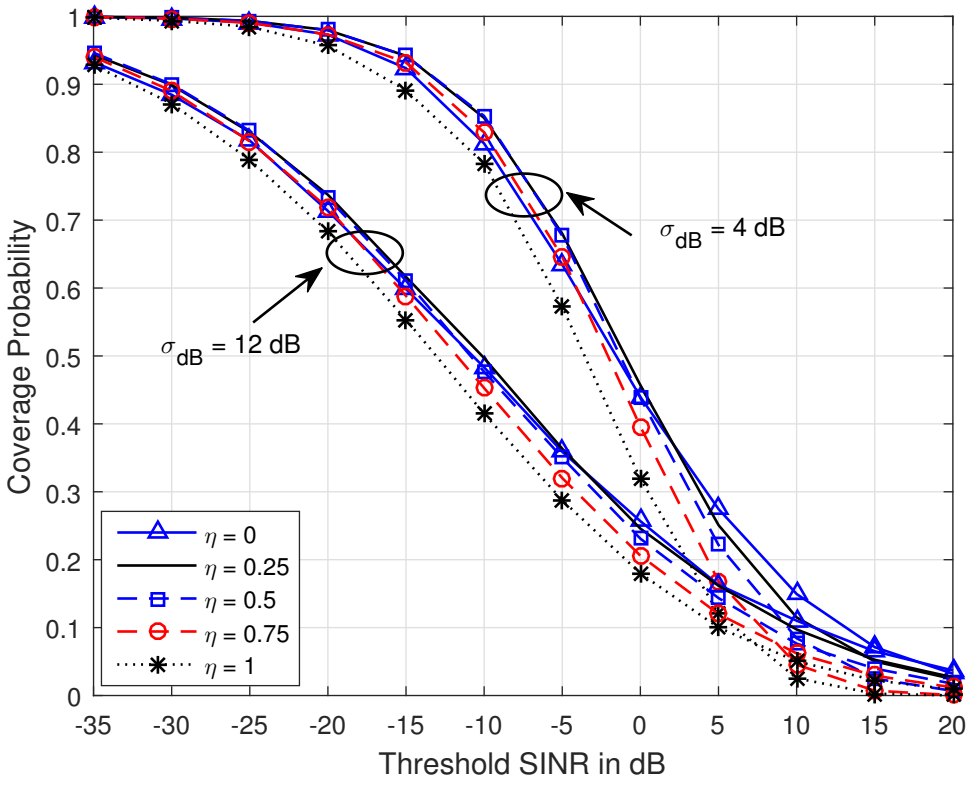

Figure 3.6: Variation of coverage of Scheme 1 vs SINR threshold for different η values. $\lambda = 0.5$ BSs/km^2, $\alpha = 3.5$, $N_0 = 0$.

shadowing severities considered.

Fig. 3.7 shows the coverage probability of Scheme 2 for various values of η and two levels of shadowing. Note that $\eta = 1$ represents complete compensation for path loss and shadowing, resulting in a constant received power level ρ at the serving BS. $\eta = 0$ represents no power control, resulting in each MS transmitting with constant power. At low SINR thresholds, complete compensation results in provides the highest coverage, while compensation for both path loss and shadowing ($\eta > 0$) results in higher coverage compared to that of no power control ($\eta = 0$). However, at high SINR thresholds, $\eta = 0$ results higher coverage probability. Also, Fig. 5 shows that the performance gap widens, when the shadowing standard deviation increases. Therefore, we can conclude that at low SINR thresholds complete elimination of shadow fading and path loss improves coverage, while at high SINR thresholds power control reduces the coverage probability.

Fig. 3.8 shows the variation of coverage probability with power control factor η

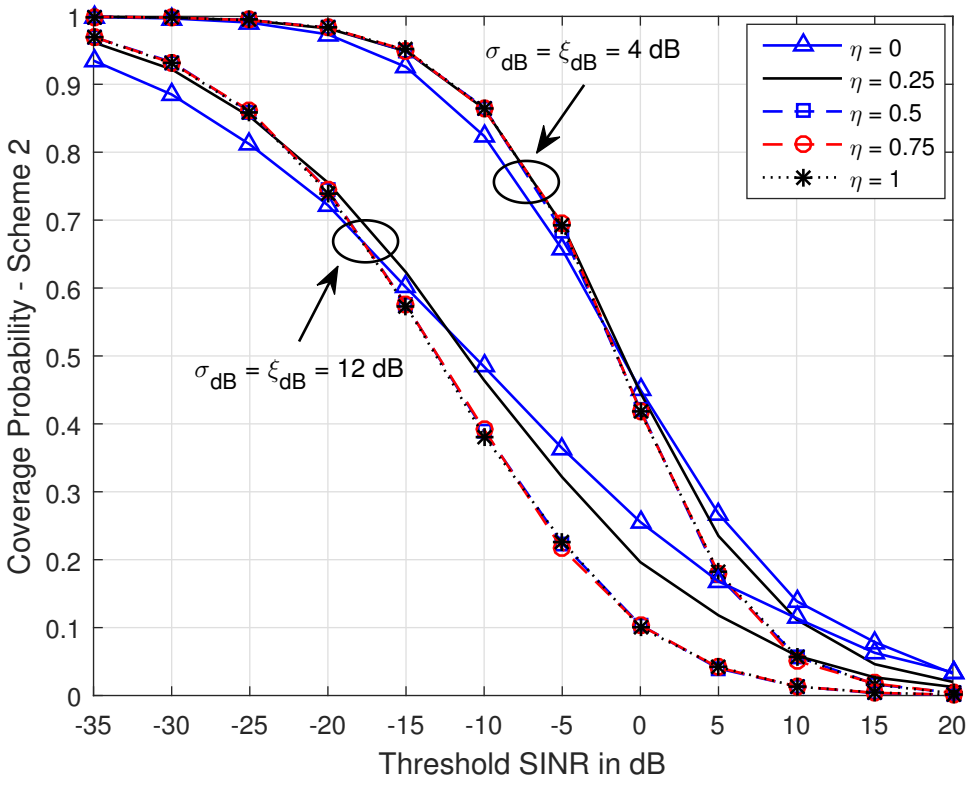

Figure 3.7: Coverage probability of Scheme 2 vs SINR threshold for different η values. $\lambda = 0.5$ BSs/km^2, $\alpha = 3.5$, $\rho = -30$ dBm, $N_0 = 0$.

for Scheme 3. When $\eta = 1$, both path loss and shadowing are fully compensated for, resulting in a constant received power level ρ at the serving BS for all the MSs regardless of the path loss and shadowing they experience. On the other hand $\eta = 0$ only compensates for shadowing. This provides higher coverage probability for higher SINR thresholds, but not otherwise. Also as the compensation factor increases above 0.5, coverage drops considerably. Therefore, we can conclude that at low SINR thresholds complete elimination of shadowing and partial compensation of path loss gives better coverage, while at high SINR thresholds inverting only the effect of shadowing improves coverage.

3.7 Conclusion

Three uplink power control schemes for cellular networks with path loss and composite Rayleigh-lognormal fading have been investigated. They are partial compensation of: (1) path loss only, (2) the aggregate effect of path loss and shadowing,

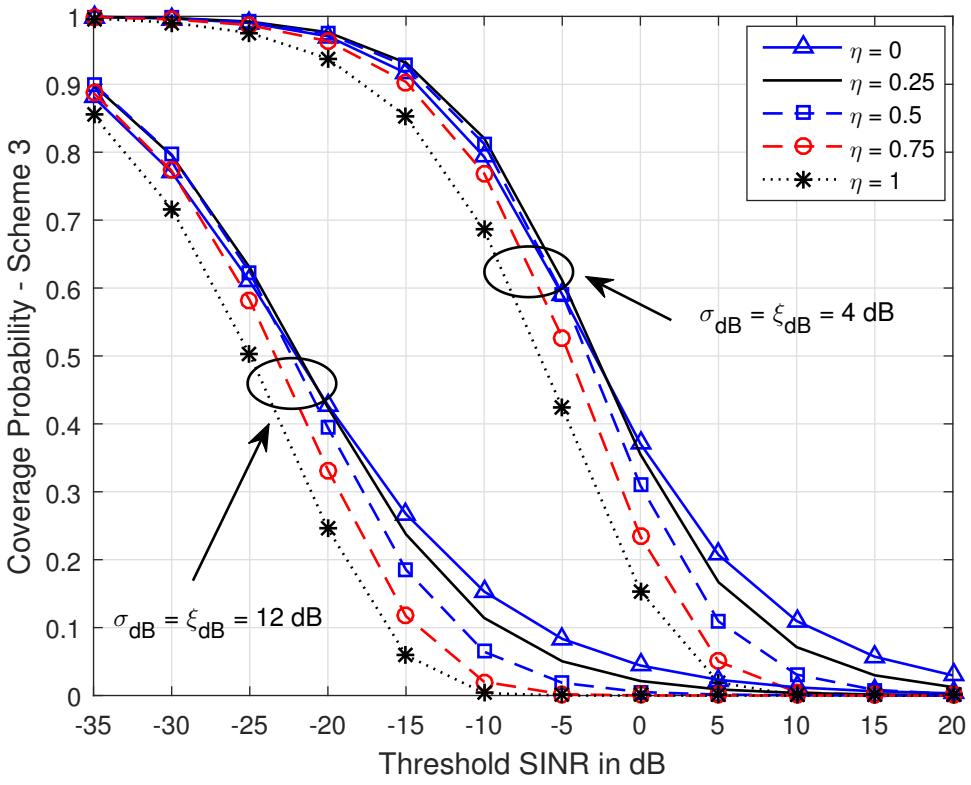

Figure 3.8: Coverage probability of Scheme 3 vs SINR threshold for different η values. $\lambda = 0.5$ BSs/km^2, $\alpha = 3.5$, $\rho = -30$ dBm, $N_0 = 0$.

and (3) path loss and complete inversion of shadowing. Approximate PDF and CDF expressions have been derived for the transmit power and the coverage probabilities. The results have been validated via simulations.

This study leads to several observations. First, shadowing clearly has negative impact on network coverage. Second, when the operating SINR is lower which is typically the case with cell-edge users or users subject to severe shadowing, compensating for the aggregate effect of path loss and shadowing (Scheme 2) improves coverage compared to the other two schemes. However, when the operating SINR is high which is the case for most cell center users or users close to the serving BS, inverting only path loss (Scheme 1) provides the best coverage. Further, of the three, power control Scheme 3 gives the worst coverage. Third, previous research has observed that the BS intensity has little effect on the coverage, when minimum path loss association and full path loss inversion power control (scheme 1 with $\eta = 1$) is used in uplink. We find the same holds true for scheme 1 and 3 for all shadowing lev-

els and $\eta < 1$. Further, it also holds for Scheme 2 under light shadowing. However, in all three schemes the extent to which path loss and shadowing are compensated has a significant effect on the coverage probability. Therefore, proper selection of uplink power control parameters is essential in cellular networks.

Chapter 4

Coverage and Rate Analysis for Limited Information Cell Association in Cellular Networks

The complexity and uncertainty inherent in large cellular networks make the acquisition of location and channel information of all but perhaps a few neighbouring network nodes [1] difficult for a given user. Therefore, a cell association policy must operate with sparse information. Thus, in this chapter [2] a new cell association policy is introduced which only requires channel state information of few neighboring users. In this policy the serving base station (BS) is the one that provides the highest instantaneous signal-to-interference-plus-noise ratio (SINR) from among all BSs providing average received signal power exceeding a predetermined minimum. This policy is evaluated for the downlink of single-tier (homogeneous) and two-tier (heterogeneous) networks, and for the latter the key advantage of the proposed policy is its capability to enable traffic off-loading. Two methods to determine the minimum average signal power are given. Coverage probabilities and average rates of mobile stations (MSs) in coverage are derived accounting for path loss, multipath fading and random locations of BSs in each tier. Analysis is verified by Monte-Carlo simulations. We observe that the instantaneous SINR and average received power of a few BSs are sufficient to achieve the coverage corresponding to the highest-SINR association, which in general requires instantaneous SINR information of a larger

[1] node = base station (BS)/access point (AP), user = mobile station (MS)

[2] A version of this chapter has been published in IEEE Transactions on Vehicular Technology [101]. A part of the contribution has also been published in 2014 IEEE 80th Vehicular Technology Conference, Vancouver, BC, Canada [102].

subset of a network. We also observe that in a two-tier network, the effect of strong interference from high power BSs, such as macro BSs, can be limited by proper choice of minimum average received power for low power BSs.

4.1 Introduction

As described in Section 1.2.2, in Heterogeneous network (HetNet) the cell association policy plays an important role in providing the best user-perceived rate [34]. Due to the uncertainty of locations of network nodes and users, many association policies have been studied under different spatial models for single-tier (homogeneous) and multi-tier (heterogeneous) networks [40,41,50,53,65,103–108]. Based on the metrics used for the serving BS selection , they can be classified into three categories

1. Closest-BS: Serving BS selection is based on BS-MS distances [40, 50, 53].
2. Highest-SINR (equivalently, highest-signal-to-interference ratio (SIR) in interference-limited networks): received SINR is used to select the serving BS [41,103–105].
3. Biased association: Serving BS selection is based on biased-SINR or biased-location [106–108].

In these studies, the locations of BSs in each tier are modeled with a homogeneous Poisson point process (PPP). The PPP [51] has extensively been used to model distributions of BSs and MSs [40–42, 49, 50, 53, 103–108] in the literature.

4.1.1 Prior related research

In the closest-BS policy, the serving BS is the closest one. Essentially, this policy ensures the highest area-averaged signal strength with the variation of the signal strength due to small- and large-scale fading are averaged out. Reference [40] investigates the coverage probability, normalized per user mean data rate and coverage gain (and mean rate loss) from static frequency reuse on the downlink of a single-tier network assuming spatial distribution of BSs follows a homogeneous PPP. The uplink performance with per-mobile power control is investigated in [53]. The downlink performance of multi-tier networks is investigated in [50]. Multiple tier BSs have different transmitted powers, supported data rates, and deployment densities. The spatial distribution of BSs in each tier is modeled using an independent homogeneous PPP.

In highest-SINR policy, the serving BS is the one offering the highest SINR. When BSs are fully loaded, transmitting and receiving packets on all their radio resource (time-frequency) blocks at all times, this strategy maximizes the sum throughput [34]. Performance of multi-tier networks under this policy is investigated in [41] and [104] assuming a system model similar to that of [50]. Reference [41] show that under this policy the coverage probability of an open access interference-limited network does not depend upon the number of tiers or the density of BSs when target threshold SIRs are the same for all the tiers. Reference [103] investigates the downlink coverage probability of a single-tier network under highest-SINR policy by characterizing the distribution of BSs with a non-homogeneous PPP.

In multi-tier networks, the area covered by each type of BS varies significantly. For example, a macro BS will provide umbrella coverage for an area covered by many pico BSs and femto access points (APs) (femto APs). Due to this reason, BSs with smaller coverage areas, such as pico BSs or femto APs, will have fewer active users and hence will be lightly loaded compared to macro BSs [34]. Therefore, smart cell association policies should be capable of off-loading users from highly loaded BSs to lightly loaded ones so that BSs offer them the best user-perceived rate [34]. This goal is achieved by introducing a bias into the association policy to account for the load of each type of BS. Performance of SINR-based biased association policies is investigated in [106,107]. In [108], Mukherjee investigates the downlink performance of both SINR- and location-based biased association policies.

Reference [109, 110] propose and investigate the performance of equivalent received power connectivity policy for multi-tier networks. In this policy a mobile user connects to the BS, from which it receives maximum equivalent power (received power in a given tier averaged over small- and large-scale fading, and divided by target SINR for that tier). When target SINRs are the same across multiple tiers, this policy is equivalent to the closest-BS association.

4.1.2 Motivation and Contribution

Contribution in this chapter is motivated by the following two key factors.

1. In large cellular networks channel state information available to an MS usually limited to only a few nodes [49]. Thus, the association policy must rely only on this limited information.

2. Due to the power-law path loss, the area-averaged received signal strength decays quickly with the distance between transmitter and receiver. In future generations of networks, this path loss may even increase with lower BS antennas and the use of higher frequencies. Therefore, higher the area-averaged received power from a BS to a user, higher the probability that it will provide the highest instantaneous SINR for the user.

These factors suggest that search for the best serving BS should be limited to a set of BSs providing the area-averaged received power (from here onward referred to as average received power) above a certain value. Motivated by these factors, we propose that a given user is served by the highest instantaneous SINR (from here onward referred to as SINR) BS from among BSs providing average received power above a predetermined value P_{th}. Thus, this policy requires only the instantaneous SINR and the average received power of a limited number of BSs, but not of the full network. The conventional highest-SINR association [41] can be considered as a special case of the new policy, i.e., when $P_{th} \to 0$. We consider two methods to determine P_{th}: (i) selecting a fixed value and (ii) iterative selection of P_{th}. We show that iterative selection of P_{th} considerably reduces the number of BSs to be tracked and hence the complexity of the cell association process.

This policy is also extended to two-tier macro pico deployments. These extensions assume different conditions for the availability of SINR and average received power of the pico BSs: (i) both SINR and average received power are available, (ii) only the average received power is available. In multi-tier networks, BSs with smaller coverage areas, such as pico BSs or femto APs, will necessarily serve fewer users and hence will be lightly loaded compared to macro BSs [34]. Therefore, a smart cell association policy should be capable of off-loading user traffic from highly loaded BSs to lightly loaded ones. It is shown that the proposed policy enables user off-loading in two-tier networks.

4.2 System Model

This section presents the system model considered in this study.

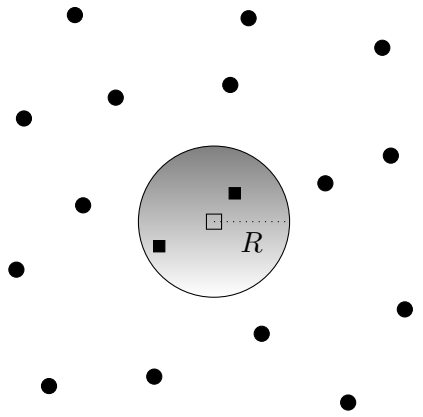

Figure 4.1: Randomly distributed BSs in $\mathbb{R}^2$ with MS at the center. Black squares - accessible BSs, black circles - inaccessible BSs.

4.2.1 System Model: Single Tier Networks

Consider downlink of a network with BSs distributed in $\mathbb{R}^d, d \in \{2, 3\}$ according to a homogeneous PPP Φ with intensity λ [42,51]. Multi-user downlink transmission is assumed. However, transmission to each user within a given cell occurs on a different time-frequency resource block; the resource blocks within each cell are orthogonal. Universal time-frequency channel reuse and a fully loaded network are also assumed. Hence, the worst intercell interference case is considered. Every BS transmits with power P_t. Rayleigh fading (with envelope power normalized to one) is assumed along with path loss. We will use the simplified power-law path loss model, where the received power P_r at a distance of r from the transmitter is given as $P_r = P_t r^{-\alpha}$. $\alpha > d$ is the path loss exponent. The condition $\alpha > d$ is necessary to maintain a finite received power at each MS. In the proposed cell association policy serving BS is the one, which provides the highest SINR among all BSs meeting average received power requirement (from here onward referred to as candidate BSs). Since simplified path loss model is assumed, P_{th} defines a maximum distance $R = \left(\frac{P_t}{P_{th}}\right)^{\frac{1}{\alpha}}$ a candidate BSs can be located from an MS (see Figure 4.1). The highest-SINR association [41] is a special case of the new policy when $P_{th} \to 0$ or equivalently $R \to \infty$.

In practice, MS-BS association is based on received signal strength indicator (RSSI) measurements from all available BSs (BSs that provide a meaningful RSSI). The association scheme proposed in this study can be implemented by imposing a cut-off threshold value for the area-averaged RSSI to select a subset of BSs out of all

the available BSs, and then choosing the BS with the highest instantaneous RSSI to serve a given MS. With that only the instantaneous RSSI of the selected subset of BSs and the average RSSI of available BSs need to be tracked. The selected subset of BSs should be updated periodically to account for the mobility of the MS and for changes in the radio wave propagation environment with time.

4.3 Coverage Probability Analysis

In this section first the coverage probability of a single-tier network is derived. Subsequently two methods for the selection of P_{th} for cell association are presented.

4.3.1 Coverage Probability Analysis: Single-Tier Network

Without loss of generality, we consider an MS located at the center of $\mathbb{R}^d$. As described in Section 4.2.1, the minimum average received power requirement for candidate BSs divides the original space $\mathbb{R}^d$, over which the BSs are distributed, into two disjoint sub-spaces: $S_1 = \{x \in \mathbb{R}^d : ||x|| \leq R\}$ and $S_2 = \{x \in \mathbb{R}^d : ||x|| > R\}$, where $R = \left(\frac{P_t}{P_{th}}\right)^{\frac{1}{\alpha}}$. Candidate BSs are distributed in the space S_1. According to the restriction theorem [52], BSs residing in S_1 and S_2 form two independent PPPs: Φ_1 and Φ_2, respectively. Assuming the MS is connected to a BS at point $y \in \Phi_1$[3], SINR of the MS can be written as

$$\text{SINR}(y) = \frac{||y||^{-\alpha} g_y}{\sum_{w \in \Phi_{1\setminus y}} ||w||^{-\alpha} g_w + \sum_{z \in \Phi_2} ||z||^{-\alpha} g_z + N_0} = \frac{||y||^{-\alpha} g_y}{I_{1\setminus y} + I_2}, \tag{4.1}$$

where g_y, g_w, and g_z represent the power gains due to multipath fading (fading coefficients). $\Phi_{1\setminus y}$ denotes Φ_1 excluding BS y. The variance of additive white Gaussian noise (AWGN) is given by N_0. $I_{1\setminus y} = \sum_{w \in \Phi_{1\setminus y}} ||w||^{-\alpha} g_w$ is the total interference power from all the BSs in Φ_1, when MS is connected to BS at the point y and all the BSs transmit with unity power. $I_2 = \sum_{z \in \Phi_2} ||z||^{-\alpha} g_z$ is the total interference power from Φ_2 when all BSs transmit with unity power. The resulting SINR at the MS is given by

$$\text{SINR} = \mathbf{max}_{y \in \Phi_1}\{\text{SINR}(y)\}. \tag{4.2}$$

[3]With slight abuse of notation we will use y to denote both the location of MS and MS itself. Similarly for w and z.

An MS is considered to be in coverage, when its SINR equals or exceeds a given threshold T. Using a similar approach to that in [41], the coverage probability $P_c(T)$ under the new cell association policy can be expressed as

$$\begin{aligned} P_c(T) &= \Pr\left(\bigcup_{y\in\Phi_1} \text{SINR}(y) \geq T\right), \\ &\leq \mathcal{E}\left[\sum_{y\in\Phi_1} \mathbf{1}\left(\text{SINR}(y) \geq T\right)\right], \end{aligned} \tag{4.3}$$

The bound is the union bound on $P_c(T)$. Using Lemma 1 of [41], it can be easily shown that the union bound is exact for threshold SINRs $T > 0$ dB and is an upper bound for $T < 0$ dB. Now (4.3) can be written as

$$\begin{aligned} P_c(T) &\overset{a}{\leq} \lambda \int_{S_1} \Pr\left(g_y \geq \frac{T(I_{1\setminus y} + I_2 + N_0)}{||y||^{-\alpha}}\right) dy, \\ &\overset{b}{\leq} \lambda \int_{S_1} \mathcal{E}_{I_{1\setminus y}+I_2}\left[\exp\left(-\frac{T(I_{1\setminus y} + I_2 + N_0)}{||y||^{-\alpha}}\right)\right] dy, \\ &\overset{c}{\leq} \lambda \int_{S_1} \exp\left(-\frac{TN_0}{||y||^{-\alpha}}\right) \mathcal{L}_{I_{1\setminus y}+I_2}\left(\frac{T}{||y||^{-\alpha}}\right) dy, \end{aligned} \tag{4.4}$$

where (a) follows from the Campbell-Mecke theorem [51] and (b) follows from $g_y \sim \exp(1)$. (c) follows form the definition of the Laplace transform. $S_1 = \{x \in \mathbb{R}^d : ||x|| \leq R\}$. $\mathcal{L}_{I_{1\setminus y}+I_2}(s)$ can be derived as shown in the following [102].

Since the fading coefficients are independent and two PPPs Φ_1 and Φ_2 are independent of each other and independent of the fading processes, $I_{1\setminus y}$ and I_2 are statistically independent. Therefore,

$$\mathcal{L}_{I_{1\setminus y}+I_2}(s) = \mathcal{E}_{\Phi_1,g_w}\Big[\exp(-s\sum_{w\in\Phi_1\setminus y} ||w||^{-\alpha} g_w)\Big] \mathcal{E}_{\Phi_2,g_z}\Big[\exp(-s\sum_{z\in\Phi_2} ||z||^{-\alpha} g_z)\Big]. \tag{4.5}$$

Since Rayleigh fading is assumed $g_w \sim \exp(1)$ and $g_z \sim \exp(1)$. Therefore,

$$\mathcal{L}_{I_{1\setminus y}+I_2}(s) = \mathcal{E}_{\Phi_1}\Big[\prod_{w\in\Phi_1\setminus y} \frac{1}{1+s||w||^{-\alpha}}\Big] \mathcal{E}_{\Phi_2}\Big[\prod_{z\in\Phi_2} \frac{1}{1+s||z||^{-\alpha}}\Big]. \tag{4.6}$$

Using the Slivnyak-Mecke theorem [51] along with the definition of probability gen-

erating functional of PPP [51] we get:

$$\begin{aligned}\mathcal{L}_{I_{1\setminus y}+I_2}(s) =& \exp\Big[-\lambda \int_{S_1} \Big(1-\frac{1}{1+s||w||^{-\alpha}}\Big)\,dw\Big],\\ &\times \exp\Big[-\lambda \int_{S_2} \Big(1-\frac{1}{1+s||z||^{-\alpha}}\Big)\,dz\Big],\\ =& \exp\Big[-\lambda \int_{\mathbb{R}^d} \Big(1-\frac{1}{1+s||u||^{-\alpha}}\Big)\,du\Big]. \end{aligned} \tag{4.7}$$

Converting from Cartesian to polar/spherical coordinates, for d-dimensional networks (4.7) can be written as

$$\begin{aligned}\mathcal{L}_{I_{1\setminus y}+I_2}(s) =& \exp\left[-\kappa_d \pi \lambda \int_0^{\infty} r^{d-1}\Big(1-\frac{1}{1+sr^{-\alpha}}\Big)dr\right],\\ =& \exp\left[\frac{-\kappa_d \pi^2 \lambda s^{\frac{d}{\alpha}}}{\alpha \sin\left(\frac{d\pi}{\alpha}\right)}\right], \end{aligned} \tag{4.8}$$

where $\kappa_2 = 2$, and $\kappa_3 = 4$. Converting (4.4) from Cartesian to polar/spherical coordinates and substituting (4.8) in this new expression, $P_c(T)$ for d-dimensional networks can be expressed as

$$P_c(T) \leq \left[1-\exp\left(\frac{-\kappa_d \pi^2 \left(\frac{P_t T}{P_{th}}\right)^{\frac{d}{\alpha}} \lambda}{\alpha \sin\left(\frac{d\pi}{\alpha}\right)}\right)\right] \frac{\alpha \sin\left(\frac{d\pi}{\alpha}\right)}{d\pi T^{\frac{d}{\alpha}}}. \tag{4.9}$$

According to (4.9), the impact of λ on $P_c(T)$ diminishes as $P_{th} \to 0$. A similar observation is made for 2-D networks in Corollary 1 of [41].

Selection of Minimum Average Received Power P_{th}

We know that if P_{th} is too large, no BS is likely to be selected as a candidate BS, which will put the MS into outage. Conversely, if P_{th} is too small, too many BSs will be selected as candidate BSs, increasing the complexity of the association. Thus, P_{th} should be chosen such that more than n (≥ 1) BSs provide average received power above P_{th} with a reasonably high probability q. For example, $n = 2$ and $q = 0.95$ will guarantee that two candidate BSs are available with a probability of 0.95. For a network with a homogeneous PPP distribution of BSs, P_{th} for selected set of values for n and q can be computed as follows.

Let P_n be the nth highest average received power from BSs. Since the average received power only depends on the path loss and BS transmitted power, which is assumed to be constant, P_n is the average received power from nth closest BS to

the MS. The cumulative distribution function (CDF) of the random variable P_n is given by

$$\begin{aligned} F_{P_n}(z) &= \Pr\left[P_t r_n^{-\alpha} \leq z\right], \\ &= 1 - \Pr\left[r_n \leq \left(\frac{P_t}{z}\right)^{\frac{1}{\alpha}}\right], \end{aligned} \tag{4.10}$$

where r_n is the Euclidean distance between an MS and its nth closest BS in $\mathbb{R}^d$. The CDF of r_n is given by [111]

$$F(r_n) = 1 - \frac{\Gamma(n, \lambda c_d r_n^d)}{(n-1)!},\ 0 < r_n < \infty, \tag{4.11}$$

where $c_2 = \pi$, $c_3 = 4\pi/3$. Substituting (4.11) in (4.10),

$$F_{P_n}(z) = \frac{\Gamma\left(n, \lambda c_d \left(\frac{P_t}{z}\right)^{\frac{d}{\alpha}}\right)}{(n-1)!},\ 0 < z < \infty. \tag{4.12}$$

Therefore, in $\mathbb{R}^d$, for a given number of BSs n and probability $q = 1 - F_{P_n}(P_{th})$, P_{th} can be computed as

$$P_{th} = P_t \left[\frac{\lambda c_d}{\Gamma^{-1}\left(n, (n-1)!(1-q)\right)}\right]^{\frac{\alpha}{d}}. \tag{4.13}$$

Improving P_c by iterative decrease of P_{th}

The second way to select P_{th} is to use an adaptive update. The problem of selecting too many BSs as candidate BSs can be alleviated by initializing the association with a large value for P_{th} (equivalently, small n and q), and decreasing it iteratively. For example, a system may select the initial minimum association received power $P_{th}^{(0)}$ by selecting lower values for n and q, $n^{(0)}$ and $q^{(0)}$ (e.g., $n^{(0)} = 1$ and $q^{(0)} = 0.9$, which guarantees at least one BS given $P_{th}^{(0)}$, 90% of the time). If no BS to associate with is found, P_{th} can be decreased iteratively N times (e.g., with $N = 2$, new minimum association received power after 1st iteration $P_{th}^{(1)}$ is selected with $n^{(1)} = 1$ and $q^{(1)} = 0.99$, which guarantees one BS 99% of the time; in the second iteration, $P_{th}^{(2)}$ with $n^{(2)} = 1$ and $q^{(2)} = 0.999$). This process is implemented by Algorithm 1 listed below. In Section 4.5 it is shown that the iterative selection of P_{th} considerably reduces the number of BSs to be scanned, therefore it lowers the complexity of the association process.

4.3.2 Extensions for Two-Tier Heterogeneous Networks

Consider a two-tier network consisting of macro and pico BSs. Two cases are considered for the availability of average received power and SINR information of pico

Algorithm 1 Cell association with iterative decrease of P_{th}

Input: $\lambda, \alpha, P_t, N, n^{(j)}$ and $q^{(j)}$ $j \in \{1, 2, ..., N\}$

$P_{th}^{(0)} \leftarrow$ *calculate starting value of* P_{th}, *use eq. (4.13) with* $n = n^{(0)}$ and $q = q^{(0)}$

$i^{(0)} \leftarrow$ number of *BSs providing* $P_{th}^{(0)}$

if $i^{(0)} \geq n^{(0)}$ **then**

  selected BS $\leftarrow$ *BS with highest SINR among those providing* $P_{th}^{(0)}$

else

  $j \leftarrow 1$

  while $i^{(j)} < n^{(j)}$, $j \leq N$ **do**

    $P_{th}^{(j)} \leftarrow$ calculate jth value of P_{th}, *use eq. (4.13)* with $n = n^{(j)}$ and $q = q^{(j)}$

    $i^{(j)} \leftarrow$ number of *BSs providing* $P_{th}^{(j)}$

    $j \leftarrow j + 1$

  end while

  selected BS $\leftarrow$ *BS with highest SINR among those providing* $P_{th}^{(j)}$

end if

BSs: (i) both SINR information and average received power are available, (ii) only the average received power is available.

For case (i), association policy attempts to select a pico BS providing average received power exceeding P_{th}. If only one pico BS is available, the MS associates with it. When more than one pico BSs are available, one providing the highest instantaneous SINR is selected. If the average received powers from all the pico BSs are lower than P_{th}, the macro BS providing the highest average SINR is selected as the serving BS. This is equivalent to associating with the closest macro BS. The ability to manage user off-loading to small cells by P_{th} is among the advantages of this association policy. For example, 70% of users will be served by pico BSs, when P_{th} is selected with $q = 0.7$ and $n = 1$ (70% of the time there is at least one pico BS providing average received power exceeding P_{th}). For case (ii), each MS connects to the pico BS providing maximum average received power (equivalently the BS providing maximum average SINR), if its received power exceeds P_{th}. If this fails, it is connected to the macro BS providing the highest average SINR.

Two-Tier Network: Network Parameters

We characterize the spatial distribution of macro and pico BSs by two independent homogeneous PPPs Φ_m and Φ_p with intensities λ_m and λ_p, respectively. Macro

BSs transmit with power P_m, while pico BSs transmit with power P_p. All the links are assumed to be subject to path loss (as in Section 4.2.1) and multipath fading. Path loss exponents of macro BSs and pico BSs are given by α_m and α_p ($\alpha_m, \alpha_p > 2$). Target SINR thresholds of macro BSs and pico BSs are T_m and T_p, respectively. Multi-user downlink transmission is assumed, as described in detail in the first paragraph of Section 4.2.1.

4.3.3 Coverage Probability Analysis: Two-Tier Networks

This section presents the coverage probability analysis for two cases, namely (i) both instantaneous SINR and average received power of pico BSs are available (ii) only average received power is available. Without loss of generality the coverage probability of an MS located at the center of the network is considered.

4.3.4 Both Instantaneous SINR and Average Received Power Available

When both SINR and average received power of pico BSs are available, the proposed association policy selects the pico BS providing the maximum instantaneous SINR from those providing average received power exceeding P_{th}. If no pico BS is found to provide such average power, the macro BS with the highest average SINR is selected as the serving BS. Using the theorem on total probability the coverage probability can be expressed as

$$P_c(T_m, T_p) = P_v P_c^{\text{macro}}(T_m) + (1 - P_v) P_{c|r_u<R_p}^{\text{pico}}(T_p), \tag{4.14}$$

where $r_u = ||u||$ is the distance between the closest pico BS $u \in \Phi_p$ and the MS. $R_p = \left(\frac{P_p}{P_{th}}\right)^{\frac{1}{\alpha_p}}$. $P_c^{\text{macro}}(T_m)$ is the coverage probability when the MS is served by the macro BS providing the highest average SINR given that there is no pico BS providing P_{th}. $P_{c|r_u<R_p}^{\text{pico}}(T_p)$ gives the coverage probability, when the MS is served by the highest SINR pico BS out of those providing P_{th}. P_v represents the probability that no pico BS is found to provide P_{th} at the MS. P_v can be derived as

$$P_v = \Pr\left(P_p r_u^{-\alpha_p} < P_{th}\right) = \Pr\left(r_u > \left(\frac{P_p}{P_{th}}\right)^{\frac{1}{\alpha_p}}\right). \tag{4.15}$$

$\Pr\left(r_u > \left(\frac{P_p}{P_{th}}\right)^{\frac{1}{\alpha_p}}\right)$ is the probability that no pico BS is found within distance $\left(\frac{P_p}{P_{th}}\right)^{\frac{1}{\alpha_p}}$ from the MS. Since pico BSs are distributed according to a PPP with

intensity λ_p,

$$P_v = \exp\left(-\lambda_p \pi \left(\frac{P_p}{P_{th}}\right)^{\frac{2}{\alpha_p}}\right). \tag{4.16}$$

Using a similar approach to the derivation of (4.3) and (4.4), $\hat{P}^{\text{pico}}_{c|r_u<R_p}(T_p) = (1 - P_v)P^{\text{pico}}_{c|r_u<R_p}(T_p)$ can be derived as follows [102]:

$$\begin{aligned}
\hat{P}^{\text{pico}}_{c|r_u<R_p}(T_p) &\leq \lambda_p \int_{\mathcal{A}_\mathcal{R}} \Pr\left(g_y \geq \frac{T_p(I_{p\setminus y} + I_m + N_0)}{P_p||y||^{-\alpha_p}}\right) dy, \\
&\overset{a}{\leq} \lambda_p \int_{\mathcal{A}_\mathcal{R}} \exp\left(-\frac{T_p N_0}{P_p||y||^{-\alpha}}\right) \mathcal{L}_{I_{p\setminus y}+I_m}\left(\frac{T_p}{P_p||y||^{-\alpha_p}}\right) dy, \\
&\leq 2\pi\lambda_p \int_0^{R_p} r \exp\left(-\frac{T_p N_0}{P_p r^{-\alpha}}\right) \mathcal{L}_{I_{p\setminus y}+I_m}\left(\frac{T_p}{P_p r^{-\alpha_p}}\right) dr,
\end{aligned} \tag{4.17}$$

where $\mathcal{A}_R$ represents the circular region around the MS with radius R_p. Step (a) follows from the Rayleigh fading assumption. $I_{p\setminus y}$ represents the aggregate interference from pico BSs when MS is served by pico BS located at $y \in \Phi_p$. I_m represents the aggregate interference from macro BSs. Similarly to (4.4), the expression (4.17) is exact for threshold SINRs $T_p > 0$ dB and is an upper bound for $T_p < 0$ dB. Since fading coefficients are independent and identically distributed (i.i.d.) and the fading processes are independent from PPPs $\mathcal{L}_{I_{p\setminus y}+I_m}(s) = \mathcal{L}_{I_{p\setminus y}}(s) \times \mathcal{L}_{I_m}(s)$. $\mathcal{L}_{I_{p\setminus y}}(s)$ can be obtained by replacing s, λ, and α in (4.8) with sP_p, λ_p, and α_p, respectively.

$$\mathcal{L}_{I_{p\setminus y}}(s) = \exp\left[\frac{-2\pi^2\lambda_p(sP_p)^{\frac{2}{\alpha_p}}}{\alpha_p \sin\left(\frac{2\pi}{\alpha_p}\right)}\right]. \tag{4.18}$$

Following similar steps to those in the derivation of (4.8), $\mathcal{L}_{I_m}(s)$ can be expressed as

$$\begin{aligned}
\mathcal{L}_{I_m}(s) &= \mathcal{E}_{\Phi_m}\left[\prod_{x\in\Phi_m} \mathcal{E}_{g_x}\left[\exp(-sP_m||x||^{-\alpha_m} g_x)\right]\right], \\
&= \exp\left[\frac{-2\pi^2\lambda_m(sP_m)^{\frac{2}{\alpha_m}}}{\alpha_m \sin\left(\frac{2\pi}{\alpha_m}\right)}\right].
\end{aligned} \tag{4.19}$$

$P^{\text{macro}}_c(T_m)$ can be derived as shown in the following. When MS is served by the highest average SINR macro BS $z \in \Phi_m$, SINR is given by

$$\text{SINR}(z) = \frac{P_m r_z^{-\alpha_m} g_z}{\sum\limits_{x\in\Phi_m\setminus z} P_m||x||^{-\alpha_m} g_x + \sum\limits_{y\in\Phi_p, ||y||>R_p} P_p||y||^{-\alpha_p} g_y + N_0}, \tag{4.20}$$

where distance between MS and the highest average SINR macro BS (equivalently, the closest macro BS) is denoted by $r_z = ||z||$. Therefore, $P_c^{\text{macro}}(T_m)$ is given by [102]:

$$\begin{aligned} P_c^{\text{macro}}(T_m) &= \Pr\Big[\frac{P_m r_z^{-\alpha_m} g_z}{I_{m\setminus z} + I_{p\setminus\mathcal{A}_\mathcal{R}} + N_0} \geq T_m\Big], \\ &= \int_0^\infty \Pr\Big[\frac{P_m r_z^{-\alpha_m} g_z}{I_{m\setminus z} + I_{p\setminus\mathcal{A}_\mathcal{R}} + N_0} \geq T_m \Big| r_z = t\Big] f_{r_z}(t)dt, \\ &= \int_0^\infty \Pr\Big[g_z \geq \frac{T_m\left(I_{m\setminus z} + I_{p\setminus\mathcal{A}_\mathcal{R}} + N_0\right)}{P_m r_z^{-\alpha_m}} \Big| r_z = t\Big] f_{r_z}(t)dt. \end{aligned} \tag{4.21}$$

Here, $I_{m\setminus z} = \sum_{x\in\Phi_{m\setminus z}} P_m||x||^{-\alpha_m} g_x$ and $I_{p\setminus\mathcal{A}_\mathcal{R}} = \sum_{y\in\Phi_p, ||y||>R_p} P_p||y||^{-\alpha_p} g_y$. As fading follows Rayleigh fading with unity variance, $g_z \sim \exp(1)$. Therefore,

$$\begin{aligned} P_c^{\text{macro}}(T_m) = \int_0^\infty \mathcal{E}_{I_{m\setminus z}+I_{p\setminus\mathcal{A}_\mathcal{R}}|r_z=t} \left[\exp\left(-\frac{T_m\left(I_{m\setminus z}+I_{p\setminus\mathcal{A}_\mathcal{R}}+N_0\right)}{P_m r_z^{-\alpha_m}}\right)\right] \\ \times f_{r_z}(t)dt. \end{aligned} \tag{4.22}$$

Using the definition of the Laplace transform

$$\begin{aligned} P_c^{\text{macro}}(T_m) = \int_0^\infty \exp\left(-\frac{T_m N_0}{P_m r_z^{-\alpha_m}}\right) \mathcal{L}_{I_{m\setminus z}+I_{p\setminus\mathcal{A}_\mathcal{R}}|r_z=t}\left(\frac{T_m}{P_m t^{-\alpha_m}}\right) \\ \times f_{r_z}(t)dt. \end{aligned} \tag{4.23}$$

The probability density function of r_z is given by [111]

$$f_{r_z}(t) = 2\pi\lambda_m t \exp\left(-\lambda_m \pi t^2\right),\ t > 0. \tag{4.24}$$

$\mathcal{L}_{I_{m\setminus z}+I_{p\setminus\mathcal{A}_\mathcal{R}}}(s)$ can be derived as shown in the following [102].

Since fading coefficients are independent and identically distributed (i.i.d.) and two PPPs Φ_m and Φ_p are independent of each other interferences $I_{m\setminus z}$ and $I_{p\setminus\mathcal{A}_\mathcal{R}}$ are statistically independent. Therefore, the Laplace transform of the sum of inference can be written and the product of individual interference terms.

$$\mathcal{L}_{I_{m\setminus z}+I_{p\setminus\mathcal{A}_\mathcal{R}}|r_z=t}(s) = \mathcal{L}_{I_{m\setminus z}|r_z=t}(s) \times \mathcal{L}_{I_{p\setminus\mathcal{A}_\mathcal{R}}}(s). \tag{4.25}$$

Using the definition of the Laplace transform

$$\begin{aligned} \mathcal{L}_{I_{m\setminus z}+I_{p\setminus\mathcal{A}_\mathcal{R}}|r_z=t}(s) = &\mathcal{E}_{\Phi_m,g_x}\left[\exp(-s\sum_{x\in\Phi_{m\setminus z}} P_m||x||^{-\alpha_m} g_x)\right] \\ &\times \mathcal{E}_{\Phi_p,g_y}\left[\exp(-s\sum_{y\in\Phi_p,||y||>R_p} P_p||y||^{-\alpha_p} g_y)\right]. \end{aligned} \tag{4.26}$$

Using the fact that PPPs and fading processes are statistically independent and fading coefficients are i.i.d.

$$\mathcal{L}_{I_{m\setminus z}+I_{p\setminus\mathcal{A}_{\mathcal{R}}}|r_z=t}(s) = \mathcal{E}_{\Phi_m}\Big[\prod_{x\in\Phi_{m\setminus z}} \mathcal{E}_{g_x}\big[\exp(-sP_m||x||^{-\alpha_m}g_x)\big]\Big] \times \mathcal{E}_{\Phi_p}\Big[\prod_{y\in\Phi_p,||y||>R_p} \mathcal{E}_{g_y}\big[\exp(-sP_p||y||^{-\alpha_p}g_y)\big]\Big]. \tag{4.27}$$

As $g_x \sim \exp(1)$ and $g_y \sim \exp(1)$, taking the expectation over g_x and g_y

$$\mathcal{L}_{I_{m\setminus z}+I_{p\setminus\mathcal{A}_{\mathcal{R}}}|r_z=t}(s) = \mathcal{E}_{\Phi_m}\Big[\prod_{x\in\Phi_{m\setminus z}} \frac{1}{1+sP_m||x||^{-\alpha_m}}\Big] \times \mathcal{E}_{\Phi_p}\Big[\prod_{y\in\Phi_p,||y||>R_p} \frac{1}{1+sP_p||y||^{-\alpha_p}}\Big]. \tag{4.28}$$

Follows from the definition of probability generating functional of PPP [51] and by converting from Cartesian to polar coordinates

$$\mathcal{L}_{I_{m\setminus z}+I_{p\setminus\mathcal{A}_{\mathcal{R}}}|r_z=t}(s) \overset{e}{=} \exp\Big[-2\pi\lambda_m\int_t^\infty u\Big(1-\frac{1}{1+sP_mu^{-\alpha_m}}\Big)du\Big] \times \exp\Big[-2\pi\lambda_p\int_{R_p}^\infty v\Big(1-\frac{1}{1+sP_pv^{-\alpha_p}}\Big)dv\Big]. \tag{4.29}$$

Solving two integrations $\mathcal{L}_{I_{m\setminus z}+I_{p\setminus\mathcal{A}_{\mathcal{R}}}|r_z=t}(s)$ can be written as

$$\mathcal{L}_{I_{m\setminus z}+I_{p\setminus\mathcal{A}_{\mathcal{R}}}|r_z=t}(s) = \exp\Big[\frac{-2\pi\lambda_mP_mt^{2-\alpha_m}s\ {}_2F_1\big[1,\frac{\alpha_m-2}{\alpha_m};2-\frac{2}{\alpha_m},\frac{-P_ms}{t^{\alpha_m}}\big]}{\alpha_m-2}\Big] \times \exp\Big[\frac{-2\pi\lambda_pP_p^{\frac{2}{\alpha_p}}P_{th}^{1-\frac{2}{\alpha_p}}s\ {}_2F_1\big[1,\frac{\alpha_p-2}{\alpha_p};2-\frac{2}{\alpha_p},-sP_{th}\big]}{\alpha_p-2}\Big]. \tag{4.30}$$

4.3.5 Only Average Received Power Available

When only average received powers of pico BSs are available, each MS attempts to connect to the pico BS with the highest average received power, if the average received power from it exceeds P_{th}. Essentially, this is connecting to the closest pico BS if it meets the minimum average received power requirement. If no pico BS is found providing P_{th}, MS associates with the macro BS providing the highest average SINR. The coverage probability of the network for this case can be derived as follows. From the theorem on total probability

$$P_c(T_m,T_p) = (1-P_v)\tilde{P}^{\text{pico}}_{c|r_u<R_p}(T_p) + P_vP_c^{\text{macro}}(T_m), \tag{4.31}$$

where $\tilde{P}^{\text{pico}}_{c|r_u<R_p}(T_p)$ is the coverage probability, when the user is served by the pico BS with the highest average received power provided that the average received power exceeds P_{th}. P_v and $P_c^{\text{macro}}(T_m)$ are given by (4.16) and (4.23), respectively. Using the definition of conditional probability $(1-P_v)\tilde{P}^{\text{pico}}_{c|r_z<R_p}(T_p)$ can be expressed as

$$(1-P_v)\tilde{P}^{\text{pico}}_{c|r_u<R_p}(T_p) = \Pr\left[\frac{P_p r_u^{-\alpha_p} g_u}{I_{p\backslash u}+I_m+N_0} \geq T_p, r_u < R_p\right],$$
$$= \int_0^{R_p} \Pr\left[g_u > \frac{T_p(I_{p\backslash u}+I_m+N_0)}{P_p r_u^{-\alpha_p}} | r_u = t\right] f_{r_u}(t)dt, \quad (4.32)$$

where $I_{p\backslash u}$ is the total interference from all other pico BSs when MS is connected to the pico BS with the highest average received power provided that the average received power exceeds P_{th}. g_u is the fading power gain. $f_{r_u}(t)$ is the PDF of r_u, distance from the MS to the pico BS with the highest average received power (equivalently, the closest pico BS) from the MS. Since $g_u \sim \exp(1)$, (4.32) can be written as

$$(1-P_v)\tilde{P}^{\text{pico}}_{c|r_u<R_p}(T_p) = 2\pi\lambda_p \int_0^{R_p} t\ \mathcal{L}_{I_{p\backslash u}+I_m|r_u=t}\left(\frac{T_p t^{\alpha_p}}{P_p}\right)$$
$$\times \exp\left(-\lambda_p \pi t^2 - \frac{T_p N_0}{P_p t^{-\alpha_p}}\right) dt, \quad (4.33)$$

where $\mathcal{L}_{I_{p\backslash u}+I_m|r_u=t}(s)$ represents the Laplace transform of $I_{p\backslash u|r_u=t}+I_m(s)$ with respect to s. Since $I_{p\backslash u|r_u=t}$ and I_m are statistically independent, $\mathcal{L}_{I_{p\backslash u}+I_m|r_u=t}(s) = \mathcal{L}_{I_{p\backslash u}|r_u=t}(s) \times \mathcal{L}_{I_m}(s)$. $\mathcal{L}_{I_m}(s)$ is given by (4.19). Following a similar approach to the derivation of $\mathcal{L}_{I_{m\backslash z}|r_z=t}(s)$ in (4.30), $\mathcal{L}_{I_{p\backslash u}|r_u=t}(s)$ can be obtained as

$$\mathcal{L}_{I_{p\backslash u}|r_u=t}(s) = \exp\left[-2\pi\lambda_p \int_t^{\infty} y\left(1-\frac{1}{1+sP_p y^{-\alpha_p}}\right)dy\right],$$
$$= \exp\left[\frac{-2\pi\lambda_p P_p t^{2-\alpha_p} s\ {}_2F_1\left[1, \frac{\alpha_p-2}{\alpha_p}; 2-\frac{2}{\alpha_p}, \frac{-P_p s}{t^{\alpha_p}}\right]}{\alpha_p - 2}\right]. \quad (4.34)$$

4.4 Achievable Rate Analysis

In this section, the average rate achievable by a randomly chosen MS in coverage is investigated. First, average rate of an MS in a single-tier network is derived. Subsequently, the derived expression is extended to two-tier networks.

4.4.1 Single-Tier Networks

The average rate achievable by a randomly chosen MS in coverage in a single-tier network can be expressed as

$$R^{\text{1-tier}} = \mathcal{E}_{\text{SINR}|\text{SINR} \geq T} \left[\ln \left(1 + \text{SINR} \right) \right]. \tag{4.35}$$

Here $\text{SINR} = \mathbf{max}_{y \in \Phi_1} \{\text{SINR}(y)\}$ where, $\text{SINR}(y)$ is given by (4.1). Since the expectation of any positive random variable X is given by $\mathcal{E}[X] = \int_0^\infty \Pr(x > z) dz$,

$$\begin{aligned} R^{\text{1-tier}} &= \int_0^\infty \Pr \left[\ln(1 + \text{SINR}) > z | \text{SINR} \geq T \right] dz, \\ &= \int_0^\infty \Pr \left[\text{SINR} > e^z - 1 | \text{SINR} \geq T \right] dz. \end{aligned} \tag{4.36}$$

Using the definition of conditional probability

$$\begin{aligned} R^{\text{1-tier}} &= \int_0^\infty \frac{\Pr \left[\text{SINR} > e^z - 1, \text{SINR} \geq T \right]}{\Pr \left[\text{SINR} \geq T \right]} dz, \\ &= \ln(1 + T) + \int_{\ln(1+T)}^\infty \frac{\Pr \left[\text{SINR} > e^z - 1 \right]}{\Pr \left[\text{SINR} > T \right]} dz, \\ &= \ln(1 + T) + \frac{1}{P_c(T)} \int_{\ln(1+T)}^\infty P_c(e^z - 1) dz, \end{aligned} \tag{4.37}$$

where $P_c(x)$ is the coverage probability in a single-tier network when threshold SINR is x, which is given by (4.9). In Section 4.3.1, it was shown that (4.9) is an exact expression for $T \geq 0$ dB and an upper bound when $T < 0$ dB. Consequently, (4.37) is an exact expression for $T \geq 0$ dB and a lower bound when $T < 0$ dB.

4.4.2 Two-Tier Networks

The achievable rate of an MS in coverage in a two-tier network $R^{\text{2-tier}}$ is analytically intractable when the SINR thresholds of two types of BSs are different. Therefore, we derive $R^{\text{2-tier}}$ assuming SINR thresholds to be the same, i.e., $T_m = T_p = T$. Following a similar approach to the derivation of (4.37), $R^{\text{2-tier}}$ has been derived as

$$R^{\text{2-tier}} = \ln(1 + T) + \frac{1}{P_c(T, T)} \int_{\ln(1+T)}^\infty P_c(e^z - 1, e^z - 1) dz, \tag{4.38}$$

where, $P_c(x, y)$ is given by (4.14) or (4.31) depending on the availability of SINR/average received power information. Similarly to (4.37), (4.38) is an exact expression for $T_m,\ T_p \geq 0$ dB and a lower bound when $T_m,\ T_p < 0$ dB.

4.5 Simulation and Numerical Results

This section first considers a single-tier network with the proposed cell association policy. Its coverage probability is compared with those of the closest-BS and the highest-SINR association policies. Secondly, the coverage probability of a two-tier network, which employs extensions of the new association policy, is investigated. Performance of the new policy is compared with those of the closest-BS, the highest-SINR and the maximum biased instantaneous received power [106] association policies. Finally the average rates of MSs in coverage of both single-tier and two-tier networks are investigated.

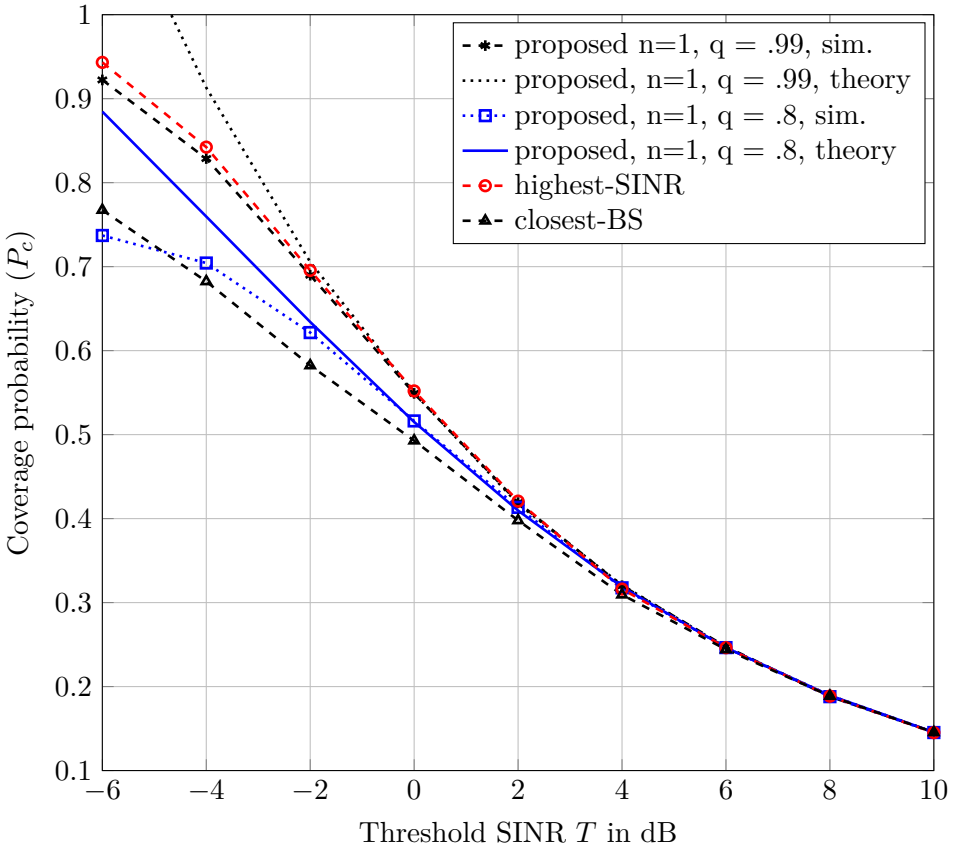

Figure 4.2: Variation of P_c in a single-tier network with T. $\alpha = 3.5$, $\lambda = 12 \times 10^{-6}$ m^{-2}, $P_t = 20$ W, $N_0 = 0$.

Figure 4.2 shows the variation of P_c in a single-tier network with the new policy. The analytical and simulation results are very close when $T > -2$ dB. Also, the coverage probability of the new policy is compared with those of the closest-BS and the highest-SINR policies. Interestingly, when P_{th} is selected appropriately (equiv-

alently, n and q are appropriately selected), this policy outperforms the closest-BS association and performs similarly to the highest-SINR policy. For example, the new policy with $n = 1$, and $q = 0.99$ achieves similar performance as the highest-SINR one. Due to path loss, to achieve a higher SINR an MS needs to associate with a much closer BS. Therefore, as can be seen, the performances of all the policies converge to that of the closest-BS policy when threshold SINR is higher ($T > 6$ dB).

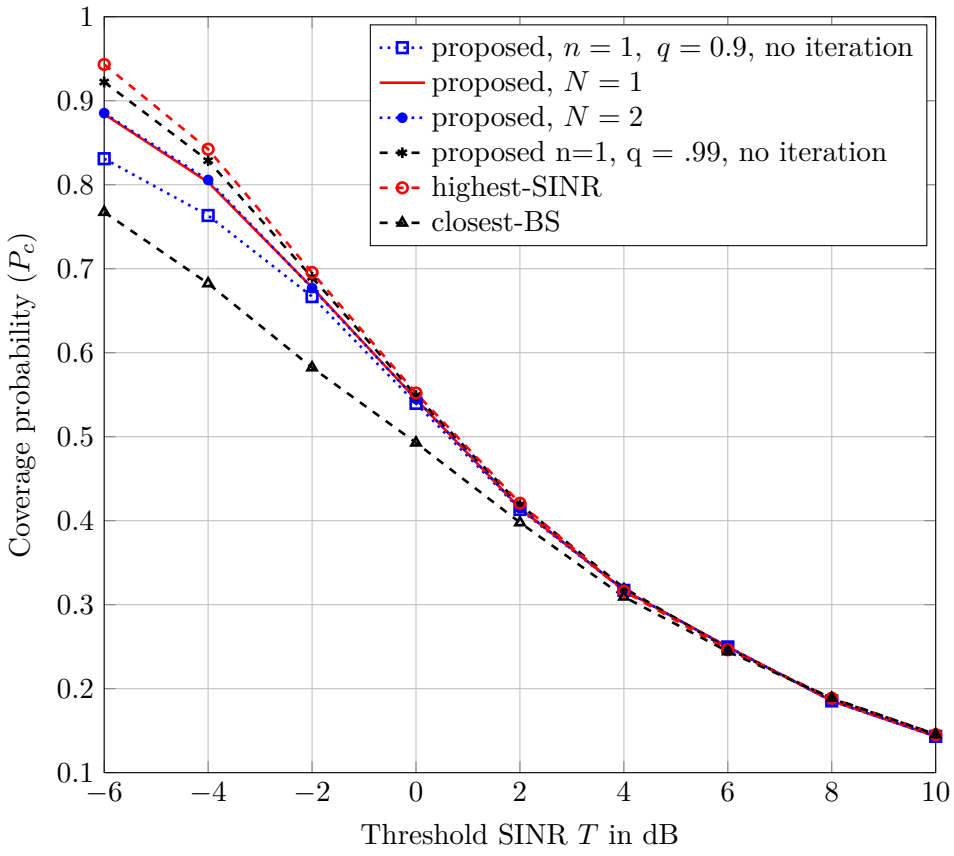

Figure 4.3: P_c in a single-tier network with adaptive P_{th} vs T. $\alpha = 3.5$, $\lambda = 12\times10^{-6}$ m^{-2}, $P_t = 20$ W, $N_0 = 0$.

Coverage probability improvement that can be achieved by adaptive selection of P_{th} is shown in Figure 4.3. In the network considered, $P_{th}^{(j)}$, $j \in \{0, 1, 2\}$ is selected with $\forall j : n^{(j)} = 1$, $q^{(0)} = 0.9$, $q^{(1)} = 0.99$, and $q^{(2)} = 0.999$. Therefore, $P_{th}^{(0)} = -40.74$ dBm, $P_{th}^{(1)} = -46.01$ dBm, and $P_{th}^{(2)} = -49.09$ dBm. Results show that P_c with no iteration outperforms the closest-BS policy. Also, it shows that the performance of the proposed policy with one iteration ($N = 1$) significantly improves P_c compared to no iterations. Further, the results indicate that only a marginal performance improvement can be achieved by having more than one

iteration. In a network with PPP distribution of BSs, the average number of BSs to be scanned with $N = 1$ is given as $q\pi\lambda\left(\frac{P_t}{P_{th}^{(0)}}\right)^{\frac{2}{\alpha}} + (1-q)\pi\lambda\left[\left(\frac{P_t}{P_{th}^{(1)}}\right)^{\frac{2}{\alpha}} - \left(\frac{P_t}{P_{th}^{(0)}}\right)^{\frac{2}{\alpha}}\right]$. For the networks considered, this figure is ≈ 2.3. Figure 4.3 also shows that P_c for $n = 1,\ q = 0.99$ no iteration case is only slightly higher compared to $N = 1$ case. However, the average number of BSs to be scanned in $n = 1,\ q = 0.99$ no iteration case is $\pi\lambda\left(\frac{P_t}{P_{th}}\right)^{\frac{2}{\alpha}} \approx 4.6$. This shows that the complexity (the number of BSs to be tracked) in the association process can be significantly reduced by using adaptive P_{th} selection at a cost of small performance degradation.

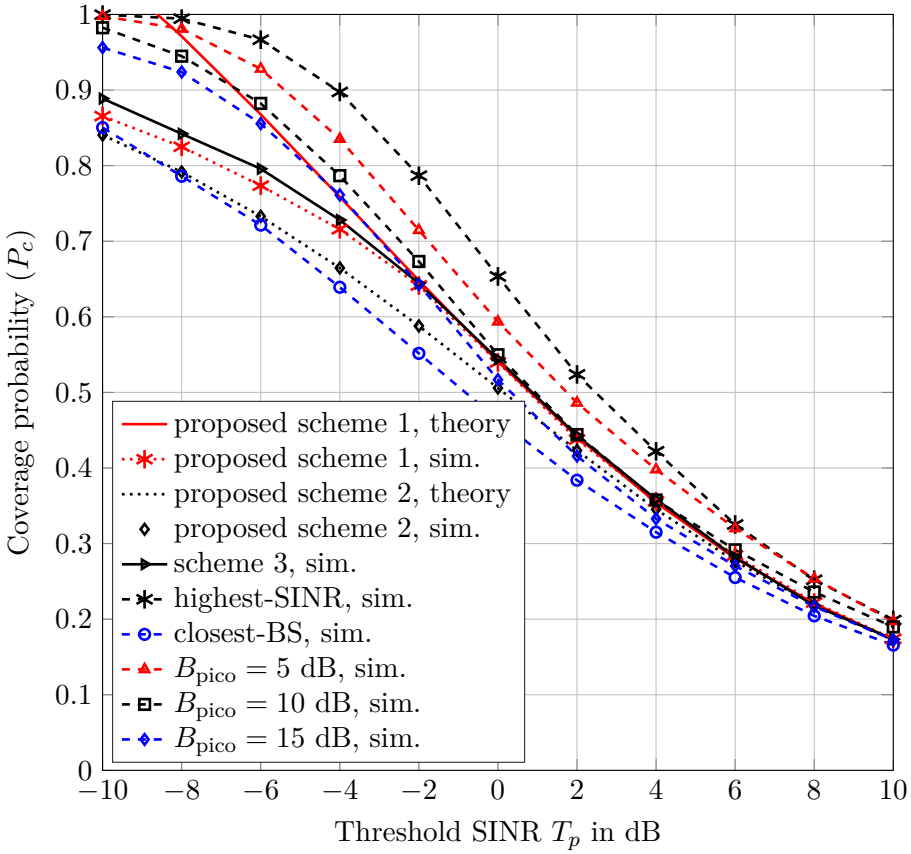

Figure 4.4: Variation of P_c in a two-tier network with T_p. $P_m = 20$ W, $P_p = 2$ W, $\alpha_m = 3.5$, $\alpha_p = 3.8$, $n = 1$, $q = 0.7$, $T_m = T_p - 5$ dB, $\lambda_m = 5 \times 10^{-7}$ m^{-2}, $\lambda_p = 20 \times 10^{-6}$ m^{-2}, $N_0 = 0$. Please see footnote[3] for the description of schemes 1-3 in the legend.

Figure 4.4 shows the variation of P_c in a two-tier network with the SINR threshold. The minimum average received power P_{th} for pico BSs was selected with $n = 1$ and $q = 0.7$. Under this configuration 70% MSs will be served by pico BSs, while the remaining 30% will be served by macro BSs. Notably, a considerable coverage probability improvement can be achieved by the availability of both instantaneous SINR and average received power (proposed scheme 1) as opposed to only average received power of pico BSs (proposed scheme 2), especially when -8 dB $< T_p < 0$ dB. Figure 4 also shows that having instantaneous SINR information for macro BSs (scheme 3), marginally improves the coverage probability at low SINR thresholds. However, at high SINR thresholds, it does not provide any coverage probability improvement compared to having average SINR. Further, Figure 4.4 compares the coverage probabilities of the proposed policy with those of closest BS, highest SINR, and maximum biased instantaneous received power [106] association policies. With the closest BS policy, an MS connects to the closest-BS, while under the highest-SINR policy an MS associates with the BS providing the highest SINR, regardless of the BS type. Therefore, these two policies fail to manage user off-loading. Clearly, the highest-SINR policy provides the best coverage probability, while the closest-BS policy provides the worst coverage probability. In maximum biased instantaneous received power [106] association, an MS associates with the macro BS providing the highest instantaneous received power, if the received power from it exceeds the maximum instantaneous received power from pico BSs with a margin of B_{pico} dB. Therefore, $B_{\text{pico}} = 0$ dB represents the highest SINR association. When B_{pico} increases, more MSs will be served by pico BSs than in highest SINR association. Clearly, when B_{pico} increases, coverage probability decreases due to interference from high power macro BSs. Results also show that at lower average SINR thresholds, biased association provides better coverage for all B_{pico} values considered compared to the proposed scheme 1. However, for lower SINR thresholds, the coverage probability of biased association can be lower than that of the proposed scheme 1 depending on

[3]Proposed scheme 1: MS is associated with the pico BS, from which it receives the highest instantaneous SINR, if the average received power from at least this pico BS exceeds P_{th}; otherwise, the MS is associated with the macro BS, from which it receives the highest average SINR. Proposed scheme 2: MS is associated with the pico BS, from which it receives the highest area-averaged received power, if the average received power from at least this pico BS exceeds P_{th}; otherwise, the MS is associated with the macro BS, from which it receives the highest average SINR. Scheme 3: MS is associated with the pico BS, from which it receives the highest instantaneous SINR, if the average received power from at least this pico BS exceeds P_{th}; otherwise, the MS is associated with the macro BS, from which it receives the highest instantaneous SINR.

the bias B_{pico}.

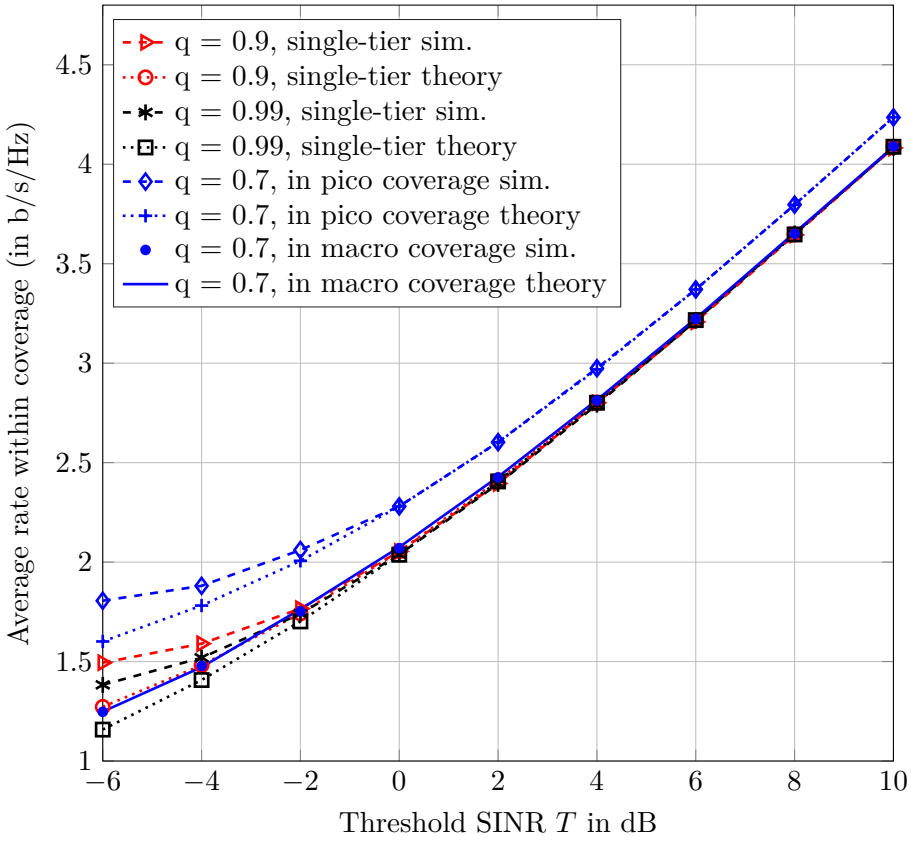

Figure 4.5: Average rate of an MS in coverage in a single-tier network, and in the coverage of pico- and macro-tiers in a two-tier network. Network configuration for single tier network: $\alpha = 3.5$, $\lambda = 12 \times 10^{-6}$ m^{-2}, $n = 1$, $P_t = 20$ W. Network configuration for two-tier network: $P_m = 20$ W, $P_p = 2$ W, $\alpha_m = 3.5$, $\alpha_p = 3.8$, $n = 1$, $q = 0.7$, $T_m = T_p = T$ dB, $\lambda_m = 5 \times 10^{-7}$ m^{-2}, $\lambda_p = 20 \times 10^{-6}$ m^{-2}, $N_0 = 0$.

Figure 4.5 shows the variation of the average rate of an MS in a single-tier network for two different values of q. A close match between theoretical and simulation results can be observed for $T > 0$ dB. When $T < 0$ dB, analytical expressions provide lower bounds. Clearly, at high SINR thresholds, MSs in coverage achieve similar average data rates regardless of the value of q. However, at low SINR thresholds, average rates slightly decrease when P_{th} decreases (or equivalently when q and/or n increase). This is because selecting a small P_{th} allows MSs to associate with BSs located far from them. Figure 4.5 also shows the average rate an MS can achieve when in coverage of macro and pico BSs assuming cell association described in Section 4.3.4.

The variation of average rates of MSs within coverage in two-tier networks is

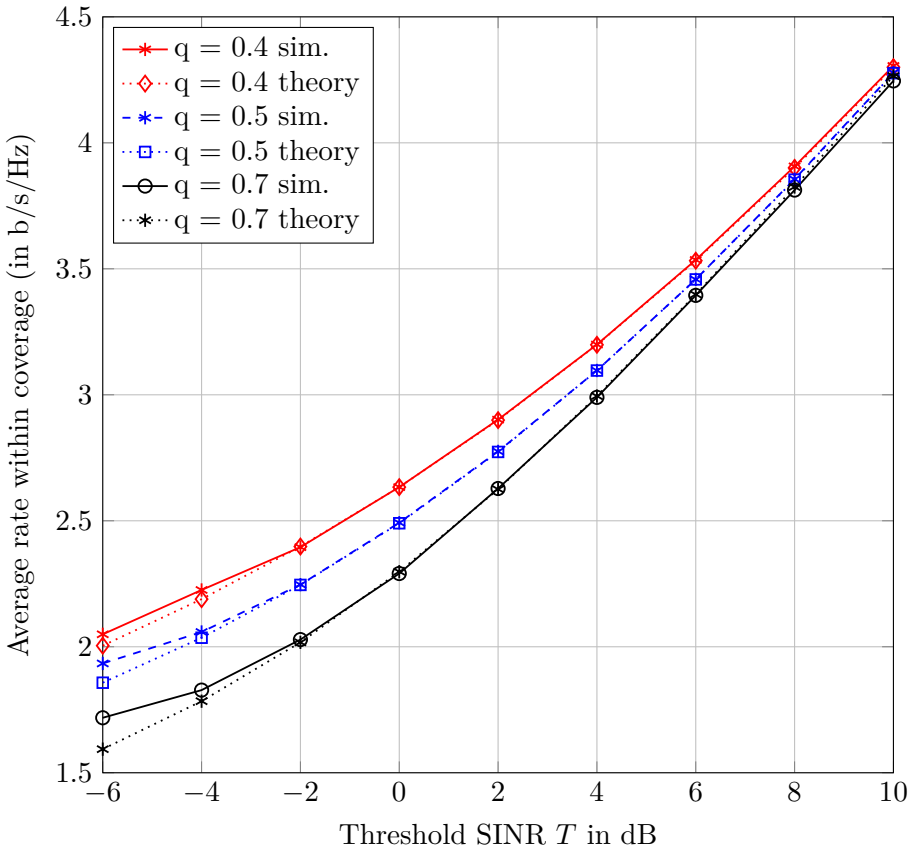

Figure 4.6: Average rate of an MS in coverage in a two-tier network for different value of q. $P_m = 20$ W, $P_p = 2$ W, $\alpha_m = 3.5$, $\alpha_p = 3.8$, $n = 1$, $T_m = T_p = T$ dB, $\lambda_m = 5 \times 10^{-7}$ m^{-2}, $\lambda_p = 20 \times 10^{-6}$ m^{-2}, $N_0 = 0$.

shown in Figure 4.6. Cell association described in Section 4.3.4 is assumed. The analytical results closely match the simulation ones. Interestingly, the results show that the average rate increases when P_{th} for pico BSs increases. When P_{th} becomes larger, an MS only associates with a pico BS that provides higher average SINR (equivalently, with a pico BS located closer to it). Otherwise, it associates with a macro BS. Therefore, the effect of strong interference from high power macro BSs, when an MS is associated with a pico BS, is limited and average rate increases. However, when P_{th} is higher, a large percentage of MSs will be associated with macro BSs, thus reducing the number of users off-loaded to pico BSs.

4.6 Conclusion

Smart cell association policies are critical for emerging heterogeneous cellular networks. This study has proposed a new cell association policy in which the serving BS

is the one that provides the highest instantaneous SINR from those providing a predetermined minimum average received signal power. The aim is to reduce the overhead associated with cell association with a minimum impact on the performance of the network. This policy includes the conventional highest-SINR association as a special case. Two methods to determine the minimum association average received power are given. Application of this policy in both single-tier and two-tier networks is investigated. It has been shown that, this policy outperforms the closest-BS policy and performs similarly to the highest-SINR association. In two-tier networks, it can be used to manage traffic off-loading to small cells which is an essential feature in HetNet to provide user-perceived rates. Coverage probability and average rate of MSs within coverage of 2- and 3-dimensional single-tier (homogeneous) and 2-dimensional two-tier (heterogeneous) networks have been derived and validated by Monte-Carlo simulations.

$\sim$

Chapter 5

Conclusion and Future Work

In this chapter, first the conclusions and the summary of the contributions of the thesis are outlined. Then, the future research directions are described.

5.1 Summary of Contributions and Conclusions

- Chapter 3 has presented three transmit power control (TPC) schemes for the cellular uplink. A refined analytical framework has also been developed by incorporating three essential radio channel impediments in the system model, namely path loss, shadowing and fading. More practical Rayleigh-lognormal fading channels have been considered, which are generally hard to incorporate in analytical models. Using the Hermite polynomial approximation approach these analytical difficulties have been circumvented. Also the developed framework has considered orthogonal channel assignment (one mobile station (MS) per time-frequency channel in each cell) to make the system model appropriate for modern cellular networks such as Long Term Evolution (LTE), Long Term Evolution-Advanced (LTE-A), and the upcoming fifth generation cellular networks (5G) new radio (NR). It has been observed that for cell-edge users or users experiencing severe shadowing, compensating for the aggregate effect of path loss and shadowing by TPC provides better coverage. However, cell center users benefit more from compensating for path loss only. Also it has been observed that increasing the density of base stations (BSs) has no significant effect on the coverage experienced by MSs.

- Chapter 4 has introduced two simple cell-association policies; one each for single-tier and two-tier networks. The motivation has been to limit the overhead involved with cell association by reducing the number of candidate BSs

considered in the selection process. This approach can be very useful in densely-deployed networks, which are expected to be common in 5G and beyond-5G communication systems. A refined analytical framework for evaluating coverage probability and achievable data rates has been developed. The trade-offs between cell-association complexity and performance have been investigated. It has been observed that considering a few candidate BSs is sufficient to achieve the same service quality as considering all active BSs for cell association. Also approaches to use the introduced policy to adaptively off-load users from large cells to small cells in a two-tier network setup has been discussed. Further, the impact of user off-loading on the achievable data rates has been quantified.

5.2 Future Research Directions

- One observation in Chapter 3 is that cell edge users or users subject to severe shadowing benefit more from compensating for the aggregate effect of path loss and shadowing in their TPC, while cell center users benefit more from compensating only for path loss. A natural problem to look at therefore is to investigate how much performance improvement can be achieved by implementing mixture of these two power control schemes depending on their operating signal-to-interference-plus-noise ratio (SINR).

- TPC in cellular networks can have a significant effect on the performance of other underlying technologies: for example, device-to-device (D2D) communications and cognitive radio networks.

- In Chapter 3 our analysis has been limited to coverage probability and transmit power of MSs. It will be interesting to see the impact of TPC schemes considered on the other performance metrics such as achievable data rates.

- In Chapter 4 we have observed that when the operating SINR is lower, user off-loading reduces the achievable data rates. However, the gains from user off-loading come from making radio resources available for more users by frequency re-use. Therefore, to evaluate the gains from user off-loading under the proposed cell association scheme, user traffic modeling should be incorporated in the system model while considering the maximum capacity for each BS.

- In Chapter 4, two-tier networks have been modeled by two independent homogeneous Poisson point processes (PPPs). However, a common deployment approach is to have more low power BSs towards the cell edge. To this end, macro BSs can be modeled by a homogeneous PPP, while the distributions of small BSs can be modeled by a Poisson hole process (PHP). Extending the study presented in this thesis to such a network arrangement will provide more insights into the applicability of the proposed cell association policy in commercially deployed networks.

$\sim$

Bibliography

[1] "Cisco visual networking index: Global mobile data traffic forecast update, 2016–2021." Cisco Systems, Tech. Rep., 2016. [Online]. Available: http://www.cisco.com/c/en/us/solutions/collateral/service-provider/visual-networking-index-vni/mobile-white-paper-c11-520862.pdf

[2] "IMT vision-framework and overall objectives of the future development of IMT for 2020 and beyond," International Telecommunication Union-Radiocommunication Sector, Tech. Rep., 2015. [Online]. Available: https://www.itu.int/dms_pubrec/itu-r/rec/m/R-REC-M.2083-0-201509-I!!PDF-E.pdf

[3] 3GPP ongoing releases. 3GPP. [Online]. Available: http://http://www.3gpp.org/specifications/releases

[4] A. Goldsmith, *Wireless Communications*. New York, NY: Cambridge University Press, 2005.

[5] I. S. Gradshteyn and I. M. Ryzhik, *Table of Integrals, Series and Products*, 7th ed. San Diego, CA: Academic Press, 2007.

[6] M. Abramowitz and I. A. Stegun, Eds., *Handbook of Mathematical Functions: with Formulas, Graphs, and Mathematical Tables*. New York, NY: Dover Publications, 1965.

[7] E. Bauer, "Improving operational efficiency of applications via cloud computing," *IEEE Cloud Computing*, vol. 5, no. 1, pp. 12–19, January 2018.

[8] S. Zhang, H. Yan, and X. Chen, "Research on key technologies of cloud computing," *Physics Procedia*, vol. 33, pp. 1791 – 1797, 2012.

[9] Y. Yuan, "Paving the road for virtual and augmented reality [standards]," *IEEE Consumer Electronics Mag.*, vol. 7, no. 1, pp. 117–128, January 2018.

[10] Y. Huang, Y. Li, H. Ren, J. Lu, and W. Zhang, "Multi-panel MIMO in 5G," *IEEE Commun. Mag.*, vol. 56, no. 3, pp. 56–61, March 2018.

[11] H. Ji, Y. Kim, J. Lee, E. Onggosanusi, Y. Nam, J. Zhang, B. Lee, and B. Shim, "Overview of full-dimension MIMO in LTE-Advanced Pro," *IEEE Commun. Mag.*, vol. 55, no. 2, pp. 176–184, February 2017.

[12] C. S. Park, Y. P. E. Wang, G. Jongren, and D. Hammarwall, "Evolution of uplink MIMO for LTE-Advanced," *IEEE Commun. Mag.*, vol. 49, no. 2, pp. 112–121, February 2011.

[13] J. Lee, J.-K. Han, and J. Zhang, "MIMO Technologies in 3GPP LTE and LTE-Advanced," *EURASIP Journal on Wireless Commun. and Networking*, vol. 2009, no. 1, pp. 1–10, July 2009.

[14] Z. Shen, A. Papasakellariou, J. Montojo, D. Gerstenberger, and F. Xu, "Overview of 3GPP LTE-Advanced carrier aggregation for 4G wireless communications," *IEEE Commun. Mag.*, vol. 50, no. 2, pp. 122–130, February 2012.

[15] C. S. Park, L. Sundstrom, A. Wallen, and A. Khayrallah, "Carrier aggregation for LTE-Advanced: Design challenges of terminals," *IEEE Commun. Mag.*, vol. 51, no. 12, pp. 76–84, December 2013.

[16] X. Lin, J. Andrews, A. Ghosh, and R. Ratasuk, "An overview of 3GPP device-to-device proximity services," *IEEE Commun. Mag.*, vol. 52, no. 4, pp. 40–48, April 2014.

[17] M. Tehrani, M. Uysal, and H. Yanikomeroglu, "Device-to-device communication in 5G cellular networks: Challenges, solutions, and future directions," *IEEE Commun. Mag.*, vol. 52, no. 5, pp. 86–92, May 2014.

[18] D. Feng, L. Lu, Y. Yuan-Wu, G. Li, S. Li, and G. Feng, "Device-to-device communications in cellular networks," *IEEE Commun. Mag.*, vol. 52, no. 4, pp. 49–55, April 2014.

[19] S. Thalanany, M. Irizarry, and N. Saxena, "License-assisted access considerations," *IEEE Commun. Standards Mag.*, vol. 1, no. 2, pp. 106–112, July 2017.

[20] M. Cierny, T. Nihtila, T. Huovinen, M. Kuusela, F. Chernogorov, K. Hooli, and A. Toskala, "Fairness vs. performance in Rel-13 LTE licensed assisted access," *IEEE Commun. Mag.*, vol. 55, no. 12, pp. 133–139, December 2017.

[21] H. J. Kwon, J. Jeon, A. Bhorkar, Q. Ye, H. Harada, Y. Jiang, L. Liu, S. Nagata, B. L. Ng, T. Novlan, J. Oh, and W. Yi, "Licensed-assisted access to unlicensed spectrum in LTE Release 13," *IEEE Commun. Mag.*, vol. 55, no. 2, pp. 201–207, February 2017.

[22] J. Lee, Y. Yi, S. Chong, and Y. Jin, "Economics of WiFi offloading: Trading delay for cellular capacity," *IEEE Trans. on Wireless Commun.*, vol. 13, no. 3, pp. 1540–1554, March 2014.

[23] T. S. Rappaport, S. Sun, R. Mayzus, H. Zhao, Y. Azar, K. Wang, G. N. Wong, J. K. Schulz, M. Samimi, and F. Gutierrez, "Millimeter wave mobile communications for 5G cellular: It will work!" *IEEE Access*, vol. 1, pp. 335–349, May 2013.

[24] T. S. Rappaport, Y. Xing, G. R. MacCartney, A. F. Molisch, E. Mellios, and J. Zhang, "Overview of millimeter wave communications for fifth-generation (5G) wireless networks-With a focus on propagation models," *IEEE Trans. on Antennas and Propagation*, vol. 65, no. 12, pp. 6213–6230, December 2017.

[25] Qualcomm, "Making 5G NR a reality," *White paper*.

[26] Huawei, "5G: A Technology vision," *White paper*.

[27] S. Parkvall, E. Dahlman, A. Furuskar, and M. Frenne, "NR: The new 5G radio access technology," *IEEE Commun. Standards Mag.*, vol. 1, no. 4, pp. 24–30, December 2017.

[28] "5G network architecture-A high level view," Huawei, Tech. Rep., 2016. [Online]. Available: http://www.huawei.com/minisite/hwmbbf16/insights/5G-Nework-Architecture-Whitepaper-en.pdf

[29] G. Brown, "Exploring 5G new radio: Use cases, capabilities & timeline," Qualcomm, Tech. Rep., September 2016. [Online]. Available: https://www.qualcomm.com/documents/heavy-reading-white-paper-exploring-5g-new-radio-use-cases-capabilities-timeline

[30] GL Stüber, *Principles of Mobile Communication*, 4th ed. Cham, Switzerland: Springer, 2017.

[31] V. Chandrasekhar, J. Andrews, and A. Gatherer, "Femtocell networks: A survey," *IEEE Commun. Mag.*, vol. 46, no. 9, pp. 59–67, September 2008.

[32] J. Zhang and J. Andrews, "Distributed antenna systems with randomness," *IEEE Trans. Wireless Commun.*, vol. 7, no. 9, pp. 3636–3646, September 2008.

[33] A. Ghosh, N. Mangalvedhe, R. Ratasuk, B. Mondal, M. Cudak, E. Visotsky, T. Thomas, J. Andrews, P. Xia, H.-S. Jo, H. Dhillon, and T. Novlan, "Heterogeneous cellular networks: From theory to practice," *IEEE Commun. Mag.*, vol. 50, no. 6, pp. 54–64, June 2012.

[34] J. Andrews, "Seven ways that HetNets are a cellular paradigm shift," *IEEE Commun. Mag.*, vol. 51, no. 3, pp. 136–144, March 2013.

[35] S. Mukherjee, *Analytical Modeling of Heterogeneous Cellular Networks: Geometry, Coverage, and Capacity.* Cambridge, UK: Cambridge University Press, 2014.

[36] G. de la Roche, A. Valcarce, D. Lopez-Perez, and J. Zhang, "Access control mechanisms for femtocells," *IEEE J. Sel. Areas Commun.*, vol. 48, no. 1, pp. 33–39, Jane 2010.

[37] R. Pabst, B. H. Walke, D. Schultz, P. Herhold, H. Yanikomeroglu, S. Mukherjee, H. Viswanathan, M. Lott, W. Zirwas, M. Dohler, H. Aghvami, D. Falconer, and G. Fettweis, "Relay-based deployment concepts for wireless and mobile broadband radio," *IEEE Commun. Mag.*, vol. 42, no. 9, pp. 80–89, September 2004.

[38] J. Gora and S. Redana, "In-band and out-band relaying configurations for dual-carrier LTE-Advanced system," in *Proc. IEEE 22nd International Symposium on Personal Indoor and Mobile Radio Communications*, September 2011, pp. 1820–1824.

[39] L. Ahumada, R. Feick, R. Valenzuela, M. Gallardo, M. Derpich, and H. Carrasco, "Empirical evaluation of the received power gain when remote radio

heads are used to enhance the coverage area in urban environments," *IEEE Trans. Wireless Commun.*, vol. 12, no. 6, pp. 2830–2839, June 2013.

[40] J. Andrews, F. Baccelli, and R. Ganti, "A tractable approach to coverage and rate in cellular networks," *IEEE Trans. Commun.*, vol. 59, no. 11, pp. 3122–3134, November 2011.

[41] H. Dhillon, R. Ganti, F. Baccelli, and J. Andrews, "Modeling and analysis of K-tier downlink heterogeneous cellular networks," *IEEE J. Sel. Areas Commun.*, vol. 30, no. 3, pp. 550–560, April 2012.

[42] M. Haenggi, *Stochastic Geometry for Wireless Networks.* New York, NY: Cambridge University Press, 2013.

[43] M. Haenggi and R. K. Ganti, *Interference in Large Wireless Networks.* Manover, MA: Now Publishers Inc., 2014.

[44] E Dahlman, S Parkvall, J Sköld, *4G, LTE evolution and the Road to 5G*, 3rd ed. Oxford, UK: Academic Press, 2016.

[45] LTE, "Technical Specification Group Radio Access Network; NR; Physical channel and modulation, Release 15, v15.1.0. 3GPP TS 38.211," 3GPP, Tech. Rep., 2018.

[46] S. Atapattu, C. Tellambura, and H. Jiang, "A mixture Gamma distribution to model the SNR of wireless channels," *IEEE Trans. Wireless Commun.*, vol. 10, no. 12, pp. 4193–4203, December 2011.

[47] W. C. Y. Lee and Y. S. Yeh, "On the estimation of the second-order statistics of log-normal fading in mobile radio environment," *IEEE J. Sel. Areas Commun.*, vol. 22, pp. 809–873, June 1974.

[48] V. Chandrasekhar and J. G. Andrews, "Uplink capacity and interference avoidance for two-tier femtocell networks," *IEEE Trans. Wireless Commun.*, vol. 8, no. 7, pp. 3498–3509, July 2009.

[49] M. Haenggi, J. Andrews, F. Baccelli, O. Dousse, and M. Franceschetti, "Stochastic geometry and random graphs for the analysis and design of wireless networks," *IEEE J. Sel. Areas Commun.*, vol. 27, no. 7, pp. 1029–1046, September 2009.

[50] S. Mukherjee, "Distribution of downlink SINR in heterogeneous cellular networks," *IEEE J. Sel. Areas Commun.*, vol. 30, no. 3, pp. 575–585, April 2012.

[51] S. N. Chiu, D. Stoyan, W. Kendall, and J. Mecke, *Stochastic Geometry and Its Applications*, 3rd ed. Chichester, UK: John Wiley and Sons, 2013.

[52] J. F. C. Kingman, *Poisson Processes*. New York, NY: Oxford University Press, 1993.

[53] T. Novlan, H. Dhillon, and J. Andrews, "Analytical modeling of uplink cellular networks," *IEEE Trans. Wireless Commun.*, vol. 12, no. 6, pp. 2669–2679, June 2013.

[54] J. Zhu and S. Govindasamy, "Performance of multi-antenna MMSE receivers in non-homogenous Poisson networks," in *Proc. IEEE International Conference on Communications*, June 2012, pp. 2404–2409.

[55] X. Zhang and M. Haenggi, "The performance of successive interference cancellation in random wireless networks," *IEEE Trans. Inf. Theory*, vol. 60, no. 10, pp. 6368–6388, October 2014.

[56] S. Srinivasa and M. Haenggi, "Distance distributions in finite uniformly random networks: Theory and applications," *IEEE Trans. Veh. Technol.*, vol. 59, no. 2, pp. 940–949, February 2010.

[57] J. Chen, M. Ding, and Q. Zhang, "Interference statistics and performance analysis of MIMO ad hoc networks in binomial fields," *IEEE Trans. Veh. Technol.*, vol. 61, no. 5, pp. 2033–2043, June 2012.

[58] K. Gulati, B. Evans, J. Andrews, and K. Tinsley, "Statistics of co-channel interference in a field of Poisson and Poisson-Poisson clustered interferers," *IEEE Trans. Signal Process.*, vol. 58, no. 12, pp. 6207–6222, December 2010.

[59] R. Ganti and M. Haenggi, "Interference and outage in clustered wireless ad hoc networks," *IEEE Trans. Inf. Theory*, vol. 55, no. 9, pp. 4067–4086, September 2009.

[60] Z. Yazdanshenasan, H. S. Dhillon, M. Afshang, and P. H. J. Chong, "Poisson hole process: Theory and applications to wireless networks," *IEEE Trans. Wireless Commun.*, vol. 15, no. 11, pp. 7531–7546, November 2016.

[61] N. Deng, W. Zhou, and M. Haenggi, "Heterogeneous cellular network models with dependence," *IEEE J. Sel. Areas Commun.*, vol. 33, no. 10, pp. 2167–2181, October 2015.

[62] M. Afshang and H. S. Dhillon, "Spatial modeling of device-to-device networks: Poisson cluster process meets Poisson hole process," in *Proc. 49th Asilomar Conference on Signals, Systems and Computers*, November 2015, pp. 317–321.

[63] C. H. Lee and M. Haenggi, "Interference and outage in Poisson cognitive networks," *IEEE Trans. Wireless Commun.*, vol. 11, no. 4, pp. 1392–1401, April 2012.

[64] F. Baccelli and B. Blaszczyszyn, *Stochastic Geometry and Wireless Networks, Volume I - Theory*, ser. Foundations and Trends in Networking Vol. 3: No 3-4, pp 249-449. NoW Publishers, 2009. [Online]. Available: https://hal.inria.fr/inria-00403039

[65] H. Dhillon, R. Ganti, and J. Andrews, "Modeling non-uniform UE distributions in downlink cellular networks," *IEEE Wireless Commun. Lett.*, vol. 2, no. 3, pp. 339–342, June 2013.

[66] H. ElSawy and E. Hossain, "On stochastic geometry modeling of cellular uplink transmission with truncated channel inversion power control," *IEEE Trans. Wireless Commun.*, vol. 13, no. 8, pp. 4454–4469, August 2014.

[67] H. ElSawy, E. Hossain, and M.-S. Alouini, "Analytical modeling of mode selection and power control for underlay D2D communication in cellular networks," *IEEE Trans. Commun.*, vol. 62, no. 11, pp. 4147–4161, November 2014.

[68] S. Kusaladharma and C. Tellambura, "Aggregate interference analysis for underlay cognitive radio networks," *IEEE Wireless Commun. Lett.*, vol. 1, no. 6, pp. 641–644, December 2012.

[69] ——, "On approximating the cognitive radio aggregate interference," *IEEE Wireless Commun. Lett.*, vol. 2, no. 1, pp. 58–61, February 2013.

[70] S. Kusaladharma, P. Herath, and C. Tellambura, "Underlay interference analysis of power control and receiver association schemes," *IEEE Trans. Veh. Technol.*, vol. 65, no. 11, pp. 8978–8991, November 2016.

[71] C. Tellambura, A. J. Mueller, and V. K. Bhargawa, "Analysis of M-ary phase-shift keying with diversity reception for land-mobile satellite channels," *IEEE Trans. Veh. Technol.*, vol. 46, no. 4, pp. 910–922, November 1997.

[72] C. Tellambura, A. Annamalai, and V. K. Bhargava, "Closed form and infinite series solutions for the MGF of a dual-diversity selection combiner output in bivariate Nakagami fading," *IEEE Trans. Commun.*, vol. 51, no. 4, pp. 539–542, April 2003.

[73] C. Tellambura, "Evaluation of the exact union bound for trellis-coded modulations over fading channels," *IEEE Trans. Commun.*, vol. 44, no. 12, pp. 1693–1699, December 1996.

[74] S. Kusaladharma, P. Herath, and C. Tellambura, "Secondary user interference characterization for underlay networks," in *Proc. IEEE 82nd Vehicular Technology Conference*, September 2015, pp. 1–5.

[75] P. Herath, C. Tellambura, and W. Krzymien, "Coverage probability analysis of three uplink power control schemes: Stochastic geometry approach," *EURASIP Journal on Wireless Communications and Networking*, vol. 141, pp. 1–14, June 2018.

[76] P. Herath, C. Tellambura, and W. A. Krzymien, "Stochastic geometry modeling of cellular uplink power control under composite Rayleigh-lognormal fading," in *Proc. IEEE 82nd Vehicular Technology Conference*, September 2015, pp. 1–5.

[77] LTE, "Technical Specification Group Radio Access Network; NR; Physical layer procedures for control, Release 15, v15.0.0. 3GPP TS 38.213," 3GPP, Tech. Rep., 2017.

[78] H. Y. Lee, Y. J. Sang, and K. S. Kim, "On the uplink SIR distributions in heterogeneous cellular networks," vol. 18, no. 12, pp. 2145–2148, December 2014.

[79] L. H. Afify, H. ElSawy, T. Y. Al-Naffouri, and M. S. Alouini, "Error performance analysis in K-tier uplink cellular networks using a stochastic geometric approach," in *Proc. IEEE International Conference on Communication Workshop*, June 2015, pp. 87–93.

[80] S. Singh, X. Zhang, and J. G. Andrews, "Uplink rate distribution in heterogeneous cellular networks with power control and load balancing," in *Proc. IEEE International Conference on Communication Workshop*, June 2015, pp. 1275–1280.

[81] M. D. Renzo and P. Guan, "Stochastic geometry modeling and system-level analysis of uplink heterogeneous cellular networks with multi-antenna base stations," *IEEE Trans. Commun.*, vol. 64, no. 6, pp. 2453–2476, June 2016.

[82] F. J. Martin-Vega, G. Gomez, M. C. Aguayo-Torres, and M. D. Renzo, "Analytical modeling of interference aware power control for the uplink of heterogeneous cellular networks," *IEEE Trans. Wireless Commun.*, vol. 15, no. 10, pp. 6742–6757, October 2016.

[83] W. Bao and B. Liang, "Uplink interference analysis for two-tier cellular networks with diverse users under random spatial patterns," *IEEE Trans. Wireless Commun.*, vol. 14, no. 3, March 2015.

[84] 3GPP, *Evolved Universal Terrestrial Radio Access (E-UTRA); Physical Layer Procedures, document TS 36.213 V12.4.0*, 3GPP Std., February 2015.

[85] A. AlAmmouri, H. ElSawy, and M. S. Alouini, "Load-aware modeling for uplink cellular networks in a multi-channel environment," in *Proc. IEEE 25th Annual International Symposium on Personal, Indoor, and Mobile Radio Communication*, September 2014, pp. 1591–1596.

[86] S. Singh, X. Zhang, and J. G. Andrews, "Joint rate and SINR coverage analysis for decoupled uplink-downlink biased cell associations in HetNets," *IEEE Trans. on Wireless Commun.*, vol. 14, no. 10, pp. 5360–5373, October 2015.

[87] T. Bai and R. W. Heath, "Analyzing uplink SINR and rate in massive MIMO systems using stochastic geometry," *IEEE Trans. on Commun.*, vol. 64, no. 11, pp. 4592–4606, November 2016.

[88] Y. Dhungana and C. Tellambura, "Multichannel analysis of cell range expansion and resource partitioning in two-tier heterogeneous cellular networks," *IEEE Trans. Wireless Commun.*, vol. 15, no. 3, pp. 2394–2406, March 2016.

[89] G. Wang, Q. Liu, R. He, F. Gao, and C. Tellambura, "Acquisition of channel state information in heterogeneous cloud radio access networks: Challenges and research directions," *IEEE Wireless Commun.*, vol. 22, no. 3, pp. 100–107, July 2015.

[90] T. Novlan, J. G. Andrews, "Analytical evaluation of uplink fractional frequency reuse," *IEEE Trans. Commun.*, vol. 61, no. 5, pp. 2098–2108, May 2013.

[91] A. Simonsson and A. Furuskar, "Uplink power control in LTE - Overview and performance," in *Proc. IEEE 68th Vehicular Technology Conference*, September 2008, pp. 1–5.

[92] Z. Zeinalpour-Yazdi and S. Jalali, "Outage analysis of uplink two-tier networks," *IEEE Trans. Commun.*, vol. 62, no. 9, pp. 3351–3362, September 2014.

[93] T. Novlan, J. G. Andrews, I. Sohn, R. K. Ganti, and A. Ghosh, "Comparison of fractional frequency reuse approaches in the OFDMA cellular downlink," in *Proc. 2010 IEEE Global Telecommunications Conference*, December 2010, pp. 1–5.

[94] N. Saquib, E. Hossain, and D. I. Kim, "Fractional frequency reuse for interference management in LTE-Advanced hetnets," *IEEE Wireless Commun. Mag.*, vol. 20, no. 2, pp. 113–122, April 2013.

[95] H. ElSawy and M. S. Alouini, "On the meta distribution of coverage probability in uplink cellular networks," *IEEE Commun. Lett.*, vol. 21, no. 7, pp. 1625–1628, April 2017.

[96] Y. Wang, M. Haenggi, and Z. Tan, "The meta distribution of the SIR for cellular networks with power control," *IEEE Trans. Commun.*, vol. 66, no. 4, pp. 1745–1757, April 2018.

[97] C. Tellambura, "Bounds on the distribution of a sum of correlated lognormal random variables and their application," *IEEE Trans. Commun.*, vol. 56, no. 8, pp. 1241–1248, August 2008.

[98] D. Senaratne and C. Tellambura, "Numerical computation of the lognormal sum distribution," in *Proc. IEEE Global Telecommunications Conference*, November 2009, pp. 1–6.

[99] G. H. Golub and J. H. Welsch, "Calculation of Gauss quadrature rules," *Mathematics of Computation*, vol. 23, no. 106, pp. 221–230, April 1969.

[100] H. ElSawy, E. Hossain, and M. S. Alouini, "Analytical modeling of mode selection and power control for underlay D2D communication in cellular networks," *IEEE Trans. Commun.*, vol. 62, no. 11, pp. 4147–4161, November 2014.

[101] P. Herath, W. A. Krzymien, and C. Tellambura, "Coverage and rate analysis for limited information cell association in stochastic-layout cellular networks," *IEEE Trans. Veh. Technol.*, vol. 65, no. 9, pp. 6962–6971, September 2016.

[102] P. Herath, W. Krzymien, and C. Tellambura, "A novel base stations - mobile stations association policy for cellular networks," in *Proc. 80th IEEE Vehicular Technology Conference*, September 2014.

[103] P. Madhusudhanan, J. Restrepo, Y. Liu, T. Brown, and K. Baker, "Stochastic ordering based carrier-to-interference ratio analysis for the shotgun cellular systems," *IEEE Wireless Commun. Lett.*", vol. 1, no. 6, pp. 565–568, December 2012.

[104] H. Dhillon, R. Ganti, and J. Andrews, "Load-aware heterogeneous cellular networks: Modeling and SIR distribution," in *Proc. IEEE Global Communications Conference*, December 2012, pp. 4314–4319.

[105] P. Madhusudhanan, J. Restrepo, Y. Liu, T. Brown, and K. Baker, "Multi-tier network performance analysis using a shotgun cellular system," in *Proc. IEEE Global Communications Conference*, December 2011, pp. 1–6.

[106] P. Madhusudhanan, J. Restrepo, Y. Liu, and T. Brown, "Downlink coverage analysis in a heterogeneous cellular network," in *Proc. IEEE Global Communications Conference*, December 2012, pp. 4170–4175.

[107] H.-S. Jo, Y. J. Sang, P. Xia, and J. G. Andrews, "Heterogeneous cellular networks with flexible cell association: A comprehensive downlink SINR analysis," *IEEE Trans. Wireless Commun.*, vol. 11, no. 10, pp. 3484–3495, October 2012.

[108] S. Mukherjee, "Downlink SINR distribution in a heterogeneous cellular wireless network with biased cell association," in *Proc. IEEE International Conference on Communications*, June 2012, pp. 6780–6786.

[109] H. Wang and M. Reed, "A novel tractable framework to analyse heterogeneous cellular networks," in *Proc. 6th IEEE Joint Workshop on Heterogeneous, Multi-Hop, Wireless and Mobile Networks, co-located with IEEE GLOBECOM 2011*, December 2011, pp. 287–292.

[110] ——, "Tractable model for heterogeneous cellular networks with directional antennas," in *Proc. Australian Communications Theory Workshop*, January 2012, pp. 61–65.

[111] M. Haenggi, "On distances in uniformly random networks," *IEEE Trans. Inf. Theory*, vol. 51, no. 10, pp. 3584–3586, October 2005.

Appendix A

Proofs for Chapter 3

A.1 Proof of Lemma 2

When the aggregate effect of path loss and shadowing is partially compensated, transmit power P_z is given by (3.2). Using (3.2), the CDF of P_z can written as

$$\begin{aligned} F_{P_z}(t) &= \Pr\left(\rho\left(r^{-\alpha}h_{zy}\right)^{-\eta} < t\right), \\ &= \mathcal{E}_{h_{zy}}\left[\Pr\left(r < \left(\frac{t}{\rho}\right)^{\frac{1}{\eta\alpha}} h_{zy}^{\frac{1}{\alpha}} | h_{zy}\right)\right], 0 < t < \infty. \end{aligned} \tag{A.1}$$

Using the PDF of r given in (3.4), (A.1) can be written as

$$F_{P_z}(t) = \mathcal{E}_{h_{zy}}\left[1 - \exp\left(-\pi\lambda\left(\frac{t}{\rho}\right)^{\frac{2}{\alpha\eta}} h_{zy}^{\frac{2}{\alpha}}\right)\right], 0 < t < \infty. \tag{A.2}$$

The PDF of h_{zy} is given by

$$f_{h_{zy}}(h) = \frac{1}{\sqrt{2\pi}\xi h}\exp\left(\frac{-\left(\ln(h)\right)^2}{2\xi^2}\right),\ 0 < h < \infty. \tag{A.3}$$

Substituting (A.3) in (A.2) and using the change of variable $u = \ln(h)/\sqrt{2}\xi$

$$F_{P_z}(t) = 1 - \frac{1}{\sqrt{\pi}}\int_{-\infty}^{\infty}\exp\Big(-u^2 - \pi\lambda\left(\frac{t}{\rho}\right)^{\frac{2}{\alpha\eta}}\exp\Big(\frac{2\sqrt{2}\xi u}{\alpha}\Big)\Big)du,\ 0 < t < \infty. \tag{A.4}$$

Solving the integration in (A.4) by Gauss-Hermite quadrature, we obtain (3.10). PDF of P_z (3.11) is obtained by differentiating (3.10).

A.2 Proof of Lemma 3

In this power control scheme, each MS transmits with power given by (3.3). The CDF of the transmit power of MS $z \in \Phi$, P_z, can be derived as follows.

$$\begin{aligned} F_{P_z(t)} &= \Pr\left(\rho r^{\alpha\eta} h_{zy}^{-1} < t\right), \\ &= \mathcal{E}_{h_{zy}}\left[\Pr\left(r < \left(\frac{h_{zy}t}{\rho}\right)^{\frac{1}{\alpha\eta}} | h_{zy}\right)\right]. \end{aligned} \tag{A.5}$$

Using the PDFs of r given by (3.4), (A.5) can be written as

$$F_{P_z(t)} = \mathcal{E}_{h_{zy}}\left[1 - \exp\left(-\pi\lambda\left(\frac{h_{zy}t}{\rho}\right)^{2/\alpha\eta}\right)\right]. \tag{A.6}$$

Substituting (A.3) in (A.6) and using the change of variable $u = \frac{\ln(h)}{\sqrt{2}\xi}$

$$F_{P_z}(t) = 1 - \frac{1}{\sqrt{\pi}}\int_{-\infty}^{\infty} \exp\left(-u^2 - \pi\lambda\left(\frac{t}{\rho}\right)^{2/\alpha\eta} \exp\left(\frac{2\sqrt{2}\xi u}{\alpha\eta}\right)\right) du. \tag{A.7}$$

Solving the integration in (A.7) by Gauss-Hermite quadrature we obtain (3.12). Now by differentiating (3.12) we can obtain (3.13).

A.3 Proof: Theorem 1

For power control Scheme 1, SINR at the BS serving MS z_0 is given by (3.14). Therefore, the coverage probability can be written as

$$P_c(T) = \Pr\left(SINR > T\right) = \Pr\left(h_{z_0} > \frac{T\left(I_{\Phi\setminus z_0} + N_0\right)}{\rho r_{z_0}^{\alpha(\eta-1)}}\right), \tag{A.8}$$

where, $I_{\Phi\setminus z_0} = \sum_{z\in\Phi\setminus z_0} P_z r_z^{-\alpha} h_z$ is the total interference power from all the co-channel MSs. Variance of additive white Gaussian noise (AWGN) is given by N_0. Since composite Rayleigh-lognormal fading is considered, $h_{z_0} \sim \exp(\mu)$ where, $\mu \sim \text{lognormal}(0, \sigma)$. Now, the PDF of h_{z_0} can be written as [30]

$$f_{h_{z_0}}(h) = \int_0^{\infty} \frac{1}{\mu}\exp\left(-\frac{h}{\mu}\right) \frac{1}{\sqrt{2\pi}\sigma\mu}\exp\left(\frac{-\left(\ln(\mu)\right)^2}{2\sigma^2}\right) d\mu. \tag{A.9}$$

Substituting (A.9) in (A.8) introduces computational and analytical difficulties. To overcome these challenges, we use an approach similar to that proposed in [46]. Using change of variable $\ln(h)/\sqrt{2}\sigma = v$, (A.9) can be written as

$$f_{h_{z_0}}(h) = \frac{1}{\sqrt{\pi}}\int_{-\infty}^{\infty} \exp\left(-\sqrt{2}\sigma v - h\,\exp\left(-\sqrt{2}\sigma v\right) - v^2\right) dv. \tag{A.10}$$

(A.10) has the form of Gauss-Hermite integration, which can be approximated as

$$f_{h_{z_0}}(h) = \sum_{i=1}^{L} \frac{\zeta_i}{\sqrt{\pi}} \exp\left(-\sqrt{2}\sigma v_i - h \exp\left(-\sqrt{2}\sigma v_i\right)\right) + O_L, \tag{A.11}$$

where ζ_i and v_i are the weights and abscissas determined by Hermite polynomial after L is chosen. L represents the remainder terms that decrease to zero as L increases to infinity.

Using (A.11) the complementary cumulative distribution function (CCDF) of h_{z_0} can be written as

$$\overline{F}_{h_{z_0}}(h) = \sum_{i=1}^{L} \frac{\zeta_i}{\sqrt{\pi}} \exp\left(-h \exp\left(-\sqrt{2}\sigma v_i\right)\right) + O'_L, \tag{A.12}$$

where O'_L is the error in the approximation due to O_L in (A.11). Substituting (A.12) in (A.8), $P_c(T)$ can be written as

$$P_c(T) = \sum_{i=1}^{L} \frac{\zeta_i}{\sqrt{\pi}} \mathcal{E}_{r_{z_0}}\left[\mathcal{E}_{I_{\Phi\setminus z_0}}\left[\exp\left(\frac{-\left(I_{\Phi\setminus z_0} + N_0\right) T \exp\left(-\sqrt{2}\sigma v_i\right)}{\rho r_{z_0}^{\alpha(\eta-1)}}\right)\right]\right] + \epsilon_L, \tag{A.13}$$

where ϵ_L is the error in the approximation due to O'_L of (A.12). Using the definition of the Laplace transform, (A.13) can be written as

$$\begin{aligned} P_c(T) = \sum_{i=1}^{L} \frac{\zeta_i}{\sqrt{\pi}} \mathcal{E}_{r_{z_0}}\Bigg[&\exp\left(-\frac{N_0 T \exp\left(-\sqrt{2}\sigma v_i\right)}{\rho r_{z_0}^{\alpha(\eta-1)}}\right) \\ &\times \mathcal{L}_{I_{\Phi\setminus z_0}}\left(s = \frac{T \exp\left(-\sqrt{2}\sigma v_i\right)}{\rho r_{z_0}^{\alpha(\eta-1)}}\right)\Bigg] + \epsilon_L, \end{aligned} \tag{A.14}$$

where $\mathcal{L}_{I_{\Phi\setminus z_0}}(s)$ is the Laplace transform of the PDF of random variable $I_{\Phi\setminus z_0}$. Substituting the PDF of r_{z_0} given by (3.4) in (A.14) we obtain (3.15). $\mathcal{L}_{I_{\Phi\setminus z_0}}(s)$, can be derived as follows.

$$\begin{aligned} \mathcal{L}_{I_{\Phi\setminus z_0}}(s) &= \mathcal{E}_{\Phi,h_z,P_z}\left[\exp\left(-s \sum_{z\in\Phi\setminus z_0} P_z r_z^{-\alpha} h_z\right)\right], \\ &= \mathcal{E}_{\Phi,h_z,P_z}\left[\prod_{z\in\Phi\setminus z_0} \exp\left(-s P_z r_z^{-\alpha} h_z\right)\right]. \end{aligned} \tag{A.15}$$

Using the definition of probability generating functional of PPP [51].

$$\mathcal{L}_{I_{\Phi\setminus z_0}}(s) = \exp\left(-2\pi\lambda \int_{r_{z_0}}^{\infty} r_z \mathcal{E}_{h_z,P_z}\left[1 - \exp\left(-s P_z r_z^{-\alpha} h_z\right)\right] dr_z\right). \tag{A.16}$$

Since P_z and h_z are statistically independent and using the PDF of where, Consider $\mathcal{I} = \mathcal{E}_{h_z,P_z}[1-\exp\left(-sP_z r_z^{-\alpha} h_z\right)]$. Using the PDF of h_z given by (A.11), $\mathcal{I}$ can be written as

$$\begin{aligned}\mathcal{I} &= \mathcal{E}_{P_z}\Bigg[1-\sum_{j=1}^{M}\frac{\kappa_j}{\sqrt{\pi}}\exp\left(-\sqrt{2}\sigma x_j\right)\\ &\qquad\times\int_0^{\infty}\exp\left(-h_z\left(\exp\left(-\sqrt{2}\sigma x_j\right)+sP_z r_z^{-\alpha}\right)\right)dh_z\Bigg]+O_M,\\ &= \mathcal{E}_{P_z}\left[1-\sum_{j=1}^{M}\frac{\kappa_j}{\sqrt{\pi}}\frac{1}{1+sP_z r_z^{-\alpha}\exp\left(\sqrt{2}\sigma x_j\right)}\right]+O_M, \end{aligned} \tag{A.17}$$

where O_M is the error due to using the approximate expression (A.11). Substituting (3.8) in (A.17) and using the fact that $\sum_{j=1}^{M}\kappa_j = \sqrt{\pi}$

$$\mathcal{I} = \frac{2\sqrt{\pi}\lambda}{\alpha\eta\rho^{\frac{2}{\alpha\eta}}}\sum_{j=1}^{M}\kappa_j\int_0^{\infty}\frac{P_z^{\frac{2}{\alpha\eta}-1}}{1+\frac{r_z^{\alpha}}{sP_z\exp\left(\sqrt{2}\sigma x_j\right)}}\exp\Big(-\pi\lambda\Big(\frac{P_z}{\rho}\Big)^{\frac{2}{\alpha\eta}}\Big)dP_z+O_M. \tag{A.18}$$

Using the change of variable $\delta = \pi\lambda\left(\frac{P_z}{\rho}\right)^{\frac{2}{\alpha\eta}}$, (A.18) can be written as

$$\mathcal{I} = \sum_{j=1}^{M}\frac{\kappa_j}{\sqrt{\pi}}\int_0^{\infty}\frac{\exp(-\delta)}{1+\frac{r_z^{\alpha}(\pi\lambda)^{\frac{\alpha\eta}{2}}}{s\rho\,\exp\left(\sqrt{2}\sigma x_j\right)\delta^{\frac{\alpha\eta}{2}}}}dy+O_M. \tag{A.19}$$

(A.19) can be approximated as a Gauss-Laguerre quadrature sum as given below.

$$\mathcal{I} = \sum_{j=1}^{M}\frac{\kappa_j}{\sqrt{\pi}}\sum_{q=1}^{Q}\beta_q\frac{1}{1+\frac{r_z^{\alpha}(\pi\lambda)^{\frac{\alpha\eta}{2}}}{s\rho\,\exp\left(\sqrt{2}\sigma x_j\right)\delta_q^{\frac{\alpha\eta}{2}}}}+O_{MQ}, \tag{A.20}$$

where β_q and δ_q are the abscissas and weight factors for the Gauss-Laguerre integration [6, Table (25.9)] and O_{MQ} is the error in the approximation. Substituting (A.20) in (A.15),

$$\mathcal{L}_{I_{\Phi\setminus z_0}}(s) = \exp\Big(-2\sqrt{\pi}\lambda\sum_{j=1}^{M}\kappa_j\sum_{q=1}^{Q}\beta_q\int_{r_{z_0}}^{\infty}\frac{r_z}{1+\frac{r_z^{\alpha}(\pi\lambda)^{\frac{\alpha\eta}{2}}}{s\rho\,\exp\left(\sqrt{2}\sigma x_j\right)\delta_q^{\frac{\alpha\eta}{2}}}}d_{r_z}\Big)+R_{MQ}, \tag{A.21}$$

where R_{MQ} is the error in the approximation. Solving (A.21) we obtain (3.16) of Theorem 1.

A.4 Proof of Theorem 2

When power control Scheme 2 is employed, SINR at the BS serving MS $z_0 \in \Phi$ is given by (3.17). Therefore, the coverage probability can be written as

$$P_c(T) = \Pr\left(\hat{h}_{z_0} > \frac{T\left(I_{\Phi\setminus z_0} + N_0\right)}{\rho r_{z_0}^{\alpha(\eta-1)}}\right). \tag{A.22}$$

The CCDF of $\hat{h}_{z_0}$ can be obtained by replacing σ by $(1-\eta)\sigma$ in (A.12). Following approach similar to the derivation of (A.14), (A.22) can be written as

$$P_c(T) = \sum_{i=1}^{L} \frac{\zeta_i}{\sqrt{\pi}} \mathcal{E}_{r_{z_0}}\Bigg[\exp\left(-\frac{TN_0 \exp\left(-\sqrt{2}(1-\eta)\sigma v_i\right)}{\rho r_{z_0}^{\alpha(\eta-1)}}\right) \times \mathcal{L}_{I_{\Phi\setminus z_0}}\Bigg(s = \frac{T\,\exp\left(-\sqrt{2}(1-\eta)\sigma v_i\right)}{\rho r_{z_0}^{\alpha(\eta-1)}}\Bigg)\Bigg] + \epsilon_L, \tag{A.23}$$

where ϵ_L is the error in the approximation. Substituting (3.4) in (A.23), we obtain (3.18). Following steps similar to the derivation of (A.15), $\mathcal{L}_{I_{\Phi\setminus z_0}}(s)$ for power control Scheme 2 can be derived as follows.

$$\mathcal{L}_{I_{\Phi\setminus z_0}}(s) = \exp\Bigg(-2\pi\lambda \int_{r_{z_0}}^{\infty} r_z \left(1 - \mathcal{E}_{P_z,h_z}\left[\exp\left(-sP_z r_z^{-\alpha} h_z\right)\right]\right) dr_z\Bigg). \tag{A.24}$$

Consider $\mathcal{B} = 1 - \mathcal{E}_{P_z,h_z}\left[\exp\left(-sP_z r_z^{-\alpha} h_z\right)\right]$. $\mathcal{B}$ is similar to $\mathcal{I}$ given in (A.17), but with the PDF of P_z given by (3.11). Therefore, $\mathcal{B}$ can be written as

$$\mathcal{B} = \frac{2\lambda}{\alpha\eta\rho^{\frac{2}{\alpha\eta}}} \sum_{k=1}^{N} w_k \sum_{j=1}^{M} \kappa_j \exp\left(\frac{2\sqrt{2}\xi u_k}{\alpha}\right) \int_0^{\infty} \frac{P_z^{\frac{2}{\alpha\eta}-1}}{1 + \frac{r_z^{\alpha}}{sP_z\,\exp\left(\sqrt{2}\sigma x_j\right)}} \times \exp\Bigg(-\pi\lambda\left(\frac{P_z}{\rho}\right)^{\frac{2}{\alpha\eta}} \exp\left(\frac{2\sqrt{2}\xi u_k}{\alpha}\right)\Bigg) dP_z + O_{NM}. \tag{A.25}$$

Here, O_{NM} is the error term due to O_M. Using the change of variable $\delta = \pi\lambda\left(\frac{P_z}{\rho}\right)^{\frac{2}{\alpha\eta}} \exp\left(\frac{2\sqrt{2}\xi u_k}{\alpha}\right)$,

$$\mathcal{B} = \frac{1}{\pi} \sum_{k=1}^{N} w_k \sum_{j=1}^{M} \kappa_j \int_0^{\infty} \frac{e^{-\delta}}{1 + \frac{r_z^{\alpha}(\pi\lambda)^{\frac{\alpha\eta}{2}} \exp\left(\sqrt{2}\xi u_k \eta\right)}{s\rho\,\exp\left(\sqrt{2}\sigma x_j\right)\delta^{\frac{\alpha\eta}{2}}}} d\delta + O_{NM}. \tag{A.26}$$

Solving the integral in (A.26) by Gauss-Laguerre quadrature

$$\mathcal{B} = \frac{1}{\pi} \sum_{k=1}^{N} w_k \sum_{j=1}^{M} \kappa_j \sum_{q=1}^{Q} \beta_q \frac{1}{1 + \frac{r_z^{\alpha}(\pi\lambda)^{\frac{\alpha\eta}{2}} \exp\left(\sqrt{2}\xi u_k \eta\right)}{s\rho\,\exp\left(\sqrt{2}\sigma x_j\right)\delta_q^{\frac{\alpha\eta}{2}}}} + O_{NMQ}. \tag{A.27}$$

Here, β_q and δ_q are the abscissas and weight factors for the Gauss-Laguerre quadrature of order $Q > 1$. O_{NMQ} is the error in the approximation. Substituting (A.27) in (A.24) and solving the integration, we obtain (3.19) of Theorem 2.

A.5 Proof of Theorem 3

When power control Scheme 3 is employed, SINR at the BS serving MS $z_0 \in \Phi$ is given by (3.20). Therefore, the coverage probability can be written as

$$P_c(T) = \Pr\left[g_{z_0} > \frac{T\left(I_{\Phi\setminus z_0} + N_0\right)}{\rho r_{z_0}^{\alpha(\eta-1)}}\right]. \tag{A.28}$$

Since $g_{z_0} \sim \exp(1)$, and random variables g_{z_0}, $I_{\Phi\setminus z_0}$, and r_{z_0} are statistically independent

$$P_c(T) = \mathcal{E}_{I_{\Phi\setminus z_0}, r_{z_0}}\left[g_{z_0} > \frac{T\left(I_{\Phi\setminus z_0} + N_0\right)}{\rho r_{z_0}^{\alpha(\eta-1)}}\right]. \tag{A.29}$$

Substituting the probability density function (PDF) of r_{z_0} given in (3.4)

$$P_c(T) = 2\pi\lambda\int_0^\infty r_{z_0}\exp\left(-\pi\lambda r_{z_0}^2 - \frac{TN_0}{\rho r_{z_0}^{\alpha(\eta-1)}}\right)\mathcal{E}_{I_{\Phi\setminus z_0}}\left[\exp\left(-\frac{I_{\Phi\setminus z_0}Tr_{z_0}^{\alpha(1-\eta)}}{\rho}\right)\right]dr_{z_0}. \tag{A.30}$$

Using the definition of the Laplace transform, $P_c(T)$ for power control Scheme 3 can be written as

$$P_c = 2\pi\lambda\int_0^\infty r_{z_0}\exp\left(-\pi\lambda r_{z_0}^2 - \frac{TN_0}{\rho r_{z_0}^{\alpha(\eta-1)}}\right)\mathcal{L}_{I_{\Phi\setminus z_0}}\left(\frac{Tr_{z_0}^{\alpha(1-\eta)}}{\rho}\right)dr_{z_0}, \tag{A.31}$$

where $\mathcal{L}_{I_{\Phi\setminus z_0}}(s)$ is the Laplace transform of the PDF of aggregate interference $I_{\Phi\setminus z_0}$. This concludes the derivation of (3.21) of Theorem 3.

Using steps similar to the derivation of (A.15), $\mathcal{L}_{I_{\Phi\setminus z_0}}(s)$ can be written as

$$\mathcal{L}_{I_{\Phi\setminus z_0}}(s) = \exp\Big(-2\pi\lambda\int_{r_{z_0}}^\infty\left(1 - \mathcal{E}_{P_z,h_z}\left[\exp(-sP_z r_z^{-\alpha}h_z)\right]\right)\Big)r_z dr_z. \tag{A.32}$$

Consider $\mathcal{A} = 1 - \mathcal{E}_{P_z,h_z}\left[\exp(-sP_z r_z^{-\alpha}h_z)\right]$. $\mathcal{A}$ is similar to $\mathcal{I}$ given in (A.17), but with the PDF of P_z given by (3.13). Therefore, $\mathcal{A}$ can be written as

$$\mathcal{A} = \frac{2\lambda}{\rho^{\frac{2}{\alpha\eta}}\alpha\eta}\sum_{k=1}^N w_k\sum_{j=1}^M\kappa_j\int_0^\infty\frac{P_z^{\frac{2}{\alpha\eta}-1}}{1+\frac{r_z^\alpha}{sP_z\exp(\sqrt{2}\sigma x_j)}} \times\exp\left(\frac{2\sqrt{2}\xi u_k}{\alpha\eta} - \frac{\pi\lambda P_z^{\frac{2}{\alpha\eta}}\exp\left(\frac{2\sqrt{2}\xi u_k}{\alpha\eta}\right)}{\rho^{\frac{2}{\alpha\eta}}}\right)dP_z + O_{NM}, \tag{A.33}$$

where O_{NM} is the error in the approximation. Using the change of variable $\delta = \pi\lambda P_z^{\frac{2}{\alpha\eta}}\exp\left(\frac{2\sqrt{2}\sigma u_i}{\alpha\eta}\right)\rho^{\frac{-2}{\alpha\eta}}$,

$$\mathcal{A} = \frac{1}{\pi}\sum_{k=1}^N w_k\sum_{j=1}^M\kappa_j\int_0^\infty\frac{\exp(-\delta)}{1+\frac{r_z^\alpha(\pi\lambda)^{\frac{\alpha\eta}{2}}\exp(\sqrt{2}\sigma u_k)}{s\rho\,\exp(\sqrt{2}\xi x_j)\delta^{\frac{\alpha\eta}{2}}}}d\delta + O_{NM}. \tag{A.34}$$

The integral in (A.34) can be approximated as a Gauss-Laguerre quadrature sum as given below.

$$\mathcal{A}=\frac{1}{\pi}\sum_{k=1}^{N} w_k \sum_{j=1}^{M} \kappa_j \sum_{q=1}^{Q} \beta_q \frac{1}{1+\frac{r_z^{\alpha}(\pi\lambda)^{\frac{\alpha\eta}{2}}\exp(\sqrt{2}\sigma u_k)}{s\rho\ \exp(\sqrt{2}\xi x_j)\delta_q^{\frac{\alpha\eta}{2}}}} + O_{NMQ}, \tag{A.35}$$

where O_{NMQ} is the error term due to O_{NM} and representing integration in (A.34) as a Gauss-Laguerre quadrature sum. Substituting (A.35) in (A.32) we obtain (3.22) of Theorem 3.

$\sim$